Vol. 107 Nº1 ISSN 2545-8655

ANALES DE LA ASOCIACIÓN QUÍMICA ARGENTINA

Enero-Junio 2020

Anales de la Asociación Química Argentina

Editada desde 1913

Asistente Editorial
Lic. Cristina E. Corbellani
e-mail: anales.aqa@gmail.com
Registro de Propiedad Intelectual Nº 164.756

Asociación Química Argentina

Sánchez de Bustamante 1749, 1425 Buenos Aires, Argentina
TE/FAX: 54-11-4822-4886
http://www.aqa.org.ar

Contenido

Vol. 107 Nº1, Enero-Junio de 2020

EDITORIAL

Estimados Lectores de Anales de la Asociación Química Argentina:

El presente número de Anales de la AQA reúne trabajos regulares de conocidos investigadores nacionales e internacionales, el trabajo "Whole bodies of the argentinian cockroach periplaneta americana: noncommercial extract fractionation/characterization, cross-reactivity and vaccine therapy", de Stella M. Battista y colaboradores, que recibió el premio del XXXII Congreso Argentino de Química en el Área Química Biológica, y el trabajo "Síntesis y Caracterización de Calix[4]areno Funcionalizado con Grupos Sulfónicos Incluido en una Matriz de Sílice-Titania", de María B. Colombo Miglioriero y colaboradores, que recibió el premio del XXXII Congreso Argentino de Química en el Área Química Industrial y Ciencia de Materiales.

Esperamos que disfruten de este nuevo número y contarlos como colaboradores en próximos números de la revista.

Dra. Susana A. Larrondo

Editora

Anales de la Asociación Química Argentina

ANS WITH METAL(II)-BIFUNCTIONAL AMINE COMPLEXES IN TOLUENE. KINETIC DETERMINATIONS AND QUANTUM CHEMICAL CALCULATIONS

SUSTITUCIÓN NUCLEOFÍLICA AROMÁTICA CON COMPLEJOS METAL(II)-AMINAS BIFUNCIONALES EN TOLUENO. DETERMINACIONES CINÉTICAS Y CÁLCULOS QUÍMICO CUÁNTICOS

Cecilia E. Silvana Alvaro[1,2*], Federico D. Bergero[3], Federico M. Bolcic[4], Susana B. Ramos[2,3], Norma S. Nudelman[5].

[1]Depto. de Química, Facultad de Ingeniería. Universidad Nacional del Comahue. Buenos Aires 1400 (8300) Neuquén, Argentina.

[2]Instituto de Investigaciones y Desarrollo en Ingeniería de Procesos, Biotecnología y Energías Alternativas (PROBIEN), CONICET - Universidad Nacional del Comahue, (8300) Neuquén, Argentina.

[3]Depto. de Física, Facultad de Ingeniería. Universidad Nacional del Comahue. Buenos Aires 1400, (8300) Neuquén, Argentina.

[4]Facultad de Ciencias Médicas, Universidad Nacional del Comahue. (8324) Cipolletti, Río Negro, Argentina.

[5]Academia Nacional de Ciencias Exactas, Físicas y Naturales, Avda. Alvear 1714, Piso 4, Buenos Aires, Argentina. Email: acad@ancefn.org.ar /sbarbati04@gmail.com

[*]Autor Corresponsal E-mail: silvanitaces@gmail.com / silvana_alvaro@hotmail.com

Resumen

Se realizaron estudios cinéticos de Sustitución Nucleofílica Aromática (SNAr) empleando complejos Metal(II)-amina en tolueno y cálculos químicos cuánticos para determinar la geometría y energía de formación de los complejos. Los estudios previamente informados del mecanismo SNAr se centran principalmente en la naturaleza del sustrato, la basicidad del nucleófilo y la polaridad del disolvente, aunque el estudio con complejos de coordinación es escaso. Los complejos metal-amina exhiben una reactividad diferencial con respecto a las aminas no complejadas dependiendo, principalmente, del metal y la estructura del ligando. El presente trabajo describe estudios cinéticos realizados en tolueno con 1-cloro-2,4-

dinitrobenceno y complejos de Cu(II) y Fe(II) con aminas bifuncionales, y se compararon con estudios previos utilizando las aminas no complejadas. Considerando la diferente reactividad de los complejos metal-amina, los resultados sugieren una diferente labilidad de los complejos atribuidos al efecto quelato y efectos estereoelectrónicos, para formar aminas no complejadas que luego reaccionarían con el sustrato, ya que los resultados cinéticos no proporcionan evidencia que los complejos metal-amina reaccionan como entidad nucleofílica. Por el contrario, se disocian antes de reaccionar y los resultados obtenidos son consistentes con el mecanismo del "Nucleófilo Dímero". Mediante cálculos teóricos basados en la Teoría Funcional Densidad determinamos la estructura de equilibrio y energía de complejación de dichos complejos. Los cálculos teóricos indican que los complejos más estables son aquellos con tres moléculas de amina como ligando, y que los complejos de Cu(II) son más estables que los de Fe(II), resultados que se correlacionan con el orden de reactividad obtenido experimentalmente

Abstract

Kinetic studies of Aromatic Nucleophilic Substitutions (ANS) of Metal(II)-amine complexes in toluene and quantum chemical calculations were carried out. Reported studies of ANS mechanism are mainly centered on the nature of substrates, nucleophile basicity and solvent polarity, while the study with coordination complexes are scarce. Amine complexes exhibit a differential reactivity with respect to uncomplexed amines depending on, among other factors, the metal center and the ligand structure. The present work describes kinetic studies carried out in toluene with 1-chloro-2,4-dinitrobenzene (DNClB) and Cu(II) and Fe(II) complexes with bifunctional amines. They were chosen considering their characteristics of bi-dentate ligands, the possible size of the metalo-cycle formed and their ability to form intra- or intermolecular hydrogen-bonds. Taking into account the dissimilar reactivity of amine-complexes, the results suggest a different stability of the complexes attributed to stereo-electronic and chelate effects, to form uncomplexed amines that would then react with the substrate, since the observed results do not provide evidence that metal-amine complexes react as a nucleophilic entity. On the contrary, they seem to dissociate prior to react rendering results consistent with a “dimer nucleophile” mechanism. To interpret kinetic results, we performed Density Functional Theory calculations to determine the equilibrium structure and the binding energy for Cu(II) and Fe(II) amine complexes. Quantum chemical calculations indicate that the most stable complexes are those with three amines molecules as ligands, and that Cu(II) complexes are more stable than those with Fe(II), results that correlate with the order of reactivity experimentally obtained.

Palabras clave: Sustitución Nucleofílica Aromática; Solventes apróticos; Complejos de coordinación; Mecanismo del Nucleófilo Dímero; Cálculos DFT.

Keywords: Aromatic Nucleophilic Substitution; Aprotic solvents; Coordination complexes; Dimer Nucleophile Mechanism; DFT calculations.

1. Introduction

Transition metal complexes are currently receiving special attention due to their special biological activity [1,2], as well as for their applications in other scientific [3,4] and technological fields [5]. Particularly, the investigation of structure and solvent effects on the reactivity of coordination metal complexes is an area of active interest [1-4]. Studies on metal coordination complexes mainly refer to transmetalation, ligand substitution, displacement of ligand from a substrate M-L (where M is the metal and L is a ligand), or displacement of a leaving group from the ligand complex by various reagents [6]. The amines form coordination complexes of particular significance in the development of Coordination Chemistry [7]; particularly amine-transition metal complexes are very important chelates due to their biological implications. As some examples it can be mentioned the recently reported electro-reduction of mixed ligand cobalt (III) complexes [8], the metal chelation-assisted amine–amine electronic coupling through the 4,4′-positions of 2,2′-bipyridine [9], the metalloenzymes feature of the metals that are chelated, usually to peptides or cofactors and prosthetic groups[10], biological applications and nutritional supplements [11-14].

Studies of the Aromatic Nucleophilic Substitution (ANS) mechanism reported in the literature are mainly centered on the nature of substrates, nucleophile basicity and solvent polarity, while the coordination complexes study in ANS reactions are very scarce. The aim of the present work is to use metal amine coordination complexes as nucleophilic entities in ANS reactions, since they have the majority of their nucleophilic atoms forming coordinated covalent bonds with the metal, and therefore are expected to be mostly non-reactive. To examine the lability of such complexes and their possible capacity to dissociate in free amines that react with the substrate we synthesized metal amine coordination complexes, developed ANS reactions, characterized the ANS products obtained, and compared them with those obtained in our previous studies in which ANS reactions were performed with the same uncomplexed amines.

Early works were carried out on several ANS performed in aprotic solvents with nitro-activated substrates and poor leaving groups, for which the second-step of the reaction is rate-determining, providing kinetic, conformational and thermodynamical evidence for a new mechanism, called the “dimer nucleophile” for ANS with amines [15].

In the last years [16-19], we have reported ANS in aprotic solvents with a substrate having a good leaving group and amines that were purposefully selected due to their special structure that make them able to form inter- or intramolecular H-bonds, as were determined by NMR measurements [20]. Theoretical calculations were also performed on these amines to provide valuable insight into the predominant type of H-bonds present in them [21,22]. Due to the self-

aggregation and other non-covalent interactions that occur in solvents of low permittivity, the predominant nucleophile is the dimer of the amine. In these cases, a third order in amine concentration, giving an overall fourth-order kinetics was determined. These reactions occur via an addition/elimination mechanism where the first step is the attack of the amine dimer to the substrate (k_1) to form a zwitterionic σ-bonded complex (SB), usually named Meisenheimer complex. In a second step, the leaving group detaches from the substrate to give the reaction product. This step can be uncatalyzed (k_2), or occur through a catalyzed route (k_3) by a third nucleophilic molecule as it has been reported in previous works [15-17].

The present paper describes ANS reactions developed with metal complexes of amines. Specifically, these reactions were carried out with 1-chloro-2,4-dinitrobenzene, (DNClB), a good nucleofugue substrate, and several coordination complexes of bifunctional amines with Cu(II) and Fe(II), in toluene. The amines are ethylenediamine (EDA), N,N-dimethyl propylamine (DMPA), 2-(1H-imidazol-4-yl)ethanamine, (histamine), and 1-(2-aminoethyl)piperidine, (2-AEPip). They were selected by considering their characteristics of bi-dentate ligands and the possible size of the metalo-cycle formed. As a way of comparison, we have previously studied ANS with the uncomplexed amines [18].

In order to provide theoretical insights on the interpretation of the kinetic results, Density Functional Theory (DFT) [23] calculations on Cu(II) and Fe(II) complexes with the above mentioned amines were carried out, determining the optimal geometries in vacuum and their binding energies. Theoretical studies based on DFT methods currently provide information about the strength, ionic character of bonds, the charge transfer effects [24-26]. Analysis based on the Atoms in Molecules [27] theory were also carried out to characterize the relevant covalent bonds and also the weak interactions present in the coordination complexes used in the study.

2. Materials and Methods

2.1. General Procedures

UV-VIS spectra and kinetic runs were recorded in a Shimadzu UV-VIS 240 graphic printer PR-1 spectrophotometer. 1H and 13C NMR spectra were recorded in a Bruker ARX-300 spectrometer instrument. NMR spectra were determined in CDCl3 spectroscopic grade as solvent and the J values are given in hertz. The infrared spectra were recorded on a Nicolet spectrophotometer, Nexus FT-IR 470/670/870. Thin-layer chromatography was performed on Merck Kiesegel 60 F254. Melting points were determined in a Kofler hot stage and are uncorrected.

2.2. Reagents and Solvents

The reagents and solvent used are the commercially available from Merck, Fluka and Sigma-Aldrich which guarantee purity ≥ 99%. Toluene was kept over sodium wire for several days and distilled twice over sodium as described previously [16]. The purification of EDA, DMPA and 2-AEPip were carry out as described previously [18] and kept in a desiccator protected from light under dry nitrogen atmosphere, prior to use. 2-(1H-imidazol-4-yl)ethanamine, (Fluka) was used without any purification and was kept in a desiccator protected from light.The substitution products were purified and characterized by NMR spectra using previously reported procedures [18].

The complexes were prepared as reported elsewhere [28], using an ethanolic solution of iron(II) and copper(II) ammonium sulfate and the respective amine. The Fe(II) complexes were prepared in the presence of drops of glacial acetic acid to avoid Fe(II) oxidation. The formation of the amine-Cu(II) complexes was shown by the appearance of a blue coloration in the colorless amine solutions after the addition of the metal ion solution; the spectra of the solutions of each ligand were performed in the absence and by adding the solution of the metal ion to the solution of the ligand in toluene and were recorded between 250 and 650 nm. After the addition of the Cu(II) solution new bands among 540-580 nm can be attributed to the amine-Cu(II) complexes formation, considering that neither the metallic ion nor the ligands absorbs in that wavelength range. A similar procedure was used for the amine-Fe(II) complexes, a green color solution was observed when adding the Fe(II) salt. Two bands, centered on 430-455 and 600-610 nm were observed in the spectra and can be attributed to the amine-Fe(II) complexes formation.

Stoichiometries of the formed complexes were determined using the Yoe-Jones method [29]. This spectrophotometric method requires the preparation of a set of solutions varying the ligand concentration [L], but keeping constant the metallic ion concentration [M]. The absorbance, A, of these solutions was measured at a wavelength which only the complexes absorb, and used to plot a graphic of A vs. [L]/[M]. The intersection points between the straight lines of the experimental data indicate the ligand:metal L:M molar ratio. It was found that the stoichiometries of the formed complexes were 3:1 ligand:metal molar composition.

The spectroscopic characterization of the substitution products was made by IR and NMR spectroscopic determinations and coincided with those obtained in the previous study where these reactions were studied with the same substrate and solvent using the uncomplexed amines [18]. The characterization results are presented below:

[N-(2,4-dinitrophenyl)ethylenediamine] (mp 108-110 °C), 1H NMR ($CDCl_3$): δ 2.30 (s, ^{1}H), 8.93 (d, ^{1}H), 6.87 (d, 1H), 8.12 (m, 1H), 3.28 (t, 2H), 3.00 (t, ^{2}H), 1, 40 (s, 2H), ^{13}C NMR ($CDCl_3$): δ

40.90, 48.31, 121.51, 121.87, 132.55, 148.10, 148.50, 149.90]. IR (KBr) ν cm^{-1}: 3320 (-N-H); 2850 (C-H, $-CH_2$); 1640 ($-NH_2$); 1590 (C-C); 1510 ($-NO_2$); 1470 (C-H $-CH_2$); 1340 ($-NO_2$); 1120 (-C-N); 890 (C-H); 780 (two bands, $-NH_2$); 710 (C-H)].

[3-dimethylamino-1-N-(2,4-dinitrophenyl)propylamine] (mp 100-102 ºC), ^{1}H NMR ($CDCl_3$): δ 2.10 (s, 1H), 9.30 (d, 1H), 7.40 (d, 1H), 8.48 (m, 1H), 3.70 (t, 2H), 2.01(t, 2H), 2.65 (t, 2H), 2.31 (s, 6H), ^{13}C NMR ($CDCl_3$): δ 27.65, 44.48, 45.40, 58.01, 119.34, 122.35, 128.87, 147.80, 148.48, 149.90]. IR (KBr) cm^{-1}: 3320 (N-H); 2850 (C-H, $-CH_2$); 1658 (-N-H); 1500 ($-NO_2$); 1470 (-C-H, $-CH_2$); 1340 ($-NO_2$); 1380 (C-H, $-CH_3$); 1120 (C-N); 860 (-C-H); 740 (C-H).

[N-(2,4-dinitrophenyl)-1-(2-aminoethyl)piperidine] (mp 122-123 ºC), ^{1}H NMR ($CDCl_3$): δ 9.04 (s, 1H), 8.15 (d, 1H), 6.81 (d, 1H), 3.36 (t, 2H), 2.63 (t, 2H), 2.40 (t, 4H), 1.49 (m, 6H), 1.02 (s, 1H). ^{13}C RMN ($CDCl_3$) δ 150.91, 148.50, 147.15, 131.52, 120.77, 115.34, 49.70, 47.90, 43.80, 27.80, 25.90. IR (KBr) ν cm^{-1}: 3480 (N-H), 1530 (N-H), 1540 and 1380, ($-NO_2$)].

[N-(2,4-dinitrophenyl)histamine] (mp 158-160 °C), ^{1}H NMR ($CDCl_3$): δ 12.60 (s, 1H), 9.03 (s, 1H), 8.25 (d, 1H, 3JHH = 9.5 Hz), 8.08 (s, 1H), 7.59 (s, 1H), 7.10 (d, 1H, 3JHH = 9.5 Hz), 3.20 (t, 2H), 3.05 (t, 2H), 2.30 (s, 1H), ^{13}C NMR (CDCl3) ppm: δ 150.91, 148.50, 147.15 , 136.20, 131.52, 122.40, 121.30, 120.77, 115.34, 38.79, 23.19. IR (KBr) ν cm^{-1}: 3450 (N-H); 2750 (C-H, $-CH_2$); 1640 (N-H); 1590 (C-C); 1510 (C-C); 1500 ($-NO_2$); 1455 (C-H, $-CH_2$); 1340 ($-NO_2$); 880 (C-H); 770 (δ C-H).

The structures of the substitution products are shown in Figure 1.

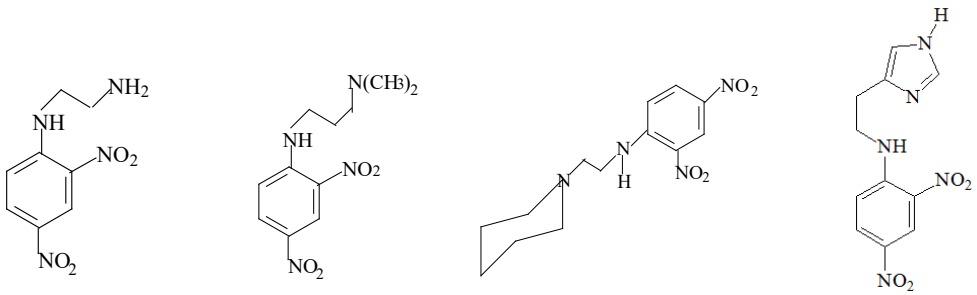

1 **2** **3** **4**

Figure 1. Molecular structures of the ANS products from 1) ethylenediamine, 2) N, N-dimethylpropylamine, 3) 1-(2-aminoethyl)piperidine, 4) histamine.

2.3. Kinetic Procedures

Kinetic measurements of ANS reactions were performed under pseudo first-order conditions by the methods previously reported at the maximum wavelength of each substitution producto [18] as follows: [2-Amino-1-N-(2,4-dinitrophenyl) ethylamine: λ_{max} = 348 nm; [4(5)-2'-(N-2,4-dinitrophenyl) aminoethyl imidazole: λ_{max} = 349 nm; [3-dimethy1amino-1-N-(2,4-dinitropheny1) propylamine: λ_{max} = 351 nm; [N-(2,4-dinitrophenyl)-1-(2-aminoethyl) piperidine: λ_{max} = 348 nm, at 25 ± 0.2 °C.

The reactions of histamine-metal complex were carried out in sealed ampoules (under nitrogen) and the reactions of EDA, DMPA and 2-AEPip complexes were followed directly in the thermostatic cell of the spectrophotometer at 25 ± 0.2 ºC. The zero-time concentration of metal-amine complexes was between 0.4 – 1.20 M, and were prepared in solution immediately before being used. At those wavelengths the reagents are transparent under the experimental conditions.

Pseudo-first-order coefficients, k_Ψ, were obtained by the least-squares method as the slope of the correlation ln $(A_\infty - A_t)/ A_\infty$ versus time, where A_∞ is the optical density of the reaction mixture measured at infinite time (more than ten half-lives). The absorption spectrum of the reaction mixture at "infinite time" corresponded within ± 4 % with the "theoretical" value calculated by application of Beer's law to solutions of the product independently prepared in toluene. No corrections for expansion coefficients were applied to the concentration values.

2.4. Computational procedures

We considered complexes formed with Cu(II) and Fe(II) and one to three ligands of the amines EDA, DMPA, histamine and 2-(AEPip).

First of all, a relaxed Monte-Carlo automatic exploration of the potential energy surface was carried out using the PM6 [30] semiempirical model for the geometrical optimizations. Out of the resulting conformations, the highest energies were discarded according to an energy criterion based on the Boltzmann distribution, usually .003 to .005 au above the lowest energy conformer. Of them, only those significantly different (i.e., different bonding pattern) were chosen, usually one to three. These semiempirical conformer searches have been recommended and the conformer energies have been found to have good correlation with the DFT ones [31].

Then, the selected conformers were optimized by the spin-unrestricted DFT [23] method and the B3LYP [24] exchange-correlation potential using the Gaussian 09 program [32]. For Fe and Cu atoms, the LANL2DZ basis set and effective core potential (ECP) were used, and for the lighter atoms, the 6-31+G(d) basis set. In some cases, namely complexes of EDA and DMPA of one to

three ligands, several spin multiplicities were tested by the unrestricted PM6 and/or the mentioned unrestricted DFT method. The multiplicities tested were mainly one and five, in the smallest complexes, also three and seven for Fe(II), and mainly two and four for Cu(II) complexes. It was found that complexes with multiplicity five for Fe(II) and two for Cu(II) have the minimal energy. Although in the case of Fe(II) this contradicts previous calculations done on porphyrines, in which the B3LYP functional favors multiplicities three or one [33a], this is consistent with experimental data referenced therein. So, all further calculations and results reported here were carried out for those spin multiplicities.

As a final step, the energies of one or two lowest energy conformers were recalculated using the LANL2TZ(f) [34] basis set and ECP for Fe and Cu atoms, and the 6-311+g (2d, p) basis set for the lighter atoms. That step included basis set superposition error (BSSE) correction using the Counterpoise (CP) method [35]. Out of those, the minimum energy conformers for each species are those presented here and discussed in the result´s section.

Amine monomers and dimers were also calculated by the same procedures and models, as their energies are used for calculating several results. Monomers do not require CP corrections. Metal atoms were also calculated with the same models. They require no geometrical optimization or CP correction.

All energies were calculated in vacuum at 0 K. In CP and in monomer and ions calculations, all unbalanced charges and unpaired electrons were assumed to be in the metal ion.

Complexes with four ligands were also searched by the same Monte Carlo semiempirical method as the other complexes. No further DFT calculations were carried out on them because in most cases the 3:1 complexes were found to be energetically more stable at the PM6 level, and also because the Yoe-Jones [29] experimental results favor the 3:1 ones (see sections 2.2 and 3).

The reported binding energy Eb of the complexes is the CP-corrected “complexation energy” as given by the G09 software [32]. It is defined as the counterpoise-corrected total energy of the complex minus the energies of each fragment calculated separately with the same geometry it has within the complex. So, it measures the binding interaction of all the parts within the complex.

We also report E_b divided by the number of ligands N_l (E_b/N_l) and by the number of N-metal coordinated covalent bonds N_b (E_b/N_b). The former is roughly the energy required to remove one amine from the complex or its tendency to provide an amine for the ANS reaction. So, it is an estimation of the lability and reactivity of the complex. The latter is roughly related to the bond

strength of the N-metal coordinated covalent bonds, although amine-amine interactions are also part of that number.

The reported complex formation energy ΔE_{form} is defined as the complex's CP corrected energy minus the energies of the isolated (and geometry optimized) ligands and metal ions, thus including the geometry effect. It is related to the relative abundance of different possible complexes that form in the solvent. Those with greater (more negative) ΔE_{form} are more abundant.

The energies ΔE_1, ΔE_2 and ΔE_3 are the energy differentials when dissociating the complexes. For example, for 3:1 complexes, ΔE_1 corresponds to removing one amine from the complex, leaving a 2:1 complex and a free amine, all with their relaxed geometries. ΔE_2 would correspond to removing two amines from it, leaving a 1:1 complex and two free amines, all geometrically relaxed. ΔE_3 would be further dissociating the remaining 1:1 complex, so it is exactly the opposite of ΔE_{form}. Likewise, ΔE_1 and ΔE_2 are equal in absolute value to the ΔE_{form} of a 1:1 and a 2:1 complex respectively.

For amine dimers, E_b is the binding energy, defined and calculated the same as for metal-amine complexes.

The presence of hydrogen bonds as well as coordinated covalent bonds was verified according to the AIM theory [27] with the multiWFN software [36]. According to this theory, a bond exists when there is a bond critical point (BCP) (a saddle point of the electron density ρ, being a minimum in the bond direction and a maximum in the other two perpendicular directions), and there is a bond path (along which ρ is a maximum in two directions) between two atoms. The density and its Laplacian $\nabla^2(\rho)$ at the BCP of H bonds have been found to be roughly proportional to the bond's stabilization energy [36]. The positive sign of the Laplacian found in all H-bonds also shows their closed-shell (non-covalent) nature [27]. The ellipticity ε at the BCP shows the electron density's deviation from circular symmetry: $\varepsilon = 0$ indicates a perfectly symmetric bond, i.e., a σ bond type, and $\varepsilon = 1$ indicates a π bond. Higher values of ε are indicative of a strained bond in a ring structure, which is about to be broken [27].

All atomic charges were also calculated according to the AIM theory. A space region called atomic basin is defined as the region bounded by closed surfaces through which the flux of the gradient vector field of the electron density is zero. The number of electrons n_e contained in the atomic basin is the integral of ρ in its volume, and the atomic charge is therefore -(ne-Z) [27]. For the metal-amine complexes, we also calculated the atomic charges of the amines alone, with the same geometry that they have in the complex. So we define a charge transfer number Δq for each atom as $q_{complex} - q_{alone}$, i.e., the charge change due to the interaction with the metal atom and the

other amines in the complex. This number is indicative of the intermolecular interactions in which each atom participates in the complex [25, 26].

3. Results and Discussion

3.1. *Kinetic results*

There is at present a considerable interest in the experimental and theoretical research of transition metal coordination complexes concerning their structures and stability [2, 8-10].

One of the first reports on the subject was informed by Shehata *et al.*[6] who proposed an ANS-like mechanism with [1-arylethanediylidene-bis-(methyldithiocarbazonoate)NN'SS'(−2)]Ni(II) complexes and morpholine in benzene in which the rate-determining step is the proton transfer process in the temperature range 20–35 ºC. The mechanism in the range 40–55 ˚C proceeds through the attack of morpholine on the carbon carrying a SCH_3 group followed by the addition of the second morpholine molecule on Ni to form an intermediate, which undergoes the elimination of morpholine and CH_3SH to give a monosubstituted complex.

The present paper reports determinations of the reactivity of Cu(II) and Fe(II)-amine complexes in ANS carry out in an aprotic solvent. The selected amines were chosen considering their characteristics of bi-dentate ligands and for the potential influence on the size of the metalo-cycle formed.

Reactions of DNClB with Cu(II) and Fe(II) amine complexes in toluene

The kinetics of the reactions between DNClB and Cu(II) and Fe(II) EDA, DMPA, 2-AEPip and histamine-metal complexes, respectively, carried out in toluene, were studied at 25 ± 0.2 ºC in the presence of variable amounts of amine complexes. The reactions proceed straightforwardly to give the expected N-substituted 2,4-dinitroaniline, shown in Figure 1.

The kinetic constants are compared with previous kinetic results obtained with the uncomplexed amines. Tables 1 and 2 shows the bimolecular rate coefficients, k_A, and third order rate coefficients, k_A/[B], for the uncomplexed amines and metal-amine complex reactions under the same reaction conditions.

Table 1: Reaction of 2,4-dinitrochlororobenzene, DNClB, with 1,2-diaminoethane (EDA), and 3-dimethylamino-1-propylamine (DMPA), and their respective complexes with Cu(II) and Fe(II) in toluene at 25.0 ± 0.2ºC. Second- (k_A), and third- (k_A/[B]) order rate coefficients are indicated.

[EDA][a*], M	0.494	0.60	0.704	0.794	0.899	1.00	1.20	1.50	----
10^3k_A, s^{-1} M^{-1}	1.69	2.25	2.84	4.11	4.52	6.21	8.39	13.50	----
10^3k_A/[B], s^{-1} M^{-2}	3.42	3.75	4.03	5.18	5.03	6.21	6.99	8.98	----
[Fe(II)-EDA][b], M	0.40	0.60	0.70	0.80	0.90	1.00	1.20	----	----
10^4k_A, s^{-1} M^{-1}	0.54	1.03	1.25	1.60	2.01	2.37	3.15	----	----
10^4k_A/[B], s^{-1} M^{-2}	1.35	1.72	1.79	2.00	2.24	2.37	2.63	----	----
Cu(II)-[EDA][b], M	0.40	0.60	0.70	0.80	0.90	1.00	1.20	----	----
10^5k_A, s^{-1} M^{-1}	0.42	0.65	0.79	0.86	1.11	1.35	1.85	----	----
10^5k_A/[B], s^{-1} M^{-2}	1.05	1.08	1.13	1.08	1.23	1.35	1.54	----	----
[DMPA][a*], M	0.497	0.601	0.697	0.800	0.897	1.00	1.20	1.50	2.01
10^3k_A, s^{-1} M^{-1}	0.480	0.72	0.99	1.26	1.55	1.98	2.59	3.93	5.92
10^3k_A/[B], s^{-1} M^{-2}	0.976	1.20	1.42	1.57	1.73	1.98	2.16	2.62	2.94
[Fe(II)-DMPA][b], M	0.40	0.60	0.70	0.80	0.90	1.00	1.20	----	----
10^4k_A, s^{-1} M^{-1}	0.45	0.96	1.21	1.93	2.40	2.75	3.93	----	----
10^4k_A/[B], s^{-1} M^{-2}	1.12	1.60	1.73	2.41	2.67	2.75	3.27	----	----
Cu(II)-[DMPA][b],M	0.40	0.60	0.70	0.80	0.90	1.00	1.20	----	----
10^5k_A, s^{-1} M^{-1}	0.33	0.56	0.72	1.03	1.29	1.49	1.98	----	----
10^5k_A/[B], s^{-1} M^{-2}	0.82	0.93	1.03	1.29	1.43	1.49	1.65	----	----

[a][DNClB] = 5.0 x 10^{-4}M. [b][DNClB] = 5.1 x 10^{-4} M.
*data taken from reference 18.

Table 2: Reaction of 2,4-dinitrochlororobenzene, DNClB, with 1-(2-aminoethyl)-piperidine, 2-AEPip and histamine (His) and their respective complexes with Cu(II) and Fe(II) in toluene at 25.0 ± 0.2ºC. Second- (k_A), and third- (k_A/[B]) order rate coefficients are indicated.

[2-AEPip][a*], M	0.496	0.597	0.79	0.99	1.20	1.51	1.73	2.01
10^3k_A, s^{-1} M^{-1}	1.92	2.48	3.12	4.88	5.98	8.73	10.09	15.40
10^3k_A/[B], s^{-1} M^{-2}	3.87	4.15	3.95	4.88	4.98	5.78	6.30	7.66
[Fe(II)-2-AEPip][b], M	0.40	0.60	0.70	0.80	0.90	1.00	1.20	----
10^4k_A, s^{-1} M^{-1}	0.65	1.12	1.35	1.73	2.19	2.49	3.35	----
10^4k_A/[B], s^{-1} M^{-2}	1.62	1.86	1.93	2.16	2.43	2.49	2.79	----
[Cu(II)-2-AEPip][b], M	0.40	0.60	0.70	0.80	0.90	1.00	1.20	----
10^5k_A, s^{-1} M^{-1}	0.45	0.63	0.80	0.96	1.16	1.40	1.62	----
10^5k_A/[B], s^{-1} M^{-2}	1.12	1.05	1.14	1.20	1.29	1.40	1.35	----
[His][*], M	0.25	0.50	0.70	0.90	1.20	1.50	1.85	2.10
10^5k_A, s^{-1} M^{-1}	1.20	3.90	5.60	7.20	9.30	10.6	12.8	15.0
[Fe(II)-His][b], M	0.40	0.60	0.70	0.80	0.90	1.00	1.20	----
10^6k_A, s^{-1} M^{-1}	0.97	1.47	1.75	2.10	2.55	2.81	3.50	----
[Cu(II)-His][b], M	0.40	0.60	0.70	0.80	0.90	1.00	1.20	----
10^7k_A, s^{-1} M^{-1}	0.30	0.51	0.65	0,78	0.93	1.02	1.27	----

[a][DNClB] = 5.09 x 10^{-4}M. [b][DNClB] = 5.12 x 10^{-4}M.
*data taken from reference 18.

Assuming that the complexes are at least partially dissociated in solution, diverse species may be present in the reaction media. However, considering the different binding energy (E_b) per bond and per ligand calculated theoretically (Table 3), it can be inferred that the species present in solution that react with the substrate are the uncomplexed amines, which can undergo self-association forming dimers, taking into account that self-aggregation of the amines prevails in non-polar aprotic solvents [15], and that the metal amine complexes partially dissociated, formed with two or three amine molecules are non-nucleophilic entities (see below Scheme 1, eq. 1). As shown in Figures 2-4, the second-order rate coefficients k_A of the reactions of metal-EDA, 2-AEPip and DMPA complexes with DNClB in toluene show a quadratic dependence with the amine complex concentrations.

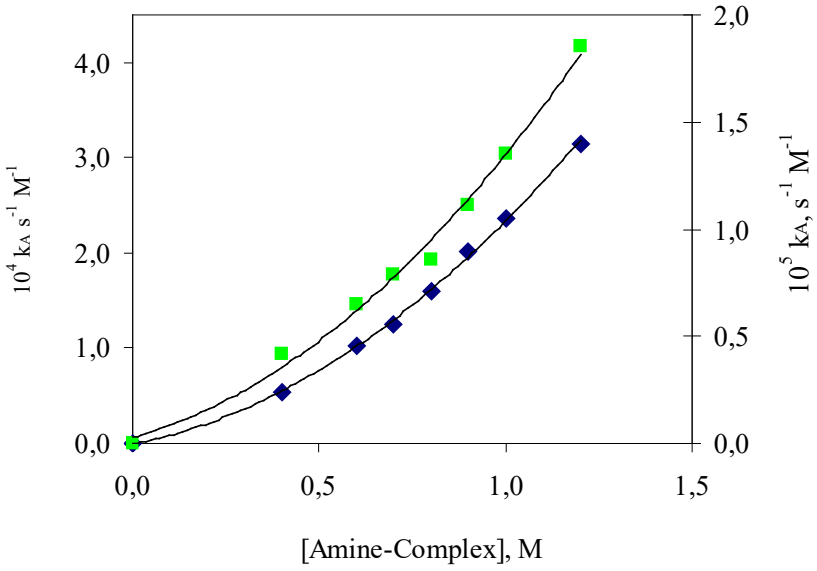

Figure 2: Second-order rate coefficients, k_A, for the reactions of 2,4- dinitrochlorobenzene (DNClB) with ■ EDA- Cu(II) complex (105 right Y-axis scale), and • EDA-Fe(II) (104 left Y-axis scale), in toluene at 25.0 ± 0.2 ºC, respectively, as a function of [amine-complex].

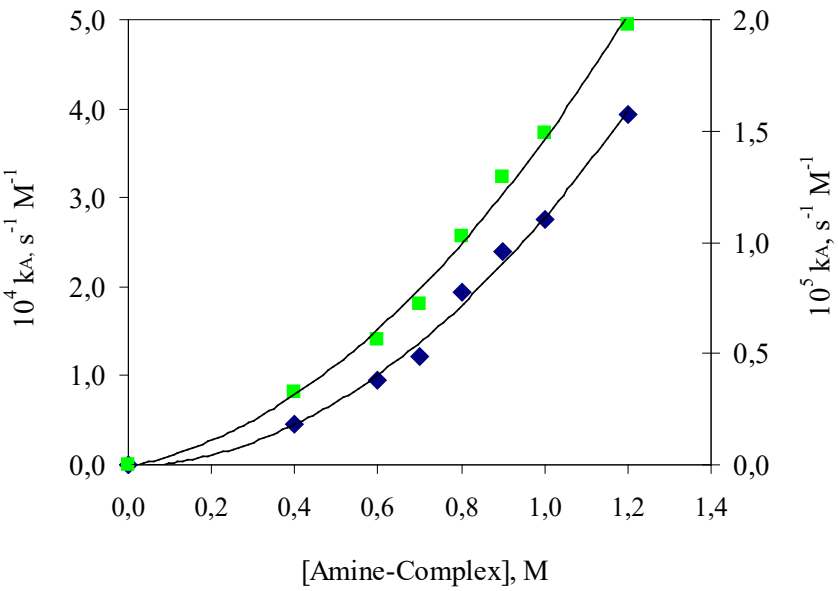

Figure 3: Second-order rate coefficients, k_A, for the reactions of 2,4- dinitrochlorobenzene (DNClB) with ♦ DMPA-Fe(II) (10^4 left Y-axis scale) and ■ DMPA-Cu(II) (10^5 right Y-axis scale) in toluene at 25.0 ± 0.2 ºC, respectively, as a function of [amine-complex].

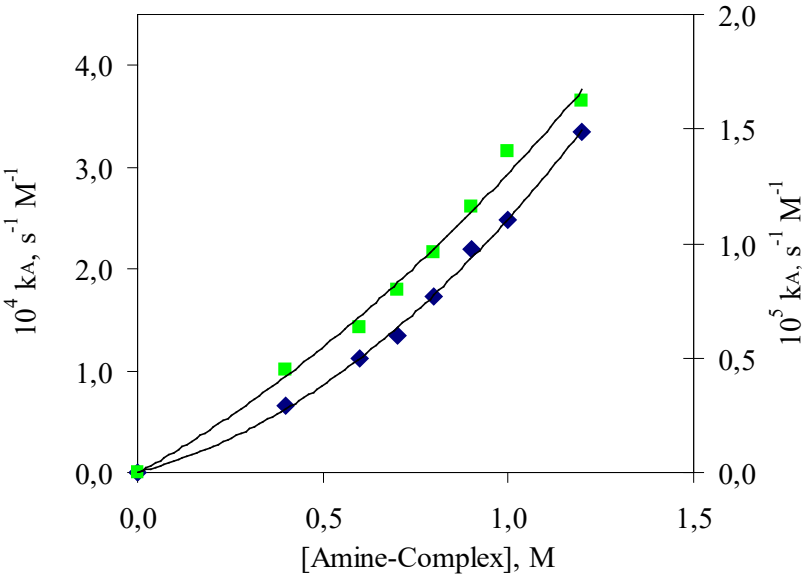

Figure 4: Second-order rate coefficients, k_A, for the reactions of 2,4- dinitrochlorobenzene (DNClB) with ■ 2-AEPip-Cu(II) (105 right Y-axis scale) and • 2-AEPip-Fe(II) (104 left Y-axis scale) in toluene at 25.0 ■ 0.2 ºC, respectively, as a function of [amine-complex].

For complexes formed with EDA, DMPA and 2-AEPip, at low concentration of metal-amine complexes, the kinetic behavior seems to be linear, however at higher concentrations an upward curvature is observed. In these Figures, different scales for the k_A values are used due to their different reactivity. Also, the third-order rate coefficients for these reactions show a straight

line (data not shown). These results are consistent with a third-order in the amine term in the kinetic law at high concentration complexes.

Regarding the self-aggregation and other non-covalent interactions that occur in solvents of low permittivity, the kinetic data shown in Figures 2-4 indicate that the predominant nucleophile is the dimer of the amine, and in these cases, a third order in amine concentration is obtained, giving an overall fourth-order kinetics. Application of the steady-state treatment to the whole mechanism gives an expression involving specific rate constant for each step and the association equilibrium constant for the nucleophile, K. Derivation of the complete expression and the limit situations that were evaluated are described in ref. 19. The simplified reaction scheme which includes the dissociation of the metal-amine complexes studied in this work, is shown in Scheme 1. The proposed mechanism does not preclude attack by the monomer, as shown in the step pathway depicted below:

$$(\text{Metal} \text{---} 3\text{NH}_2 \text{---} \text{R})_{\text{complex}} \overset{K_{dis}}{\rightleftharpoons} (\text{Metal} \text{---} 2\ \text{NH}_2 \text{---} \text{R})_{\text{complex}} + \text{NH}_2 \text{---} \text{R} \qquad (1)$$

$$2\ \text{RNH}_2 \rightleftharpoons \text{RNH}_2 \cdots\cdots \text{NH}_2\text{R} \qquad (2)$$

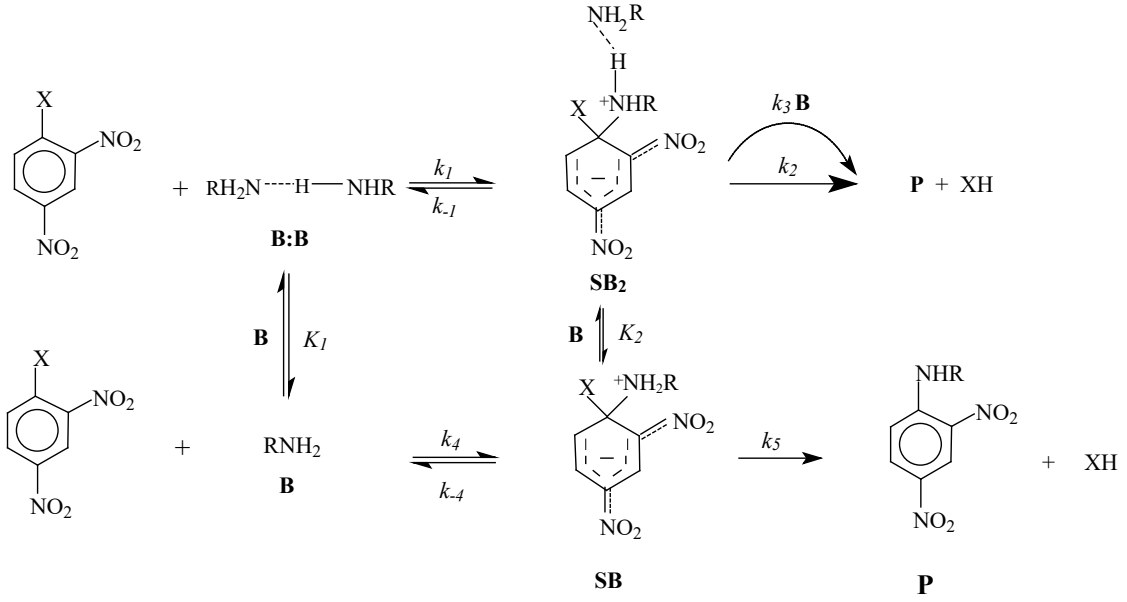

(3)

$$k_A = \frac{k_1 k_2 K[B] + k_1 k_3 K[B]^2}{k_{-1} + k_2 + k_3[B]} \qquad (4)$$

Scheme 1: Reaction for metal-amine complexes and EWG substrate of Dimer Nucleophile Mechanism by amine dimer and monomer amines and the corresponding kinetic expression for the reaction.

Eq. 1 of Scheme 1 represents the first dissociation equilibrium reaction of a amine-metal complex formed with three amine molecules, which liberates one amine molecule. Eq. 2 represents

the auto-association of the free amines that exists in solution, through H-bonding. While the complex with two amine molecules could further dissociate, the first dissociation of a single amine molecule appears to be the most likely, according to the calculated binding energies (E_b/N) of each ligand in the complex (see Table 3).

By the contrary, a linear dependency is observed in the case of histamine.

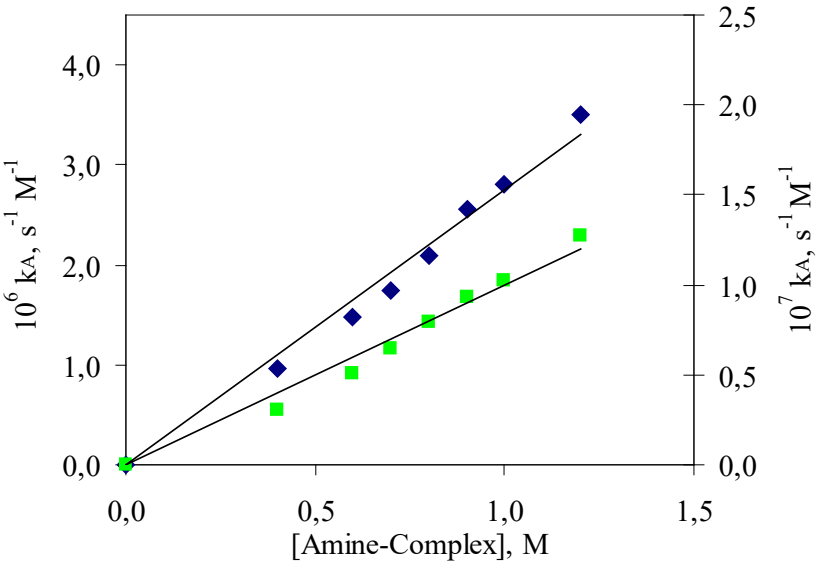

Figure 5: Second-order rate coefficients, k_A, for the reactions of 2,4- dinitrochlorobenzene (DNClB) with ■ histamine-Cu(II) (10^7 right Y-axis scale) and ♦ histamine-Fe(II) (10^6 left Y-axis scale) in toluene at 25.0 ± 0.2ºC as a function of [amine-complex].

Figure 5 shows the kinetic behavior of histamine-metal(II) complexes with DNClB in toluene, in presence of variable amounts of the nucleophile. The second-order rate coefficients increase steadily with [histamine-complex] (eq. 5); the plot of k_A vs. nucleophile is a straight line with a null intercept and a correlation coefficient of R2 = 0.984 for histamine-Fe(II) complex and R^2 = 0.977 for Cu(II). In histamine, an intramolecular hydrogen bond prevents the formation of intermolecular dimers (Scheme 2) and the classical mechanism of base-catalyzed decomposition of SB (eq. 5) is obeyed [18]. The null intercept indicates that the spontaneous decomposition of SB is negligible. The proposed histamine structure that should act as a nucleophile is shown below, where a six-membered ring is formed by an intramolecular hydrogen bond:

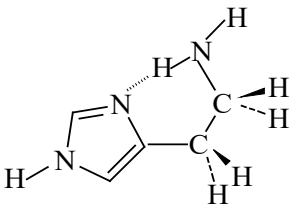

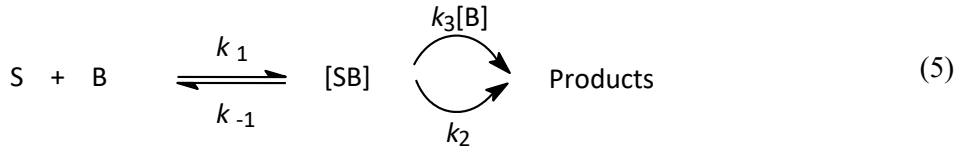

(5)

Scheme 2: Intramolecular hydrogen bond established in histamine in aprotic solvents and the reaction scheme.

Considering the self-aggregation of amines in aprotic solvents and the different reaction rates obtained with the different metal-amine complexes, these results suggest distinct stabilities for each complex, attributed to stereo-electronic and chelate effects. Differences in the stability of the complexes, can also be presumed from the theoretical results (see below).

Therefore, the different stability of the metal-amine complexes appears as the main determinant factor controlling the nucleophilic attack process in these ANS reactions. The observed kinetic results do not provide evidence that the metal-amine complexes react as a nucleophilic entity. On the contrary, they seem to dissociate prior to react rendering results consistent with a "dimer nucleophile" mechanism for ANS. The structures of these amines may allow the formation of intra- or intermolecular H-bond in the complex structure influencing its stabilization energy, serving as an indicator of the gradual change of strength and reactivity of many types of complexes [37].

In the present study, the reaction rates of the complexes are one and two orders of magnitude lower with respect to uncomplexed amines [18]. Reactions with Cu(II) complexes are slower than those obtained with Fe(II) complexes, consistently with the relative stabilities (see Tables 1 and 2). In summary, the reactivity trends are controlled by the lability of the different complexes, as has been recently reported [38].

3.2. Theoretical results

Figure 6 (a) to (h) shows the most stable complexes (greater negative ΔE_{form}) of EDA, DMPA, histamine and 2-AEPip with Fe(II) and Cu(II). All of them are those with a coordination number of three. The coordinated covalent bonds and H-bonds found by the AIM method are shown in dashed lines.

In both EDA-Fe(II) and histamine-Fe (II), six N atoms form coordinated bonds to the Fe ion, leading to an approximately symmetrical tetragonal geometry. For EDA-Fe(II), the N-Fe-N dihedral angles for the same ligand are ≈ 75º and in histamine-Fe, ≈ 88º.

In all 3:1 amine-Cu(II) complexes and in 2-AEPip-Fe(II) and DMPA-Fe(II) 3:1 complexes, only five N atoms form coordinated bonds with the metal ions, and the remaining one forms a hydrogen bond. This could be due to steric effects preventing all molecules from fully approaching the metal ion and to the stabilization effect of the H-bond.

In EDA-Cu(II) the geometry is nearly square pyramidal, with both dihedral and out-of-plane angles ≈ 99º maximum. So it is in histamine-Cu(II), with dihedrals of ≈ 88º and out-of planes of ≈ 104º maximum, and in 2-AEPip-Cu(II), with dihedrals of ≈ 83º to ≈ 96º and an out-of plane of ≈ 105º maximum. In DMPA-Cu(II), the geometry is trigonal bipyramidal, with dihedral angles ≈ 109º to 127º for the base of the pyramid and out-of planes angles of ≈ 83º minimum. DMPA-Fe(II) has the same geometry, with dihedral angles of ≈ 112º to 129º and out-of plane angles of ≈ 84º minimum. So does 2-AEPip Fe(II), with dihedrals of ≈ 108º to 137º and out-of-planes of ≈ 79º minimum.

The coordination numbers and geometries found are consistent with previous studies on Cu(II) [33b] and Fe(II) [33a] complexes, which also found five or six bonds, four of them planar and the other or others on a perpendicular axis.

In all cases of the intra- or intermolecular H bonds formed, the proton donor is a primary nitrogen which is also engaged in a coordinated bond to the metal atom. In both DMPA complexes, H bonds are intramolecular and the acceptor is a tertiary nitrogen. The same H-bonding pattern was found in a previous study of the uncomplexed amines [22]. 2-AEPip-Fe(II) has an intramolecular H-bond between a primary and a tertiary nitrogen, which was not seen in the mentioned study. In the remaining complexes, H-bonds are intermolecular, and in 2-AEPip-Cu(II), the proton acceptor is a tertiary N, while in EDA-Cu(II) and histamine-Cu(II), it is a primary N.

Table 3 shows characteristics of complexes of Fe(II) and Cu(II) with EDA, DMPA, histamine and 2-AEPip, with a number of amine ligands (N_l) of one to three. These characteristics are: the total number of coordinated covalent bonds (N_b) between amine N atoms and the metal atom, (as shown in Figure 5), the binding energy (E_b), the binding energy per N-metal bond (E_b/N_b), the binding energy per ligand (E_b/N_l), and the complex formation energy (ΔE_{form}), all calculated as described in the Computational Procedure section.

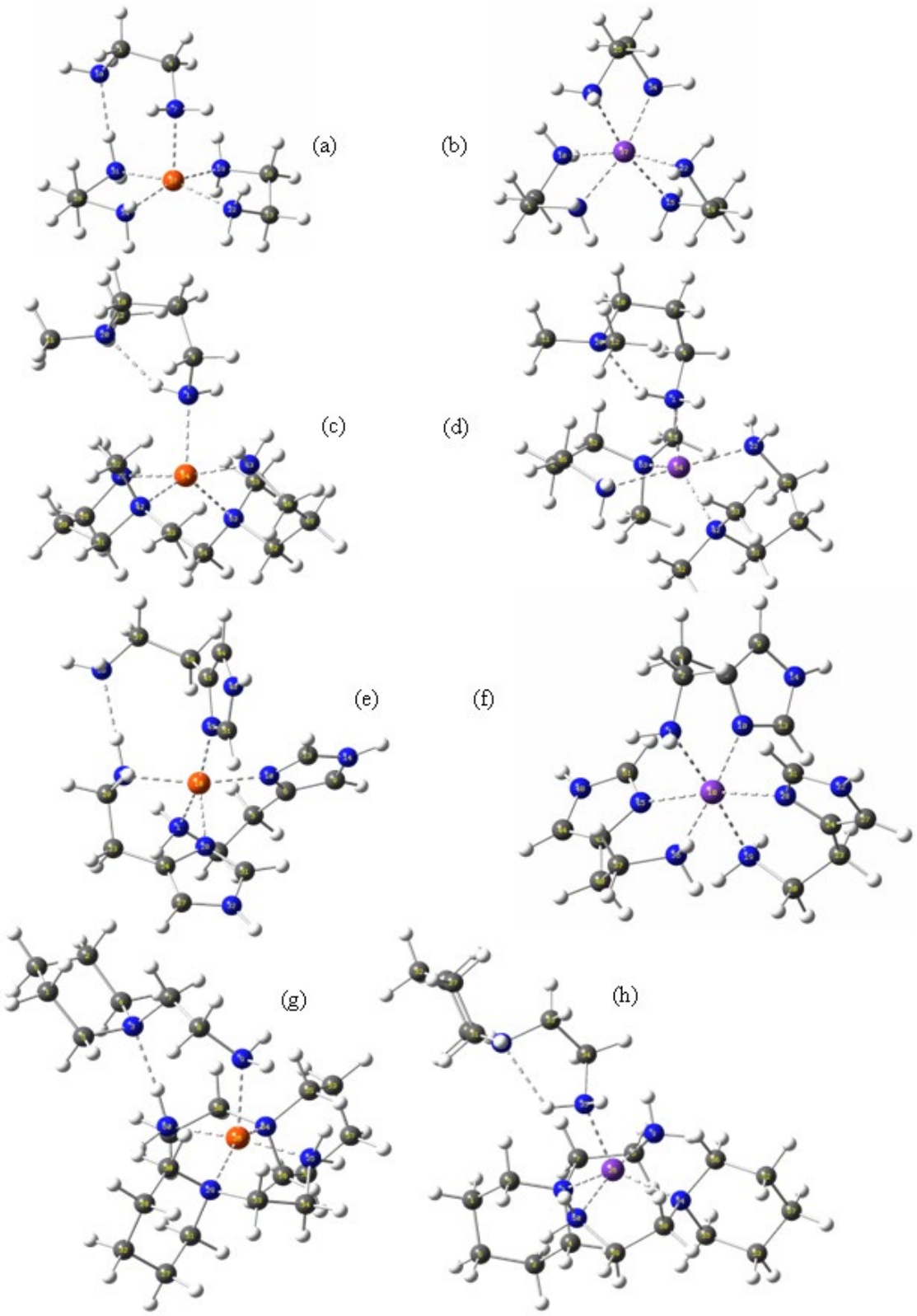

Figure 6: Calculated structure and bonding of 3:1 amine-metal complexes. (a) EDA-Cu(II); (b) EDA-Fe(II); (c) DMPA-Cu(II); (d) DMPA-Fe(II); (e) Histamine-Cu(II); (f) Histamine-Fe(II); (g) 2-AEPip-Cu(II); (h) 2-AEPip-Fe(II).

Note: Grey: C; white: H; blue: N; purple: Fe; red: Cu. Dashed line: H-bond or coordinated bond.

Table 3: Number of amine ligands, number of N-metal bonds, formation and binding energies (kcal/mol), for complexes of Cu(II) and Fe(II) with 1 to 3 EDA, DMPA, histamine and 2-AEPip ligands. See abbreviations in the text.

Amine-Fe(II)									
	N_l	N_b	E_b	E_b/N_b	E_b/N_l	ΔE_1	ΔE_2	ΔE_3	ΔE_{form}
EDA	**1**	2	-207.8	-103.9	-207.8	199.8			-199.8
	2	4	-328.4	-82.1	-164.2	114.4	314.2		-314.2
	3	6	-379.1	-63.2	-126.4	46.9	161.3	361.1	-361.1
DMPA	**1**	2	-237.2	-118.6	-237.2	227.7			-227.7
	2	4	-339.9	-85.0	-170.0	92.4	320.2		-320.2
	3	5	-382.8	-76.6	-127.6	38.0	130.4	358.1	-358.1
Histamine	**1**	2	-249.6	-124.8	-249.6	238.7			-238.7
	2	4	-372.3	-93.1	-186.2	117.1	355.7		-355.7
	3	6	-415.1	-69.2	-138.4	37.6	154.6	393.3	-393.3
2-AEPip	**1**	2	-237.7	-118.9	-237.7	226.6			-226.6
	2	4	-345.6	-86.4	-172.8	95.8	322.5		-322.5
	3	5	-380.1	-76.0	-126.7	31.4	127.2	353.9	-353.9
Amine-Cu(II)									
	N_l	N_b	E_b	E_b/N_b	E_b/N_l	ΔE_1	ΔE_2	ΔE_3	ΔE_{form}
EDA	**1**	2	-266.4	-133.2	-266.4	257.1			-257.1
	2	4	-393.3	-98.3	-196.6	120.5	377.6		-377.6
	3	5	-429.0	-85.8	-143.0	30.2	150.7	407.8	-407.8
DMPA	**1**	1	-316.3	-316.3	-316.3	307.3			-307.3
	2	4	-400.6	-100.2	-200.3	79.1	386.4		-386.4
	3	5	-425.5	-85.1	-141.8	25.2	104.3	411.6	-411.6
Histamine	**1**	2	-304.9	-152.5	-304.9	295.1			-295.1
	2	4	-427.0	-106.8	-213.5	112.3	407.4		-407.4
	3	5	-462.6	-92.5	-154.2	34.4	146.7	441.8	-441.8
2-AEPip	**1**	1	-309.4	-309.4	-309.4	298.7			-298.7
	2	4	-402.1	-100.5	-201.0	84.0	382.7		-382.7
	3	5	-440.1	-88.0	-146.7	26.5	110.5	409.2	-409.2

It is observed that ΔE_{form} and E_b are bigger (more negative) for the 3:1 complexes. This indicates that 3:1 complexes are more stable and most likely to be present in solution, provided there are enough available amines. This agrees with the Yoe-Jones [29] experimental results. Cu(II) complexes are also more stable than Fe(II) complexes in all cases. On the other hand, the binding energies per bond E_b/N_b and per ligand E_b/N_l decrease (in absolute values) as the number of bonds and ligand number increases. This could be due to steric effects, and indicates the 3:1 complexes are the most labile and reactive.

In all cases, ΔE_1 is the lowest compared to ΔE_2 and ΔE_3, and the lowest ΔE_1 is by far the one corresponding to a 3:1 complex. This indicates that the prevalent mechanism for the reactions starts with the dissociation of one amine from a 3:1 complex, and if a dimer is formed from free

amines, it is most likely to be with the first amine dissociated from another 3:1 complex. All this supports the proposed equations (1) and (2) from Scheme 1.

Cu(II) complexes have greater binding energies per amine than the corresponding Fe(II) ones, so they are less labile and reactive, consistently with experimental results that indicate that the reactions with Cu(II) complexes are slower than those with Fe(II) complexes. Nevertheless, it is noticeable that the overall energy differential for reactions (1) and (1) + (2) is smaller for Cu(II) complexes than for Fe(II) complexes.

The relative E_b/N_l for the different amine 3:1 complexes are: histamine >> DMPA ≥ 2-(AEPip) ≥ EDA for the Fe complexes, and histamine >> 2-AEPip > EDA > DMPA for Cu complexes. Histamine is the least labile and, therefore, the least reactive of all them, while the labilities of the other amine complexes are similar.

In Table 4, we show the covalent coordinated N-metal and hydrogen bonds present in the 3:1 complexes of histamine and 2-AEPip, having selected them as examples. The columns "Atom 1" and "Atom 2" show the bonded atoms and the bond type (see Figure 6). The calculated properties are: the relevant interatomic distance d, the angle α (in the case of H-bonds); AIM results for the bond critical point: electron density ρ, its Laplacian $\nabla^2(\rho)$, and its ellipticity ε; and the charge transference Δq of the bonded atoms, as described in the theoretical method section. Averages include the N-metal bonds only. For the complexes shown in the table, bond strengths, as inferred from the average bond distance, electron density at the BCP and charge transfer of the metal atom, are stronger for Cu complexes, showing the same trend in lability as the one inferred from the E_b/N_l value.

4. Conclusions

The present paper describes the kinetic determinations for ANS carried out with 1-chloro-2,4-dinitrobenzene, (DNClB), a good nucleofugue substrate, and several bifunctional amine coordination complexes with Cu(II) and Fe(II), in toluene. The amines selected as ligands were ethylenediamine (EDA), N,N-dimethyl propylamine (DMPA), histamine and 1-(2-aminoethyl)piperidine, 2-AEPip, because of their characteristics of bi-dentate ligands and the possible size of the metalo-cycle formed.

Table 4: N-metal coordinated bond characteristics. Bonded atoms, bond distance (Å), bond angle, electron density and its Laplacian at the BCP (au), ellipticity, and charge transfer (au) of the atoms. See abbreviations in the text.

atom 1...	...atom 2	d	α	ρ	$\nabla^2(\rho)$	ε	Δq 1	Δq 2
				Histamine-Fe(II)				
N1...	...Fe	2.294	-	0.04630	0.22044	0.495	-0.06643	-0.60252
N10...	...Fe	2.246	-	0.04985	0.24984	0.445	-0.13936	"
N19…	...Fe	2.296	-	0.04620	0.21951	0.508	-0.09042	"
N28…	...Fe	2.222	-	0.05393	0.24015	0.095	-0.15646	"
N36…	...Fe	2.318	-	0.04424	0.20869	0.552	-0.10294	"
N45…	...Fe	2.226	-	0.05353	0.23677	0.038	-0.16165	"
average		2.267		0.04901				
				Histamine-Cu(II)				
N1...	...Cu	2.124	-	0.06531	0.30644	0.022	-0.08142	-0.85221
N10...	...Cu	2.081	-	0.06935	0.34723	0.029	-0.14300	"
N19…	...Cu	2.095	-	0.07065	0.32166	0.018	-0.12443	"
N28…	...Cu	2.256	-	0.04741	0.23568	0.057	-0.15413	"
N45…	...Cu	2.098	-	0.06686	0.33444	0.077	-0.11363	"
N19-H...	...N36	1.959	176.5	0.03175	0.07933	0.006	-0.12443	-0.05705
average		2.131		0.06392				
				2-AEPip-Fe(II)				
N3...	...Fe	2.235	-	0.05734	0.23102	0.085	-0.14183	-0.65984
N9...	...Fe	2.259	-	0.05121	0.23932	0.434	-0.09320	"
N35…	...Fe	2.184	-	0.06027	0.27733	0.396	-0.11773	"
N54…	...Fe	2.241	-	0.05692	0.21930	0.044	-0.16076	"
N60…	...Fe	2.267	-	0.05006	0.23659	0.518	-0.09530	"
N29...	...H-N35	2.154	118.7	0.02444	0.07690	0.483	-0.02548	-0.11773
average		2.237		0.05516				
				2-AEPip-Cu(II)				
N9...	...Cu	2.393	-	0.03764	0.14861	0.028	-0.05443	-0.94867
N29…	...Cu	2.236	-	0.05393	0.22606	0.014	-0.08260	"
N35…	...Cu	2.086	-	0.07063	0.34286	0.017	-0.06654	"
N54…	...Cu	2.238	-	0.05381	0.22306	0.007	-0.09276	"
N60…	...Cu	2.026	-	0.08281	0.37628	0.009	-0.12789	"
N60-H…	...N3	1.859	175.0	0.04186	0.08409	0.010	-0.12789	-0.06871
average		2.196		0.05976				

DFT calculations were performed to determine the geometries and energies of the complexes, considering one to three ligands. Results indicate that the most stable complexes are those with three amine molecules, while those with Cu(II) are more stable than those of Fe(II) in all cases. The binding energy of the amine-complexes, which correlates with other bond strength indicators, was found to be determinant in the reaction rate, and it correlates satisfactorily with the order of reactivity observed in the kinetic experiments, which indicate that histamine complexes are least reactive, and Cu(II) complexes are less reactive than their Fe(II) counterparts. The studied

amine structures were quantum-chemically calculated in previous works and in the present study several H-bonds pattern were found in the complexes as well.

Finally, we believe that other effects that influence the different lability of complexes are the stereo electronic and chelating effects of the different ligands, both attributed to the structure of each amine, and to the existence of intra- or intermolecular hydrogen bonds.

Regarding the biological interest in the mechanism of action of metallo species chelated to peptides and other amine containing groups, if the studied system is considered as a simplified model, it can be concluded that the amine-metal complexes should partly dissociate prior to reaction with a potential biological site in a lipophilic media.

Acknowledgements

Financial help from the Universidad Nacional del Comahue (grants no. I221 and I238-UNCo) and from Research and Development Institute of Process Engineering, Biotechnology and Alternatives Energies (PROBIEN), CONICET–Universidad Nacional del Comahue is gratefully acknowledged.

References

(1) Abdel-Mohsen Ebain Nassr, L. *Int. J. Chem. Kinet.* 2010, 42, 372-379 and referentes therein.

(2) Muñoz, V. A.; Ferrari, G. B.; Sancho, M. I.; Montaña, M. P. *J. Chem. Eng. Data* 2016, 61, 987-995.

(3) El-Subruit, G. M.; Younes, G. O.; Zeitouni, F. S.; Amira, M. F. *Int. J. Chem. Kinet*. 2008, 40, 416-422.

(4) Escudero, D.; González, L. J. *Chem. Theory Comput*. 2012, 8, 203-213.

(5) Shubina, V. S.; Kozina, V. I.; Shatalin, Yu. V. *Russian Journal of Bioorganic Chemistry* 2017, 43, 463-470.

(6) Shehata, A. K.; Fathalla, M.; Header, H. M. A.; Hamed, E. A. *Int. J. Chem. Kinet*. 2012, 44, 27-40.

(7) von Zelewsky, A. *Stereochemistry of Coordination Compounds*, John Wiley, Chichester, England, 1995.

(8) Sivaraj, K.; Elango, K. P. *J. Solution Chem*. 2010, 39, 1681-1697.

(9) Nie, H.-J.; Yang, W.-W.; Zheng, R.-H.; Shi, Q.; Chen, H.; Yao, J.; Zhong, Y.-W. *Inorg. Chem.*, 2015, 54, 1272-1282.

(10) Nelson, D. L.; Cox, M.; Lehninger *Principles of Biochemistry*, 7thed., W. H. Freeman & Co (Sd), USA, 2017.

(11) Campbell, N. R.; Hasinoff, B. *British Journal of Clinical Pharmacology* 1991, 31, 251-255.

(13) Al Zoubi, W.; Al-Hamdani, A. A. S.; Ahmed, S. D.; Ko, Y. G. *J Phys Org Chem*. 2018, 31, e3752. https://doi.org/10.1002/poc.3752.

(14) Ejidike, I. P.; Ajibade, P. A. *Molecules* 2015, 20, 9788-9802.

(15) Nudelman, N. S.; *ANS Reactions of Amines in Aprotic Solvents in The Chemistry of Amino, Nitroso, Nitro and Related Groups Supplement F2*, Eds. S. Patai, John Wiley & Sons, Ltd, London, UK, 1996.

(16) a) Alvaro, C. E. S.; Nudelman, N. S.; *ARKIVOC*, 2003, 10, 95-106. b) Nudelman, N. S.; Alvaro, C. E. S.; Yankelevich, J. S. *J. Chem. Soc. Perkin Trans*. 2, 1997, 2125-2130.

(17) a) Alvaro, C. E. S.; Bergero, F. D.; Bolcic, F. M.; Ramos, S. B.; Nudelman, N. S. *J. Phys. Org. Chem.* 2016, 29, 565-573. b) Alvaro, C. E. S.; Nudelman, N. S.; *Trends in Org. Chem*. 2011, 15, 95-107, and references therein.

(18) Alvaro, C. E. S.; Nudelman N. S. *Phys. Chem. Special Issue: Chemical Kinetics* 2013, 3, 39-47.

(19) Alvaro, C. E. S.; Nudelman, N. S., *Int. J. Chem. Kinet.* 2010, 42, 735-742.

(20) Nudelman, N. S., Alvaro, C. E. S. *J. Phys. Org. Chem.* 2011, 24, 1067-1071.

(21) Bergero, F. D.; Alvaro, C. E. S.; Nudelman, N. S., Ramos de Debiaggi, S. *J. Mol. Struct. (Theochem)* 2009, 896, 18-24.

(22) Bergero, F. D.; Alvaro, C. E. S.; Nudelman, N. S.; Ramos de Debiaggi, S. J. *Argent. Chem. Soc*. 2013, 100, 35-47.

(23) Parr, R. G.; Yang, D.; *Density- Functional Theory of Atoms and Molecules*, Ed. Oxford University Press, New York, 1989.

(24) a) Becke, A. D. *J. Chem. Phys*. 1993, 98, 5648.5652. b) Lee, C.; Yang, C. W.; Parr, R. G. *Phys. Rev. B*, 1988, 37, 785-793.

(25) Schwöbel, J.; Ebert, R.-U.; Kühne, R.; Schürmann, G. *J. Chem. Inf. Model*. 2009, 49, 956-962.

(26) Ribeiro, R. F.; Marenich, A. V.; Cramer, C. J.; Truhlar, D. G. *Phys. Chem. Chem. Phys*. 2011, 13, 10908-10922.

(27) Bader, R. F. W. *Chem. Rev.* 1991, 91, 893-928.

(28) Shaker, A. M.; Abdel-Mohsen Ebain Nassr, L.; Adam, M. S. S.; Mohamed, I. M. A. *Russian Journal of General Chemistry*, 2014, 84, 2037–2042.

(29) Yoe, J. H.; Jones, A. L. *Ind. Eng. Chem. Anal*. Ed. 1944, 16, 111–115.

(30) Stewart, J. P. *J. Mol. Model*. 2007, 13, 1173-1213.

(31) Kanal, Y.; Keith, J.; Hutchison, G., *Int. J. Quantum Chem*. 2018, 118, (5), e25512.

(32) Frisch, M. J.; Trucks, G. W.; Schlegel, H. B.; Scuseria, G. E.; Robb, M. A.; Cheeseman, J. R.; Scalmani, G.; Barone, V.; Mennucci, B.; Petersson, G. A. et al. Gaussian 09, Revision A.01, Gaussian, Inc., Wallingford CT, 2009.

(33) a) Scherlis, D. A.; Estrin, D.A., *Int. J. Quantum Chem.* 2002, 87, 158-188, and references therein. b) Conry, R. R. "Copper: Inorganic & Coordination Chemistry". *Encyclopedia of Inorganic Chemistry*, First Edition. Wiley, 2006.

(34) a) Feller, D. J. Comp. Chem. 1996, 17, 1571-1586. b) Schuchardt, K. L.; Didier, B. T.; Elsethagen, T.; Sun, L.; Gurumoorthi, V.; Chase, J.; Li, J.; Windus, T. L. *J. Chem. Inf. Model* 2007, 47, 1045-1052.

(35) Boys, S. F.; Bernardi, F. *Mol. Phys.* 1970, 19, 553-556.

(36) Lu, T.; Chen, F. Multiwfn: A multifunctional wavefunction analyzer. *J. Comput. Chem.* 2012, 33, 580-592.

(37) Parthasarathi, R.; Subramanian, V.; Sathyamurthy, N. *J. Phys. Chem. A* 2006, 110, 3349-3351.

(38) Reiners, M.; Maekawa, M.; Daniliuc, C. G.; Freytag, M.; Jones, P. G.; White, P. S.; Hohenberger, J.; Sutter, J.; Meyer, K.; Maron, L.; Walter, M. D. *Chem. Sci.* 2017, 8, 4108-4122.

Anales de la Asociación Química Argentina

VIBRATIONAL SPECTRA OF TWO BISMUTH (III) OXALATES: $Bi(OH)C_2O_4$ and $Bi_2(C_2O_4)_3{\cdot}7H_2O$

Ana C. González-Baró, Vicente L. Barone and Enrique J. Baran*

Centro de Química Inorgánica (CEQUINOR, CONICET/UNLP), Facultad de Ciencias Exactas, Universidad Nacional de La Plata, Bvd.120 N° 1465, 1900-La Plata, Argentina.

Autor Corresponsal E-mail:baran@quimica.unlp.edu.ar

Resumen

Se sintetizaron los dos oxalatos de Bi(III) del título y se registraron sus espectros de infrarrojo y Raman, los que resultaron ser bastante similares en su forma y ordenamiento espectral. Los espectros del $Bi(OH)C_2O_4$ resultaron consistentes con sus peculiaridades estructurales conocidas. En el caso del $Bi_2(C_2O_4)_3{\cdot}7H2O$ el análisis espectroscópico está de acuerdo con la presencia de grupos oxalato tetradentados fuertemente distorsionados, que generan un ordenamiento estructural tridimensional muy complejo, similar a los encontrados en los dos hidratos relacionados de estructuras conocidas, esto es $Bi_2(C_2O_4)_3{\cdot}6H_2O$ y $Bi_2(C_2O_4)_3{\cdot}8H_2O$.

Abstract

The two Bi(III) oxalates of the title were synthesized. Their infrared and Raman spectra were recorded and showed relatively similar spectral patterns. The spectra of $Bi(OH)C_2O_4$ are consistent with their known structural peculiarities. In the case of $Bi_2(C_2O_4)_3{\cdot}7H_2O$ the spectroscopic analysis is in agreement with presence of highly distorted tetradentate oxalate groups, generating a complex three-dimensional structural arrangement similar to those found in the two related hydrates of known structures, i. e. $Bi_2(C_2O_4)_3{\cdot}6H_2O$ and $Bi_2(C_2O_4)_3{\cdot}8H_2O$.

Palabras clave: Oxalatos de bismuto(III); espectros de IR y Raman; comportamiento vibracional; características estructurales.

Keywords: Bismuth(III) oxalates; IR and Raman spectra; vibrational behavior; structural characteristics.

1. Introduction

As a continuation of our spectroscopic studies of heavy metal oxalates [1-6] we have now investigated the vibrational spectroscopic behavior of two Bi(III) oxalates, namely $Bi(OH)C_2O_4$ and $Bi_2(C_2O_4)_3 \cdot 7H_2O$.

Although different Bi(III) oxalates have been reported in the past, information on their chemical and structural properties remains relatively scarce [7]. However, on the other hand, in recent years there is a growing interest not only in bismuth oxalates themselves, but also in mixed metal oxalates containing bismuth, as precursors for the synthesis of catalysts, ferroelectrics, and high Tc-superconductors [8]. In this context, $Bi(OH)C_2O_4$ is also considered a novel and interesting type of photocatalytic material [8,9]. Therefore, a deeper characterization of this type of materials seems timely and highly desirable.

2. Materials and Methods

2.1. Synthesis of the compounds

Bismuth nitrate pentahydrate was supplied by Aldrich (St. Louis, Mo., USA), while all the other reagents used were from Merck (Darmstadt, Germany), analytical grade, and were used as purchased.

The two Bi(III) oxalates were prepared using known synthetic procedures [8,10] with slight modifications. Bismuth nitrate (0.2M) in HNO_3 (1M) and aqueous oxalic acid (0.3M) solutions were the starting reagents. The syntheses of both oxalates were performed as follows:

a) $Bi(OH)C_2O_4$. To 100 mL of distilled water at room temperature, 60 mL of the Bi(III) solution and 30 mL of the oxalic acid solution were added dropwise, under constant stirring. The pH of the reaction mixture was continuously adjusted to the value 6–7, with ammonia. Once the reaction was complete, the mixture was stirred for another hour. The white precipitate was filtered using a G3 glass fritted funnel, washed several times with ethanol and finally dried under vacuum over H_2SO_4.

b) $Bi_2(C_2O_4)_3 \cdot 7H_2O$. This oxalate was prepared as above, using 60 mL of the Bi(III) solution and 50 mL of the oxalic acid solution. During the reaction, the pH value was maintained at 0-1, by the addition of HCl. Aging, filtration, washing and drying were also the same as above.

2.2. Characterization of the compounds

The two oxalates obtained were characterized by X-ray powder diffractometry [8,10], with a Rigaku-Denki diffractometer and monochromatic (Ni-filtered) Cu-Kα radiation (λ = 1.5418 Å), using NaCl as an external calibration standard. The analysis of the obtained powder diagrams, shows the presence of totally pure samples without traces of impurities or any additional phases.

2.3. Vibrational spectra

The infrared spectra, in the spectral range between 4000 and 400 cm^{-1}, were recorded with an FTIR-Bruker-EQUINOX-55 spectrophotometer, using the KBr pellet technique. Raman spectra were obtained in the same spectral range with a Thermo Scientific DXR Raman microscope, using the 532 nm line of a Thermo Scientific solid-state laser diode pump for excitation.

3. Results and Discussion

3.1. Structural characteristics of the complexes

The structure of $Bi(OH)C_2O_4$ was solved by Rivenet et al.[11]; it belongs to the orthorhombic space group Pnma with Z = 4 formulas in the unit cell. On the other hand, the structure of $Bi_2(C_2O_4)_3{\cdot}7H_2O$ remains unknown, although some years ago those of some other similar hydrates were reported, namely $Bi_2(C_2O_4)_3{\cdot}6H_2O$ and $Bi_2(C_2O_4)_3{\cdot}8H_2O$ [7].

In $Bi(OH)C_2O_4$ the Bi(III) coordination is a BiO_6E pentagonal bipyramid with the lone pair E sitting on an axial vertex. The opposite axial vertex is occupied by a hydroxyl O-atom, which is also an equatorial corner of a neighboring BiO_6E bipyramid. Oxalate groups act as bidentate ligands. The BiO_6E moieties are connected via shared oxygen hydroxyl atoms leading to $[BiO_5E]$ zig-zag chains that run down the [100] direction. These chains are aligned on a sheet parallel to the (010) plane, through oxalate moieties that now act as tetradentate units, and are further connected via "secondary" oxalate bonds to form a three-dimensional arrangement [11].

In the cases of $Bi_2(C_2O_4)_3{\cdot}6H_2O$ and $Bi_2(C_2O_4)_3{\cdot}8H_2O$, the coordination of Bi(III) is BiO_9 and consists of four oxalate O-atoms of two different oxalate anions, which act as tetradentate ligands, two O-atoms from water molecules and three O-atoms from vicinal oxalate groups, generating a complex three dimensional set. It can be speculated that in the case of $Bi_2(C_2O_4)_3{\cdot}7H_2O$ now investigated a similar structural arrangement may be present.

3.2. Vibrational spectra

In their general structure and appearance, the FTIR and FT-Raman spectra of both compounds are not very different, suggesting the presence of similar overall binding characteristics. On the other hand, the IR spectra closely resemble those recently published by Roumanille et al.[8], but show an appreciably better resolution in our cases and also some aspects of the proposed assignments are not coincident.

3.2.1. $Bi(OH)C_2O_4$

The FTIR and FT-Raman spectra in the spectral range between 4000 and 400 cm^{-1} are shown in Figure 1 and the proposed assignment is presented in Table 1, and is briefly commented as follows:

- The stretching vibration of the OH-group is found at 3390 cm^{-1} in the infrared spectrum and was not observed in the Raman spectrum.

- Weak combinational modes found slightly above 2900 cm^{-1} surely originated from combinations of stretching vibrations of the oxalate anions.

- Both, the ν_{as} and ν_s vibrations, of the oxalate moieties are found at lower energies than those measured in other crystalline oxalates coordinated in a tetradentate fashion to the metal cations (for example, in $MgC_2O_4{\cdot}2H_2O$ [12] or in the dihydrated oxalates of Co, Ni and Zn [13]). This decrease in energy probably originates from the fact that, in the present case, the oxalate ligand not only coordinates simultaneously with two different Bi(III) centers, but its O-atoms are also involved in secondary bondings to vicinal Bi(III) centers, lowering the strength of the C-O bonds.

- Another interesting difference, probably related to the same binding characteristics, is the fact that in the case of complexes derived from tetradentate coordinated oxalate, one of the vibrations assigned to ν_s(C-O) + δ(OCO) looks like as a well-resolved doublet [12-14], while in the present case it appears as a unique feature.

- We have also tried to find any spectroscopic evidence of motions involving the Bi-OH moiety (i.e. a ν(Bi-O) and/or a δ(Bi-OH) vibration). In this context, it is interesting to mention that the stretching vibrations of the Bi=O bond, for example in bismuth oxohalides, XBiO [15] or in $(BiO)_2CO_3{\cdot}0.5H_2O$ [16] are around to 500 cm^{-1}. Therefore, a vibration associated with ν(Bi-O) may be expected at energies lower than this value. The possible location of a δ(Bi-OH) vibration is more difficult to predict.

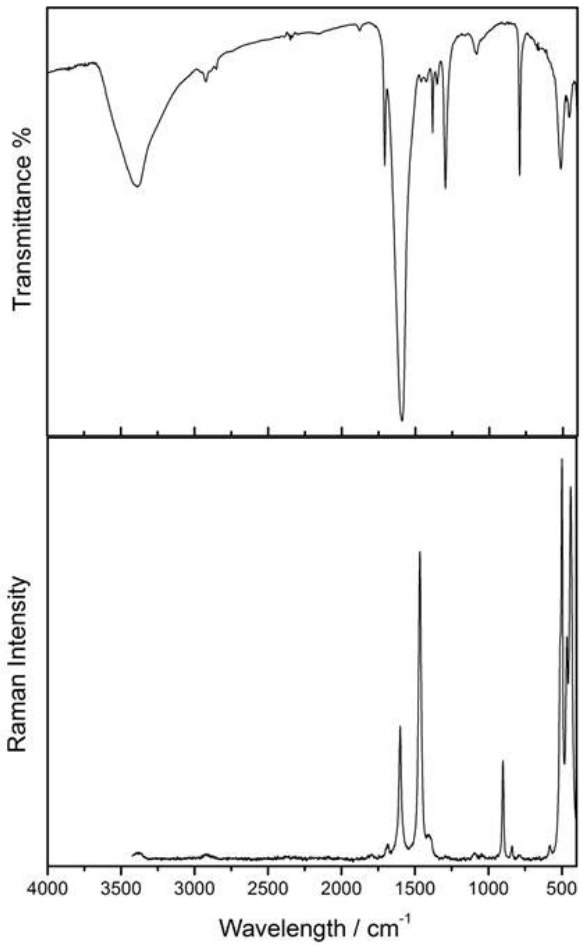

Figure 1. FTIR (above) and Raman spectra (below) of $Bi(OH)C_2O_4$.

Table 1. Assignments of the FTIR and FT-Raman spectra of $Bi(OH)C_2O_4$ (Band positions in cm^{-1}).

Infrared	Raman	Assignments
3390 vs, br		ν(O-H)
2922 w, 2852 vw		Combination modes
1709 m, 1590 vs	1682 w, 1600 s	ν_{as}(C-O)
1460 vw, 1426 vw	1466 vs	ν_s(C-O) + ν(C-C)
1384 m, 1353 w	1380 w	ν_s(C-O) + δ(OCO)
1296 s		ν_s(C-O) + δ(OCO)
1084 w	1091 vw, 1046 vw	ν(C-C)
	901 s, 839 w	ν(C-C) + δ(OCO)
793 s		ν(C-C) + δ(OCO)
513 s, 474 w, 456 w	499 vs, 466 s, 439 vs	δ_{ring}

vs, very strong; s, strong; m, medium; w, weak; vw, very weak; br, broad.

3.2.2. $Bi_2(C_2O_4)_3 \cdot 7H_2O$

The FTIR and FT-Raman spectra in the spectral range between 4000 and 400 cm^{-1} are shown in Figure 2 and the proposed assignment is presented in Table 2, and is briefly commented as follows:

- The OH-stretching vibrations of the water molecules are found as a broad band with components at 3382 and 3549 cm^{-1} in the infrared spectrum and were, also in this case, not observed in the Raman spectrum. The appearance of a doublet structure clearly suggests the presence of at least two types of water molecules. This fact implies a structural situation similar to that observed in the case of the hexa- and octahydrated bismuth oxalates previously investigated [7], in which some of the H_2O molecules coordinate directly with the metal center and the other ones are located in the crystal channels as hydration water. The position of these OH-stretching motions suggests the participation of water molecules in H-bridges of medium strength [17, 18].

- The deformational modes of water molecules, $\delta(H_2O)$, are surely overlapped with the very strong ν_{as}(C-O) vibrational mode. Also, the characteristic $\rho(H_2O)$ mode is surely overlapped with one of the lowest frequency bands identified in the FTIR spectrum below 700 cm^{-1}. In Table 2 we have made a tentative assignment for this vibration.

- The weak combinational modes found around 2900 cm^{-1} are also here surely originated from combinations of stretching vibrations of oxalate anions.

- Also in this case, all the characteristic oxalate vibrations show a decrease in energy compared to similar vibrations found in complexes with simple bonded tetradentate oxalate groups. In addition, the typical doublet structure of one of the ν_s(C-O) + δ(OCO) vibrations is absent in $Bi_2(C_2O_4)_3 \cdot 7H_2O$.

- The important number of ring deformational modes found in this case supports the presence of a relatively complex three-dimensional arrangement around the Bi(III) center.

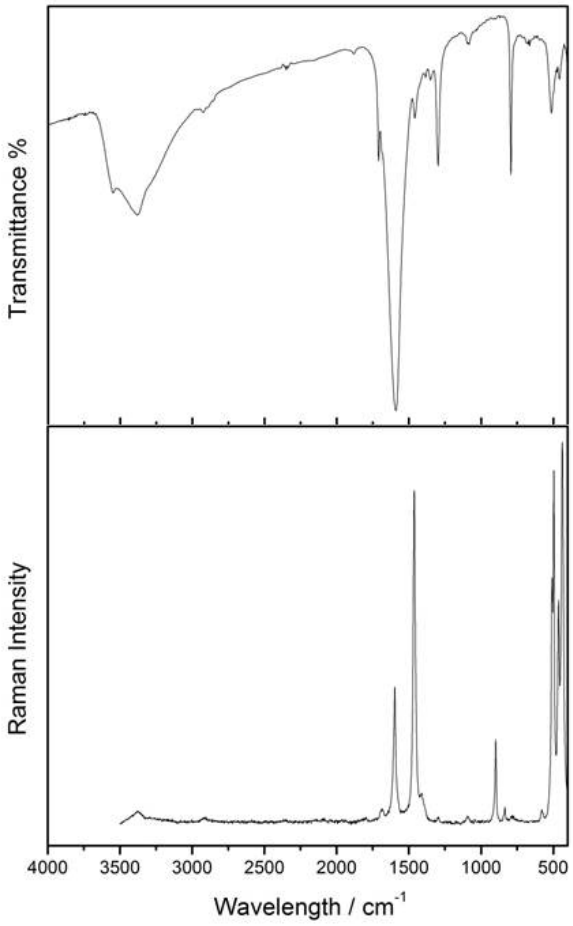

Figure 2. FTIR (above) and Raman spectra (below) of $Bi_2C_2O_4)_3 \cdot 7H_2O$.

Table 2. Assignments of the FTIR and FT-Raman spectra of $Bi_2(C_2O_4)_3 \cdot 7H_2O$ (Band positions in cm^{-1}).

Infrared	Raman	Assignments
3549 m, 3383 vs, br		ν(O-H)
2924 w, 2880 vw		Combination modes
1709 w, 1590 vs	1685 w, 1597 s	ν_{as}(C-O)
1458 w	1462 vs	ν_s(C-O) + ν(C-C)
1384 vw, 1351 w	1367 w	ν_s(C-O) + δ(OCO)
1297 s	1280 vw	ν_s(C-O) + δ(OCO)
1083 w	1094 vw	ν(C-C)
	898 m, 835 w, 784 vw	ν(C-C) + δ(OCO)
793 s		ν(C-C) + δ(OCO)
673 vw, 663 vw		δ_{ring} + $\rho(H_2O)$ (?)
	579 w, 508 s, 498 vs	δ_{ring}
512 m, 456 w		δ_{ring}
	465 s, 437 vs	δ_{ring}

vs, very strong; s, strong; m, medium; w, weak; vw, very weak; br, broad.

4. Conclusions

The FTIR and FT-Raman spectra of $Bi(OH)C_2O_4$ and $Bi_2(C_2O_4)_3{\cdot}7H_2O$ were recorded and analyzed. Interestingly, the spectral patterns of both compounds are not very different. In the case of $Bi(OH)C_2O_4$, the general spectral features are compatible with the known structural peculiarities. For $Bi_2(C_2O_4)_3{\cdot}7H_2O$ structural arrangements similar to those found in $Bi_2(C_2O_4)_3{\cdot}6H_2O$ and $Bi_2(C_2O_4)_3{\cdot}8H_2O$ can be proposed, that is, Bi(III) are bridged by tetradentate oxalate ligands, which also interact with vicinal cations by means of their O-atoms, generating secondary bonds. Part of the water molecules are directly bound to the metal centers and the rest are present as crystallization water.

Acknowledgements

This work was supported by the UNLP. ACGB is a member of the Research Career from CONICET.

References

(1) N. Mancilla, M.C. D'Antonio, A.C. González-Baró, E.J. Baran, *J. Raman Spectr*, 2009, 40, 2050-2052.

(2) A. Wladimirsky, D. Palacios, M.C. D'Antonio, A.C. González-Baró, E.J. Baran, *Spectrochim. Acta*, 2010, 77A, 334-335.

(3) D. Palacios, A. Wladimirsky, M.C. D'Antonio, A.C. González-Baró, E.J. Baran, *Phys. Chem., An Indian J.*, 2014, 9, 336-339.

(4) O.E. Piro, G.A. Echeverría, A.C. González-Baró, E.J. Baran, Z. *Naturforsch.*, 2015, 70b, 249-252.

(5) A.C. González-Baró, E.J. Baran, *Phys. Chem., An Indian J.*, 2015, 10, 121-124.

(6) M.M. Torres, D. Palacios, M.C. D'Antonio, A.C. González-Baró, E.J. Baran, *Spectr. Lett.*, 2016, 49, 238-240.

(7) U. Kolitsch, *Acta Crystallogr.*, 2003,59C, m501-m504.

(8) P. Roumanille, V. Baco-Carles, C. Bonningue, M. Gougeon, B. Duployer, P. Monfraix, H.L. Trong, P. Tailhades, *Inorg. Chem.*, 2017, 56 9486-9496.

(9) K. Xiao, N. Tian, Y. Guo, H. Huang, X. Li, Y. Zhang, *Inorg. Chem. Commun*, 2015, 52, 5-8.

(10) L. Tortet, O. Monnereau, P. Conflant, G. Vacquier, *Ann. Chim. Sci. Mater.*, 2007, 32, 69-80.

(11) M. Rivenet, P. Roussel, F. Abraham, *J. Solid State Chem.*, 2008, 181, 2586-2590.

(12) M.C. D'Antonio, N. Mancilla, A. Wladimirsky, D. Palacios, A.C. González-Baró, E.J. Baran, *Vibrat. Spectr.*, 2010, 53, 218-221.

(13) A. Wladimirsky, D. Palacios, M.C. D'Antonio, A.C. González-Baró, E.J. Baran, *J. Argent. Chem. Soc.*, 2011, 98, 71-77.

(14) M.C. D'Antonio, A. Wladimirsky, D. Palacios, L. Coggiola, A.C. González-Baró, E.J. Baran, R.C. Mercader, J. *Braz. Chem. Soc.*, 2009, 20, 445-450.

(15) A. Rulmont, *Spectrochim. Acta*, 1972, 28A, 1287-1296.

(16) G.E. Tobón-Zapata, S.B. Etcheverry, E.J. Baran, *J. Mater. Sci. Lett.*, 1997, 16, 656-657.

(17) E. Libowitzky, *Monatsh. Chem.*, 1999, 130, 1047-1059.

(18) H. Siebert, *Anwendungen der Schwingungsspektroskopie in der Anorganischen Chemie*, Springer, Berlin, 1966.

Anales de la Asociación Química Argentina

ESTUDIO TEÓRICO DE ACETILACIÓN DE ALCOHOLES CATALIZADA POR ÁCIDOS DE LEWIS E INFLUENCIA DE SOLVENTES

Silvana C. Caglieri*, Héctor R. Macaño, Gustavo I. Servetti

CIQA-Centro de Investigación y Transferencia en Ingeniería Química Ambiental, Facultad Regional Córdoba, Universidad Tecnológica Nacional. Córdoba. República Argentina

**Autor Corresponsal E-mail: scaglieri@frc.utn.edu.ar*

Resumen

Se llevó a cabo un estudio teórico de reactividad de alcoholes alifáticos y aromáticos, frente a la reacción de acetilación con anhídrido acético, catalizada por iones metálicos: Zn^{2+}; Co^{2+}, Mn^{2+}; Cu^{2+} y Ni^{2+}, a través del análisis de los intermediarios de reacción correspondientes. Las energías de activación y las energías de los intermediarios de reacción, se calcularon con el método Universal Force Field (UFF). Los valores obtenidos se compararon con datos de literatura. El p-metilfenol presentó la mayor reactividad frente a la acetilación en todos los casos y el Zn^{2+} resultó ser el ion metálico más reactivo, reportando los valores más bajos de energía. Se completó el estudio comparando la reactividad de etanol y fenol frente a la reacción de acetilación, en presencia de diferentes solventes polares apróticos y no polares, a través del análisis de los intermediarios de reacción correspondientes. Las energías de los mismos y las energías de activación se calcularon con el nivel de teoría funcional de densidad (DFT) con el estándar B3LYP combinado con el conjunto de base 6-31G**. Para estudiar la influencia de los diferentes solventes se utilizó el modelo IEFPCM. Los valores obtenidos se compararon con datos de literatura. El etanol presentó la mayor reactividad en todos los casos y el acetonitrilo resultó ser el solvente óptimo para la reacción de acetilación de ambos alcoholes.

Abstract

A theoretical study of reactivity of aliphatic and aromatic alcohols in the acetylation catalyzed with metallic ions: Zn^{2+}; Co^{2+}, Mn^{2+}; Cu^{2+} y Ni^{2+}, through the analysis of the corresponding reaction intermediates was carried out. The activation energies and the reaction intermediates energies were calculated with the method Universal Force Field (UFF). The calculated values were compared with literature data. The p-methylphenol presented the higher reactivity in the acetylation reaction and the Zn^{2+} reported the lower

energy values. This was completed with a comparative theoretical study of reactivity of ethanol and phenol in the acetylation with several aprotic polar and nonpolar solvents, through the analysis of the corresponding reaction intermediates. The activation energies and the reaction intermediates energies were calculated with the level density functional theory (DFT) with the standard B3LYP combined with basis set 6-31G*. The IEFPCM model used to study the influence of different solvents. The values obtained were compared with literature data. The ethanol presented the higher reactivity in the acetylation reaction and the acetonitrile turned out to be the best solvent for the reaction of acetylation of both alcohols.

Palabras clave: acetilación, ácido Lewis, alcoholes, DFT-IEFPCM, UFF.

Keywords: acetylation, Lewis acid, alcohols, DFT- IEFPCM, UFF.

1. Introducción

La síntesis de ésteres es de gran importancia dentro de la industria química, por su utilidad para la formulación de aditivos para alimentos [(1)], por su empleo como antioxidantes y surfactantes [(2)], como materias primas para la síntesis de poliésteres [(3,4)] y en la síntesis de insecticidas [(5)]. También se encuentran grupos acetilados en formulaciones de cosméticos, alimentos, disolventes, perfumes, plastificantes, pesticidas y productos farmacéuticos [(6,7,8)]. Los ésteres se pueden sintetizar a partir de la acetilación de alcoholes, reacción usada en síntesis orgánica para proteger el grupo hidroxilo en un determinado proceso [(9)].

La acetilación de un alcohol es una reacción de sustitución nucleofílica sobre carbono insaturado, actuando el alcohol como nucleófilo, produciendo un ataque al carbono del carbonilo del anhídrido acético formando un intermediario tetraédrico. Se han llevado a cabo estudios teóricos sobre la reacción de acetilación de metanol con anhídrido acético [(10)] y trabajos experimentales sobre la reacción de acetilación de diferentes alcoholes con el mismo reactivo [(11)] y ambos coinciden en que la misma transcurre a través de la formación del intermediario tetraédrico.

Dicha reacción puede ser catalizada por medio de una base [(12)], de un ácido de Brönsted [(13)], de un ácido de Lewis [(14)] y en la búsqueda de procesos alternativos, ambientalmente favorables, se han llevado a cabo estudios experimentales de la acetilación de alcoholes empleando iones metálicos [(15)] como ácidos de Lewis –Ni^{2+}, utilizando ácido acético y sales de cobre [(16)], SiO_2 -$Co(acac)_2$ y SiO_2 -$Cu(acac)_2$ [(17)] y $CoCl_2$ [(18)].

El objetivo de este trabajo consiste en efectuar un estudio teórico comparativo de reactividad de diferentes alcoholes alifáticos y aromáticos frente a la reacción de acetilación catalizada por una variedad de iones metálicos, mediante el análisis de los intermediarios de

reacción correspondientes, completando el estudio con un análisis de la influencia de diferentes solventes polares apróticos y no polares en la acetilación de etanol y fenol en ausencia de catalizador.

2. Materiales y Métodos

Se empleó el método UFF - Universal Force Field para comparar la reactividad de los siguientes alcoholes: n-propanol, isopropanol, fenol, p-metilfenol y p-nitrofenol frente a la acetilación catalizada por diferentes iones metálicos, a saber M^{2+}: Mn^{2+}, Ni^{2+}, Zn^{2+}, Co^{2+} y Cu^{2+}. Siendo M: metal.

En la Figura 1 se indica el esquema general y el mecanismo de reacción de la acetilación de propanol ($R=CH_2$-CH_2-CH_3), isopropanol ($R=CH$-$(CH_3)_2$), fenol ($R=C_6H_5$), p-nitrofenol ($R=C_6H_4NO_2$), y p-metilfenol ($R=C_7H_7$) con anhídrido acético, catalizada por iones metálicos, cuyos productos de reacción son: ácido acético y los ésteres acetato de n-propilo, acetato de isopropilo, acetato de fenilo, acetato de p-nitrofenilo y acetato de p-metilfenilo, respectivamente.

Los iones metálicos actúan como ácidos de Lewis catalizando la reacción de acetilación, debido a la formación de un complejo con el oxígeno del carbonilo, facilitando la polarización del mismo y favoreciendo de esta manera el ataque del agente nucleofílico (alcohol) al carbono del carbonilo. Se han realizado estudios de acetilación de alcoholes empleando ácidos de Lewis [14,18,19] y coinciden en que dicha reacción transcurre de esta manera.

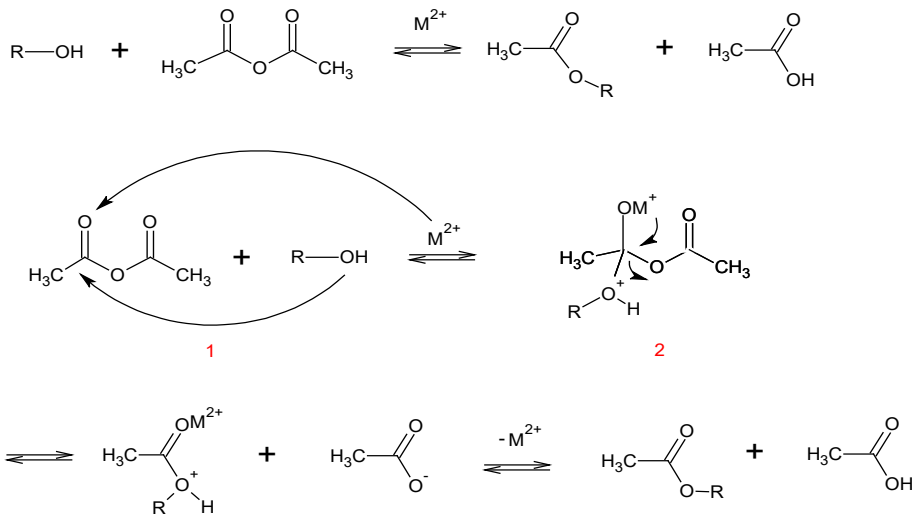

Figura 1. Mecanismo de acetilación catalizada por iones metálicos

Se calcularon las energías de activación (E_a) de cada una de las reacciones, las mismas resultan de la diferencia de energía entre las etapas 1 y 2 (intermediario de reacción), indicadas en el esquema general del mecanismo de reacción.

Para estudiar teóricamente la influencia de solventes no polares (dietiléter, cloroformo, tolueno y ciclohexano) y solventes polares apróticos (acetonitrilo, acetona, y tetrahidrofurano - THF), en las acetilaciones de etanol y fenol, a través del análisis de los intermediarios correspondientes, se utilizó el modelo IEFPCM o PCM (Polarizable Continuum Model). Se han llevado a cabo estudios sobre la influencia del solvente en la acetilación de alcohol bencílico [13].

En la Figura 2 se indica el esquema general y el mecanismo de reacción de la acetilación de etanol ($R=CH_2$-CH_3) y fenol ($R=C_6H_5$) con anhídrido acético, en ausencia de catalizador, cuyos productos de reacción son: ácido acético y los ésteres acetato de etilo y acetato de fenilo, respectivamente.

Las energías de activación y las energías de los intermediarios de reacción se calcularon con el nivel de teoría DFT basado en la teoría de funcionales de densidad [20] y dentro de este se utilizó el B3LYP [21], combinado con el conjunto de base 6-31G*, que indica que se emplean seis funciones gaussianas para representar los orbitales atómicos internos, mientras que los externos, capa de valencia, se representan mediante tres funciones para la parte contraída y una para la parte difusa, más una función de polarización para átomos pesados, indicada mediante el *, que representa el efecto de los orbitales tipo d, respectivamente. Este método ha sido empleado para calcular las energías de activación de la acetilación de diferentes aminas en presencia de ácidos de Lewis [22], las energías de activación de la acetilación de diferentes aminas en ausencia de catalizador [23] y para calcular las energías de activación de la hidrólisis de diferentes amidas, siendo esta reacción también una sustitución nucleofílica sobre carbonilo [24]. Se empleó el programa Gaussian´09 [25] para la realización de todos los cálculos.

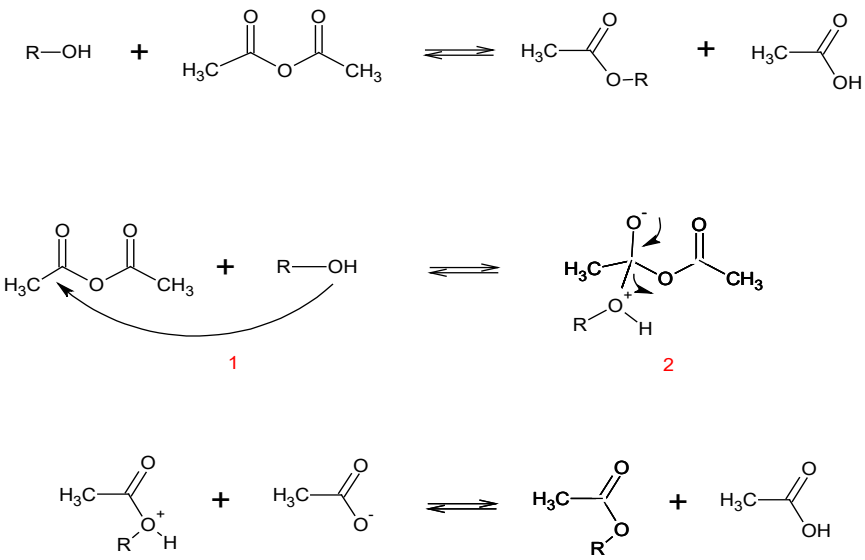

Figura 2. Mecanismo de acetilación en ausencia de catalizador

3. Resultados

Las Tablas 1 y 2 reportan los valores de energías, en Hartree, de los alcoholes reactivos (E_r), a saber: n-propanol, isopropanol, fenol, p-metilfenol, p-nitrofenol y las energías del anhídrido acético (E_r) y de los intermediarios tetraédricos (E_i) de cada una de las acetilaciones motivo de estudio para los diferentes iones metálicos, respectivamente. Datos obtenidos de la aplicación del método indicado.

Tabla 1. Energías de alcoholes reactivos en Hartree

reactivos	**n-propanol**	**isopropanol**	**fenol**	**p-metilfenol**	**p-nitrofenol**
E_r	0,0070	0,0081	0,0194	0,0212	0,0254

Tabla 2: Energías de reactivos e intermediarios de reacción en Hartree

M^{2+} ion metálico	**E_r anhídrido acético**	**E_i n-propanol**	**E_i isopropanol**	**E_i fenol**	**E_i p-metilfenol**	**E_i p-nitrofenol**
Zn^{2+}	0,0526	0,0949	0,1007	0,1123	0,1046	0,1187
Cu^{2+}	0,0525	0,0968	0,1026	0,1144	0,1068	0,1208
Ni^{2+}	0,0526	0,1021	0,1079	0,1190	0,1114	0,1254
Co^{2+}	0,0527	0,1033	0,1090	0,1200	0,1124	0,1264
Mn^{2+}	0,0538	0,1085	0,1142	0,1251	0,1175	0,1316

En la Tabla 3 se indican las energías de activación ($E_a = E_i - E$) en kcal/mol, de las diferentes acetilaciones catalizadas por los iones metálicos motivo de estudio. Siendo E_i la energía del intermediario tetraédrico y E la suma de las energías del anhídrido acético y el alcohol correspondiente. La conversión 1 Hartree equivale a 627,51 kcal.mol^{-1}.

Tabla 3. Energías de activación de las diferentes acetilaciones en kcal.mol^{-1}

radio atómico (Å)	**M^{2+}**	**n-propanol E_a**	**isopropanol E_a**	**fenol E_a**	**p-metilfenol E_a**	**p-nitrofenol E_a**
1,53	Zn^{2+}	22,15	25,10	25,29	19,33	25,54
1,57	Cu^{2+}	23,41	26,35	26,67	20,77	26,92
1,62	Ni^{2+}	26,67	29,62	29,49	23,59	29,74
1,67	Co^{2+}	27,36	30,24	30,06	24,16	30,31
1,79	Mn^{2+}	29,93	32,82	32,57	26,67	32,88

Siendo M^{2+}: ion metálico y E_a: la energía de activación de la acetilación en kcal/mol. Se observa que una disminución del radio atómico del metal, lo cual implica una disminución del tamaño del átomo, se puede asociar a un menor impedimento estérico, que se traduce en una mayor estabilidad del intermediario de reacción, disminuyendo la energía del mismo y por consiguiente disminuyendo la energía de activación de la acetilación.

Los iones metálicos, ácidos de Lewis, empleados como catalizadores en la acetilación de n-propanol, isopropanol, fenol, p-nitrofenol y p-metilfenol, reportaron el siguiente orden creciente de reactividad: $Zn^{2+} > Cu^{2+} > Ni^{2+} > Co^{2+} > Mn^{2+}$. Trabajos sobre acetilaciones de fenol y alcoholes indican un orden de reactivad Ni > Co [26], Cu > Co [17], Zn > Cu [27] y un orden de reactivad Cu > Co > Mn [28].

La Tabla 4 reporta los valores de energías en Hartree de los reactivos (E_r) y de los intermediarios tetraédricos (E_i) de cada una de las acetilaciones motivo de estudio para los diferentes solventes no polares y polares apróticos, datos obtenidos de la aplicación de los métodos indicados.

Tabla 4. Energías de reactivos e intermediarios, sin catalizador y con solventes en Hartree

Disolventes	E_r- Etanol	E_r- Fenol	E_r - Anhídrido Acético	E_i - Etanol	E_i- Fenol
acetonitrilo	-154,9963	-307,3863	-381,9804	-536,9535	-689,3385
acetona	-154,9961	-307,3861	-381,9785	-536,9512	-689,3362
tetrahidrofurano	-154,9953	-307,3851	-381,9708	-536,9419	-689,3267
cloroformo	-154,9946	-307,3842	-381,9639	-536,9336	-689,3182
dietiléter	-154,9944	-307,3840	-381,9618	-536,9312	-689,3158
tolueno	-154,9930	-307,3824	-381,9457	-536,9136	-689,2980
ciclohexano	-154,9925	-307,3819	-381,9393	-536,9066	-689,2910

La Tabla 5 reporta las constantes dieléctricas, momentos dipolares de los solventes empleados en las acetilaciones de etanol y fenol y los correspondientes valores de energías de activación ($E_a = E_i - E$) en kcal.mol^{-1}. Siendo Ei la energía del intermediario tetraédrico y E la suma de las energías del anhídrido acético y el alcohol correspondiente. La conversión 1 Hartree equivale a 627,51 kcal.mol^{-1}.

Para ambas acilaciones, de etanol y fenol con anhídrido acético, la menor energía de activación se observó para el acetonitrilo, solvente con la mayor constante dieléctrica y alta polaridad. Además, se reportó una mayor energía de activación al emplear solventes con constante dieléctrica menor a 5.

Tabla 5: Energías de activación acetilación etanol y fenol, sin catalizador y con solventes en kcal.mol^{-1}

Solventes	Constante dieléctrica a 25 ºC	Momento dipolar Debye (D)	Etanol - E_a	Fenol - E_a
acetonitrilo	37	3,92	14,56	17,69
acetona	21	2,88	14,68	17,82
tetrahidrofurano	7,5	1,75	15,18	18,32
cloroformo	4,8	1,04	15,62	18,76
dietiléter	4,3	1,15	15,69	18,82
tolueno	2,3	0,36	15,75	18,89
Ciclohexano	2	0,00	15,81	18,95

4. Discusión

El n-propanol resultó ser más reactivo que el isopropanol frente a todos los iones metálicos catalizadores de la acetilación, esto puede asociarse al mayor impedimento estérico que presenta

una ramificación de la cadena carbonada que se traduce en un aumento en la correspondiente energía de activación. Estudios experimentales de acetilación empleando cloruro de acetilo y SiO_2-$Cu(acac)_2$ como catalizador, reportan un rendimiento para esta reacción de 85 % y 84 % para el n-propanol e isopropanol, respectivamente [17]. Otros estudios experimentales coinciden que los alcoholes no ramificados son más reactivos que los ramificados frente a la acetilación [14].

El p-metilfenol resultó ser más reactivo que el fenol frente a todos los iones metálicos catalizadores de la acetilación. Al reemplazar un hidrógeno del anillo aromático por un grupo metilo, en posición para respecto del grupo hidroxilo, se genera un efecto inductivo adicional por diferencia de hibridación $Csp^3 \rightarrow Csp^2$, que favorece la disposición electrónica por parte del oxígeno del alcohol, aumentando su carácter nucleofílico y su reactividad.

Por el contrario el p-nitrofenol resultó ser menos reactivo que el fenol frente a todos los iones metálicos catalizadores de dicha reacción. Esto puede asociarse al efecto de atracción de electrones ejercido por el grupo nitro sobre el anillo aromático, por diferencia de electronegatividad, que favorece la deslocalización electrónica, en el anillo aromático, de los electrones no enlazados del oxígeno del alcohol, disminuyendo el carácter nucleofílico del mismo.

Coincidiendo con estudios experimentales de acetilación empleando anhídrido acético y nanopartículas de fosfato de cobre zirconio, que reportan un rendimiento para esta reacción de 95%, 90% y 80% para p-metilfenol, fenol y p-nitrofenol, respectivamente [19].

El Zn resultó ser el metal más eficiente para la acetilación de n-propanol, isopropanol, fenol, p-nitrofenol y p-metilfenol, mientras que el Mn resultó ser el metal menos eficiente para la acetilación de todos los alcoholes, coincidiendo con estudios experimentales [27,28].

Tanto la acetilación de etanol como la de fenol son más reactivas en solventes polares apróticos que en solventes no polares. El aumento de la polaridad del disolvente, se puede asociar con una mayor estabilización del intermediario tetraédrico, lo que involucra una menor energía y esto se traduce en una disminución de la energía de activación de la acetilación.

Ambas acetilaciones son más reactivas en acetonitrilo que en dietiléter, coincidiendo con estudios experimentales de acetilación de alcohol 4-nitro bencílico con un rendimiento del mismo de 90 % y 75 % en acetonitrilo y dietiéter respectivamente [11].

Tanto la acetilación de etanol como la de fenol son más reactivas en acetonitrilo que en tolueno, coincidiendo con estudios experimentales de acetilación de β-naftol con un rendimiento del mismo de 91% y 85 % en acetonitrilo y tolueno respectivamente [29] y son más reactivas en acetonitrilo que en cloroformo, coincidiendo con estudios experimentales de acetilación de alcohol

bencílico con un rendimiento del mismo de 87 % y 58 % en acetonitrilo y cloroformo respectivamente [13].

5. Conclusiones

Luego del análisis y discusión de los resultados presentados en este trabajo, se observó que el p-metilfenol presentó la mayor reactividad frente a la acetilación catalizada por los diferentes iones metálicos, siendo el Zn^{2+} el ion metálico más reactivo, ya que reportó los valores más bajos de energía.

En cuanto al estudio de solventes, el etanol reportó una mayor reactividad, en comparación con el fenol, frente a la acetilación en presencia de todos los solventes y el acetonitrilo resultó ser el solvente más óptimo para ambas acetilaciones.

La existencia de una marcada concordancia entre los resultados teóricos y datos de literatura, valida el empleo del método Mechanics-UFF y del método DFT- IEFPCM como herramientas para el estudio de sistemas que involucran enlaces carbono-metal y para el estudio de la influencia de solventes en la acetilación de alcoholes, respectivamente.

El empleo de alcoholes alifáticos con cadenas alquílicas no ramificadas, de alcoholes aromáticos con anillos sustituidos con grupos dadores de electrones y de solventes polares apróticos, optimiza y favorece cualquier proceso químico que involucre una reacción de acetilación. El uso de ácidos de Lewis como catalizadores, reemplazando la utilización de sustancias tóxicas como la piridina, permite considerar a dicha reacción como una síntesis ambientalmente favorable.

Agradecimientos

Agradecemos a UTN por el financiamiento del Proyecto homologadoUTI4703TC.

Referencias

(1) Staroń, J.; Dąbrowski, J.M.; Cichoń, E.; Guzik, M. *Crit. Rev. Biotechnol.*, 2017, 38(2), 245−258.

(2) Karmee, S.K. *Lipid Technol*., 2011, 23 (10), 227−229.

(3) KobayashI, S. *Polym Adv Technol*., 2015, 26 (7), 677−686.

(4) Namekawa, S.; Uyama, H.; Kobayashi, S. *Biomacromolecules*, 2000, 1(3), 335–338.

(5) Song, Z.; Li, S.; Chen, X.; Liu, L.; Song, Z. *For. Stud. China*. 2006, 8(3), 26−29.

(6) Yoon, H.J.; Lee, S.M.; Kim, J.H.; Cho, H.J.; Choi, J.W.; Lee, S.H.; Lee, Y.S., *Tetrahedron Lett.*, 2008, 49(19), 3165−3171.

(7) Sharghi, H.; Jokar, M.; Doroodmand, M.M. *Adv. Synth. Catal.*, 2011, 353, 426−442.

(8) Taghavi, S.A.; Moghada, M.M.; Mohammadpoor-Baltork, I.; Tangestaninejad, S.; Mirkhani, V.; KhosropouR, A.R. *Inorganica Chim Acta.*, 2001, 377 (1), 159−164.

(9) Adinolfi, M.; Barone, G.; Iadonisi, A.; Schiattarella, M. *Tetrahedron Lett.*, 2003, 44, 4661−4663.

(10) Kruger, H.G. *J Mol Struc-Theochem.*, 2002, 577, 281−285.

(11) Lugemwa, F.N.; Shaikh, K.; Hochstedt, E. *Catalysts.*, 2013, 3, 954−965.

(12) Yadav, V.K.; Babu, K.G.; Mittal, M. *Tetrahedron.*, 2001, 57,7047−7051.

(13) Esmaeilpour, M.; Sardarian, A.R. *Iran J Sci Technol A.*, 2014, 38, 175−186.

(14) Farhadi, S.; Panahandehjoo, S. *Appl. Catal., A.*, 2010, 382, 293−302.

(15) Meshram, G.A.; Patil, V.D. *Synth. Commun.*, 2009, 39 (14), 2516−2528.

(16) Iranpoor, N.; Firouzabadi, H.; Zolfigol, M. A. *Synth. Commun.*, 1998, 28(11), 1923−1934.

(17) Kour Sodhi, R.; Kumar, V.; Satya, P. *The Open Catalysis Journal.*, 2013, 6, 1−7.

(18) Mulla, S.A.R.; InamdaR, S.M.; Pathan, M.Y.; Chavan, S.S. *Open J. Synth. Theory Appl.*, 2012, 1, 31−35.

(19) Hajipour, A.R.; Karimi, H. *Chin. J. Catal.*, 2014, 35, 1982−1989.

(20) Parr, R.G.; Yang, W.; *Density-functional theory of atoms and molecules*, 1th ed., Oxford University Press, Nueva York, 1989.

(21) Becke, A.D. *J Chem Phys.*, 1997, 107, 8554−8560.

(22) Caglieri, S.C.; Macaño, H.R. *Ingeniería Investigación y Tecnología.*, 2018, 19 (2), 239−244.

(23) Caglieri, S.C.; Macaño, H.R. *Inf. Tecnol.*, 2016, 27 (2), 105−110.

(24) Caglieri, S.C.; PAGNAN, M. *Inf. Tecnol.*, 2013, 24 (3), 35−40.

(25) Frisch, M.J.; Trucks, G.W.; y otros 71 autores. *Gaussian 09*, Revision D.1., 2th Edition. USA: Gaussian, Inc., 2013.

(26) Hajipour, A.R.; Karimi, H.; Masti, A. *Chinese J Catal.*, 2015, 36, 595−602.

(27) Chandra, K.L.; Saravanan, P.; Singh, R.K.; Singh, V. K. *Tetrahedron.*, 2002, 58, 1369−1374.

(28) Jeyakumar, K.; Chand, D.K. *J Mol Catal A-Chem.*, 2006, 255, 275−282.

(29) Ghosh, R.; Maiti, S.; Chakraborty, A. *Tetrahedron Lett.* 2005, 46, 147−151.

(30) Fikee, W. *J Chromatogr Sci.*, 1973, 11 (1), 25–27.

Anales de la Asociación Química Argentina

WHOLE BODIES OF THE ARGENTINIAN COCKROACH *PERIPLANETA AMERICANA*: NONCOMMERCIAL EXTRACT FRACTIONATION/CHARACTERIZATION, CROSS-REACTIVITY AND VACCINE THERAPY

CUERPOS ENTEROS DE LA CUCARACHA ARGENTINA *PERIPLANETA AMERICANA*: FRACCIONAMIENTO/CARACTERIZACIÓN DEL EXTRACTO NO COMERCIAL, REACTIVIDAD CRUZADA Y VACUNOTERAPIA

Stella M. Battista [1], Santiago R. Rodríguez [1], Ángel Alonso [1], Alicia B. Pomilio [2*]

[1] División Alergia e Inmunología, Hospital de Clínicas "José de San Martín", Buenos Aires, Argentina.

[1] Cátedra de Microbiología e Inmunología, Facultad de Medicina, Universidad de Buenos Aires, Argentina. battistasm@yahoo.com.ar

[2] Departamento de Bioquímica Clínica, Área Hematología, Hospital de Clínicas "José de San Martín", Universidad de Buenos Aires, CONICET, Av. Córdoba 2351, C1120AAF Buenos Aires, Argentina.

[*]Autor Corresponsal E-mail: abpomilio@sinectis.com.ar; pomilio@ffyb.uba.ar

Resumen

Los restos de cucarachas y los ácaros del polvo doméstico provocan algunos cuadros de alergia, siendo especialmente responsables del asma y otras enfermedades alérgicas de las vías respiratorias, como rinitis, bronquitis y rinoconjuntivitis alérgica en áreas urbanas. *Periplaneta americana* y *Blatella germanica* son dos de las cucarachas más frecuentes en la ciudad de Buenos Aires y sus alrededores, mientras que *Triatoma infestans* (vinchuca) se encuentra en las zonas rurales de Argentina, el resto de Sudamérica, Centroamérica y América del Norte. Por lo tanto, se analizaron y caracterizaron extractos naturales de ambas cucarachas de Argentina, obteniendo glicoproteínas alergénicas. La reactividad cruzada entre *P. americana* y *B. germanica* de Argentina se evaluó mediante pruebas inmunoserológicas. *Dermatophagoides pteronyssinus* y *D. farinae* son ácaros del polvo doméstico que se encuentran en nuestro país, siendo el primero el más extendido de estos arácnidos. Los sueros de conejos inmunizados con cada extracto de insecto, junto con el adyuvante completo de Freund, también se analizaron contra extractos de

P. americana y *D. pteronyssinus*, lo cual demostró que el ácaro provoca principalmente reacciones de tipo I y no respuestas de inmunoglobulina G (IgG) circulantes. La terapia con vacunas en pacientes atópicos mostró resultados exitosos en comparación con los controles. La disminución de IgE, el aumento de IgG y la mejora de los signos/síntomas alérgicos respaldaron la eficacia del tratamiento de tres años. La caracterización de proteínas por electroforesis capilar de extractos argentinos de P. americana y T. infestans no sólo mostró algunos epítopes en común, sino que también demostró ser una herramienta útil para la caracterización de extractos de proteínas de cucarachas. Los perfiles de electroferogramas son apropiados para la comparación y distinción de extractos de diferentes regiones geográficas. La reactividad cruzada entre las proteínas alergénicas de *P. americana* y *T. infestans* enfatizó los problemas de salud de hipersensibilidad por los síntomas alérgicos que empeoran en pacientes atópicos urbanos cuando viajan a áreas rurales.

Abstract

Cockroach debris and house dust mites trigger some allergy frames, being especially responsible for asthma and other allergic airway diseases, such as rhinitis, bronchitis, and allergic rhinoconjunctivitis in urban areas. *Periplaneta americana* and *Blatella germanica* are two of the most frequent cockroaches in the city of Buenos Aires and surroundings, while *Triatoma infestans* (vinchuca) is found in rural areas from Argentine to North America. Therefore, natural extracts of both cockroaches from Argentine were analyzed and characterized, obtaining allergenic glycoproteins. Cross-reactivity between argentinian P. americana and *B. germ*anica was assessed by immunoserological tests. *Dermatophagoides pteronyssinus* and *D. farinae* are house dust mites occurring in our country, the former being the most widespread of these arachnids. Sera from immunized rabbits with each insect extract, together with complete Freund's adjuvant, were also tested against *P. americana* and *D. pteronyssinus* extracts, demonstrating that the mite mainly elicit type I reactions and not circulating immunoglobulin G (IgG) responses. Successful results were shown by vaccine therapy of atopic patients compared to controls. IgE decrease, IgG increase, and allergic signs/symptoms improvement supported the efficiency of three-years-treatment. Capillary electrophoresis protein characterization of argentinian *P. americana* and *T. infestans* extracts not only showed some epitopes in common, but also proved to be a useful tool for characterization of cockroach protein extracts. Electropherogram profiles are appropriate for comparison and distinction of extracts from different geographical regions. Cross-reactivity between *P. americana* and *T. infestans* allergenic proteins stressed the hypersensitivity health problems due to allergic symptoms that worsen in urban atopic patients when they travel to rural areas.

Palabras clave: Periplaneta americana; cucaracha de Argentina; IgE; IgG; reactividad cruzada; inmunoterapia alergénica específica; alergia respiratoria.

Keywords: Periplaneta americana; cockroach from Argentine; IgE; IgG; cross-reactivity; allergen-specific immunotherapy; airway allergy.

1. Introduction

The Allergy Division of the Hospital de Clínicas "José de San Martín" of Buenos Aires has been devoted for years to treat allergic patients, and to study indoor and outdoor allergens, under the guidance of Prof. A. Alonso. In 1980 glycoprotein fractions of the mite *Dermatophagoides farinae* were isolated and characterized [1]. Allergens from house dust [1, 2], air pollutants [3], food (oranges) [4], mites (Acari) [1, 2], and insects (Insecta) were reported [5-9]. In the latter case, cockroaches in cities, and *Triatoma infestans* (called "vinchuca" in Argentine, Uruguay, Chile and Bolivia, also known as "kissing bug" or "barber bug" in English spoken countries), which is a vector for the American trypanosomiasis and other diseases in rural areas, were studied [10-14]. Daily seven-weeks aerosolization of guinea pigs with *T. infestans* antigens (glycoproteins) induced interstitial pneumonitis as shown histopathologically, and resulted in the production of specific antibodies (IgG and IgE) by serological techniques [15]. Recently, Alonso's research group reported the successful subcutaneous immunotherapy applied to a young woman anaphylactic case after a *Pseudomyrmex acanthobius* or *P. favidulus* ant sting in Argentine [16].

Allergic diseases, such as asthma, rhinitis, rhinoconjunctivitis, and atopic dermatitis, are worldwide distributed, showing geographical variations, i.e., allergy frequency is stressed in the Tropics [17]. Therefore, characteristics of allergy and immunology in the Tropics [17], in particular in Africa [18], have been recently reported. World Health Organization (WHO) has reported on urban pests, pestborne diseases and pest management, based on contributions from international experts, highlighting the risk of developing allergic sensitization due to exposure to allergens [19].

House dust, insects and arachnids are currently related to asthma and airway diseases in urban areas of Argentine. Therefore, contributions in this field are usually welcome. The present study refers to the cockroach *Periplaneta americana* from Argentine, characterization of the whole body extract and antigenicity, together with cross-reactivity with the other cochroach *B. germanica*, the vinchuca *T. infestans*, and house dust mite *D. pteronyssinus* from Argentine.

Periplaneta americana L. (Phylum: *Arthropoda*; Class: *Insecta*; Order: *Blattodea*; Family: *Blattidae*), also called "American cockroach", "US cockroach", and "red cockroach", is native to Tropical Africa and Middle East, but it occurs in Asia (China), Oceania (Australia), and the American continent [North (USA), Central, and South America (Argentine)]. This cockroach is the largest one of all common species (mean length nearly 5 cm and about 1 cm tall). Females are higher than males (sexual dimorphism). Taxonomical controversies were in part resolved by regional entomological reports, such as an identification key of the orders of South American insects [20]. However, there are marked morphological and behavior variations in specimens from

different geographical sources, probably due to epigenetics. That is why it is relevant to study the allergens and antigenicity of cockroaches from each region.

More than 4,600 species of *Blattodea* are known and worldwide spread. The best investigated domestic cockroaches are *Periplaneta americana* and *Blattella germanica* ("German cockroach", although numerous specimen occur in USA), and the oriental cockroach (*Blatta orientalis*). These cockroaches and the "smoky brown cockroach" (*Periplaneta fuliginosa*) are the main indoor cockroach species responsible for human allergy worldwide. *Periplaneta fuliginosa* was indigenous to Japan, Southeast Asia and the Southern United States, but now is spread worldwide by infesting air and ship containers. At present, extracts from three cockroach species, *P. americana*, *Blatella germanica* and *Blatta orientalis* are commercially available [21]. The cockroaches found in Buenos Aires and surroundings are *P. americana*, *B. germanica*, and *Blaptica dubia* (Phylum: *Arthropoda*; Class: *Insecta*; Order: *Blattodea*; Family: *Blaberidae*), also called "Argentinian wood roach" that is found in Central America (Costa Rica) and South America (common from French Guiana and Brazil to Argentine). *B. dubia* is sold as feeder insect for reptiles, tarantulas and amphibians all over the world [22-24]. As far as we know, there are no reports on *B. dubia* allergy.

Various arthropod allergens have been already well characterized and some are available as recombinant molecules. Comparison of the allergens of commercially available *B. germanica* and *P. americana* cockroach extracts has been reported [25]. Also, bioassay-guided extracts of *P. americana* have been studied [26] to explain the chemotherapeutic traditional uses in southwestern China as alternative medicine.

Cockroach allergy arises mainly by powdered proteins derived from debris, secretions, and dead bodies of cockroaches, which induce IgE-mediated hypersensitivity [27].

Cockroaches are known as carriers of pathogens (bacteria, fungi and molds, viruses), several types of parasites, and other microorganisms, thus giving rise to a serious health problem because of food contamination by contact. Pathogenic bacteria have been isolated from gut contents of domestic cockroaches from household facilities, hotels and hospital pipes and sewers [28, 29]. Furthermore, mite and cockroach debris are responsible for respiratory system pathologies in responding individuals worldwide, and from Argentine.

Research on human sensitization by inhalation of mite-containing house dust was carried out in Argentine [1,2]. Mites are microscopic arachnids, whose genera vary geographically, *Dermatophagoides* being more common in temperate climates and *Blomia* being found only in tropical climates [30]. *Dermatophagoides pteronyssinus*, *Dermatophagoides farinae*, and *Euroglyphus maynei* (Phylum: *Arthropoda*; Class: *Arachnida*; Subclass: *Acari*; Superorder:

Acariformes; Family: *Pyroglyphidae*) are the three most known dust mite species, being *D. pteronyssinus* and *E. maynei* the most common in Europe, but found worldwide in humid and temperate climates. Both species of *Dermatophagoides* are common in Buenos Aires. The mean size of *D. pteronyssinus* (*Dp*) is 350 μm in length for females, and 285 μm for males. Thirty-eight allergens were characterized to date from the European house dust mite, Der p 1 to Der p 38 [31]. *D. pteronyssinus* is the dominant mite in homes, where it is found in mattresses, pillows, and carpets [32].

There is strong cross-reactivity between extracts from storage, house dust and flour mites, but little IgE cross-reactivity between house dust mites and storage mites [21]. The tropomyosin from storage mites, such as *Lepidoglyphus destructor* (Lep d 10), has a high degree of identity with Der f 10 and Der p 10 from house dust mites, showing high cross-reactivity with them [21]. The tropomyosin Lep s 1 from *Lepisma saccharina* ("silver fish") showed cross-reactivity with tropomyosin of other arthropods, such as house dust mite, cockroach, and shrimp [21].

D. pteronyssinus contains cysteine-type peptidases in its composition as previously demonstrated [2]. *D. pteronyssinus* (*Dp*) and *D. farinae* (*Df*) contain enzymes between 25 and 30 kDa, which are serine-proteases, with the characteristics of trypsin, chymotrypsin, and elastase-type [33]. Proteases cause an increase in vascular permeability, massive nonspecific release of low MW cytokines, and amplification of endothelial transmigration. All these facts are important in the genesis and maintenance of allergic inflammation.

Western blot bands of MWs about 200 kDa, 110 kDa, 65 kDa, 60 kDa, and 43 kDa showed to be involved in the specific immune response against *D. pteronyssinus* antigens in rabbits and in atopic patients. The 200 kDa band, with gelatinolytic activity, showed the greatest antigenicity against the atopics antisera and was a trypsin-like serine-peptidase by using specific inhibitors [2,33].

Therefore, *D. pteronyssinus* was demonstrated to contain two types of peptidases (cysteine and serine proteases), thus providing activity as enzymatic molecules and as intense immunogenic antigens [33].

The effects of bats and mites on respiratory system allergy have been also investigated by Alonso *et al*. [33-36]. Mites (*D. pteronyssinus*) may be ingested by bats, thus mite antigens being part of bat manure. Therefore, mites are indirectly allergenic for atopic patients, who have shown hypersensitivity to these feces [33-36].

Although this research group has carried out several studies on *Periplaneta americana* from Argentine [5, 6, 8, 9, 15, 37], more research is necessary on this subject to explain some chemical,

biochemical and medical issues related to this cockroach. The fact that cockroach sensitization plays an important role in the development of asthma and other airway diseases, and the results obtained so far encourage further investigation.

According to previous results on the chitinous exoskeleton, the extract of *P. americana* whole bodies was fractionated in order to locate the active fraction(s), based on the evaluation of the antigenicity, and specific immunoglobulins obtained by immunostimulation.

The goals of the present study are (a) fractionation and characterization of the cockroach *Periplaneta americana* extract from Argentine, and quantitation of the proteins and sugars; (b) antigenicity assessment of the chromatographic fractions of the extract; (c) analysis of cross-reactivity with the cockroach *Blattella germanica*, house dust mite *Dermatophagoides pteronyssinus* and vinchuca *Triatoma infestans* from Argentine; (c) evaluation of a three-years-vaccine therapy in allergic patients (with rhinitis syndrome/asthma).

2. Materials and Methods

2.1. Ethics Statement

The study protocol was approved by the Ethical Committee of the Facultad de Medicina, Universidad de Buenos Aires (UBA), Argentine. Written informed consent for the use of blood samples and testing was obtained from all participants (patients and controls) before study entry, according to the declaration of Helsinki.

2.2. Approval of research protocols involving patients and experimental animals

The experimental protocol was favorably analyzed by the Human Ethics Committee (*Comité de Ética Humana*: CEH), and the Committee for Care and Use of Laboratory Animals (*Comité Institucional para el Cuidado y Uso de Animales de Laboratorio*: CICUAL) of the Facultad de Medicina, UBA, in accordance with the Bioethics Committee, and the Principles of Laboratory Animal Care and Use in Research (UBA and CONICET, Argentina), respectively.

2.3. Preparation of cockroach and vinchuca extracts

Antigens. Allergenic extracts of the whole bodies of the argentinian *Periplaneta americana* and *Triatoma infestans* were prepared as previously reported [5, 6]. The whole bodies of argentinian *P. americana* were first defatted with ethyl ether. Proteins were extracted with phosphate buffered saline (PBS) (1:5, w/v) under stirring at 4°C. The crude protein extract was centrifuged at 4°C for 30 min, and the supernatant was dialyzed in PBS. Thereafter, the extract was sterilized through

0.22 μm filter membrane (Millipore, Bedford, MA, USA), and stored at -20°C. Protein content (Bradford) was assessed with bovine serum albumin as standard. The same procedure was applied to argentinian *T. infestans* for comparison purposes.

2.4. Preparation of immune rabbit sera

Adult rabbits were immunized for 13 weeks with 0.5 mL of *P. americana* extract plus 0.5 mL of the complete Freund's adjuvant as previously reported [(7)]. After 10 days of the last inoculation rabbits were bled. Sera were kept at -20 °C.

Triatoma infestans extract also developed antigenicity in rabbits, thus producing specific IgG after 8 weeks immunization, as detected by several serological techniques [(10)].

2.5. Fractionation of the extract

The *P. americana* extract (5 mL) was fractionated separately in Sephadex G-200 (22 mm x 780 mm), and DEAE-cellulose (25 mm x 380 mm) columns, eluting with 0.15 M NaCl phosphate buffers, pH 8 at 4 °C, in Sephadex, and with 0.01 M to 0.5 M, pH 8 to pH 6, in DEAE-cellulose.

2.6. Quantitation of proteins, and hexoses

Assessment of molecular weights (MWs). The proteins were quantified by the Bradford method and the sugars by the indole method on a Metrolab spectrophotometer at 280 nm and 470 nm, respectively. MWs were determined by comparison with commercial known markers of twelve recombinant unstained proteins ranging from 10 kDa to 200 kDa (Merck KGaA, Darmstadt, Germany).

2.7. Immunological techniques

Ouchterlony method [(38)], the Boyden passive hemagglutination, and immunoelectrophoresis were applied to the rabbit sera after the respective separate inoculation with cockroach *P. americana* and vinchuca *T. infestans* extracts, as previously reported [(6)]. Chromatographic fractions containing the highest protein content were also tested.

2.8. Patients

A total of 75 subjects were recruited in the study and were divided into two groups. **Group A:** 50 atopic patients (29 women and 21 men; aged 19-54 years old) with perennial

rhinitis/bronchial asthma, worsening with house dust, and positive skin test of ≥10 mm with *Dermatophagoides pteronyssinus*, residents of Buenos Aires city and surroundings. Patients were chosen according to the American Thoracic Society criteria [6]. **Group B (control group):** 25 subjects (10 women and 15 men of Buenos Aires and surroundings; aged 25-55 years old), without respiratory disease or a family history of atopy.

Peripheral venous blood was collected from each patient and control, allowed to coagulate at 4°C, and centrifuged for 15 min at 1000 *g*. Patients and controls sera were stored at -70 °C until use.

2.9. Radioimmunoassays

The paper radioimmunosorbent test (PRIST) assessed total serum IgE; values were expressed in kiloUnits per liter (normal IgE values up to 120 kU/L). The radioallergosorbent test (RAST; Phadebas, Pharmacia Laboratories) was prepared with the extracts of *P. americana* and *T. infestans* (13 mg/mL each), covalently bound to a solid phase, such as cellulose discs (SS547), under cyanogen bromide at pH 11 for 2 hours in alkaline medium. Values were expressed in PRU/mL (Phadebas RAST Units per milliliter) (> 0.35 PRU/mL were significant) [39, 40].

2.10. Sodium dodecyl sulphate polyacrylamide gel electrophoresis (SDS–PAGE)

P. americana extract (20 mcL) and standard molecular weight markers were run in 15% polyacrylamide gels in the presence of SDS (Laemmli). Upon mixing the protein sample with the tensoactive agent SDS, the proteins were unfolded into linear chains and coated with a negative charge. Proteins were separated according to size by gel electrophoresis, and were detected in gels using an ultrasensitive silver staining [41].

2.11. Western-blots [42]

After running, SDS-polyacrylamide gel electropherograms were transferred onto blotting nitrocellulose membranes. Then, the membranes were subjected for 90 min to a blocking treatment, thus preventing antibodies from binding to the membrane nonspecifically. The blocking solution was Tris-buffered saline (TBS) (10x: concentrated TBS), 50 mM Tris, 150 mM NaCl, pH was adjusted to 7.6, containing 3% dry skim milk. The blocking step reduced the background. Each membrane was then incubated with a 1/10 dilution of *Pa*-hypersensitive patient serum (anti-*Pa*; primary antibody), in phosphate buffered saline (PBS) overnight at 4°C, which was specifically bound to the antigenic protein. Any unbound primary antibody was washed away, and

the membrane was further incubated for 90 min with a 1:1000 diluted goat anti-human IgE-peroxidase conjugate (secondary antibody) at room temperature. Non-atopic sera were the negative controls. The secondary antibody was linked to a reporter enzyme for colorimetric detection. Color detection was achieved with 4-chloro-1-naphthol and hydrogen peroxide in a methanol/PBS solution. Therefore, this methodology showed to be appropriate for detecting a specific protein from a mixture of proteins.

Besides, after blocking, membranes were tested with a human serum (1:100 dilution), followed by 90-min incubation with rabbit antisera. After washing, membranes were treated for 90 min with a goat anti-rabbit IgG antibody (1:2000) coupled to phosphatase alkaline at room temperature. Sera from non-atopic subjects and normal rabbits were negative controls. For IgG- and IgE-protein extract bands recognition, membranes were incubated before and after immunotherapy by immunoblotting.

2.12. Capillary electrophoresis.

Extracts of *P. americana* and *T. infestans* were analyzed in a Bio-Focus 3000, Bio-Rad equipment (Hercules, California, USA). Capillary: 24 cm x 50 um ID; uncoated; setpoint temp: 20 °C; injection: 120 psi*sec; polarity: - to +; wavelength: single 220 nm. Electropherograms were obtained and compared.

2.13. Vaccine therapy (immunotherapy) with *P. americana* antigens.

Atopic patients received weekly subcutaneous injections of various concentrations of P. americana extract (3 mg/mL to 13 mg/mL) for 3 years, assessing serum levels of IgE and IgG-anti-*Pa*.

2.14. Statistics. Data were expressed as mean ± SEM.

All experiments were carried out in duplicate. Statistical significance between mean values was analyzed by one-way ANOVA and the Student's-*t*-test. $P < 0.05$ was considered significant.

3. Results and Discussion

The extract of *Periplaneta americana* (*Pa*) whole bodies was chromatographed yielding one broad protein peak in tubes of both Sephadex G-200 and DEAE-cellulose columns, at 280 nm absorbance. Three main peaks of hexoses were detected in tubes of the Sephadex G-200 column, and seven in the DEAE-cellulose column, by changing molarity and pH throughout the elution, at 470 μm absorbance. Quantitation yielded 42 mg/mL of proteins, and 2000 μg/mL of hexoses for

P. americana (both values greater than those found in *Triatoma infestans*), thus supporting the glycoprotein nature of *P. americana* immunogens (as those of *T. infestans*). These *P. americana* antigens showed a MW of nearly 180 kDa, and produced specific antibodies in rabbits as shown by Ouchterlony (Figure 1), Boyden, and immunoelectrophoresis.

Therefore, rabbits were immunized with the antigens of the argentinian cockroach *Pa* extract together with complete Freund's adjuvant. As it is known, the concentration of the immunoglobulin G (IgG) is higher in the serum of Freund's complete adjuvant-treated rabbits than in normal rabbit serum. Therefore, after injection of *Pa* extract antigens and Freund's adjuvant into rabbits for thirteen weeks, IgG-type circulating antibodies, precipitins and hemagglutinins were produced as detected by the double immunodiffusion Ouchterlony method, immunoelectrophoresis, and Boyden's passive hemagglutination.

Anti-*Pa* antibodies were analyzed against the antigens of *Blattella germanica* (*Bg*) and *P. americana* (*Pa*) extract, and also against the mite *Dermatophagoides pteronyssinus* (*Dp*) antigens. The IgG in the rabbit antiserum against *Pa* (anti-*Pa* serum) showed the highest reactivity to Bg and *Pa* extracts. No reactivity to *Dp* was detected in the Ouchterlony system (Figure 1).

Precipitation bands with total and partial identities were observed between the antiserum (anti-*Pa* rabbit serum) and antigens from *B. germanica* extract in an Ouchterlony system (figure not shown), thus showing immunological cross-reaction of both cockroach extracts. Also, specific antibodies (titer 1/1024) were detected by Boyden. Matching bands were detected by isoelectric focusing of *P. americana* and *B. germanica* extracts, the most significant correlation accounting for *p*I of 4.5.

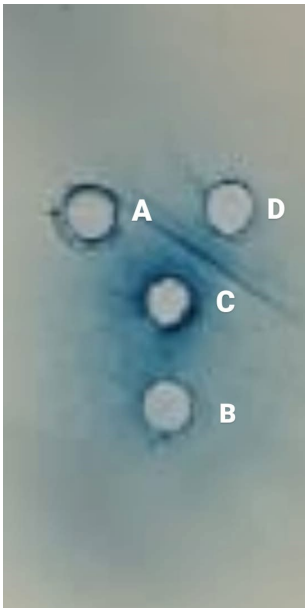

Figure 1. Precipitation bands. Mite extract (**A**); physiological solution (**B,** negative control); rabbit serum anti-*Pa* antibodies (**C**); and *Periplaneta americana* extract (**D).**

Ouchterlony revealed two precipitin lines in the *Pa*-anti-*Pa* system. Therefore, two precipitation bands were detected between the serum rabbit anti-*Pa* (C) and the extract of *P. americana* (*D*) (Figure 1). So that, the rabbit serum antibodies recognized and bound to the antigens of the *P. americana* extract, forming two immune complexes due to antigen-antibody reactivity that gave two precipitin lines. Immunoelectrophoresis also showed precipitation bands between anti-*Pa* rabbit serum and *P. americana* extract accounting for IgG.

Non-precipitation against the mite extract (*A*) was observed, as occurred with the negative control (*B*) (Figure 1). Therefore, anti-*Pa* serum did not contain antibodies against mite extract antigens. These results supported the fact that the mite extract antigens are likely to produce type I reactions instead of circulating IgG class antibodies.

These results are in agreement with the IgE cross-reactivity reported between cockroach and house dust mite allergens in Chinese patients with allergic rhinitis and asthma [(43)].

IgE is usually associated with allergy. However, many allergic reactions are not dependent on IgE and occur even in the absence of allergen specific and also total IgE. In these instances, IgG plasma cells are involved in induction, and pathogenesis of allergic diseases as recently reported [(44)].

Previously, a poor rabbit immunization with mite extract was reported [(1)], thus resulting in only one slight precipitin band by the Ouchterlony technique, and a 1:20 titer of hemagglutinating antibodies. Also, immunotherapy due to human sensitization by *Dermatophagoides* species is difficult to apply. Nevertheless, there are some reports on house dust mite subcutaneous and sublingual allergen immunotherapy, but more rigorous, long-term, double-blind, placebo-controlled randomized clinical trials are required [(45)].

The cockroach *Periplaneta americana* (*Pa*) and the reduviid *Triatoma infestans* (*Ti*) are strongly immunogenic arthropods for animals and for atopic patients [(11)]. Several immunoserological procedures, and also capillary electrophoresis were applied in order to establish the occurrence of common glycoprotein epitopes in both insects. Specific antibodies (IgG

and IgE) were detected in rabbit and human sera. RAST and RAST-inhibition supported cross-reactivity between both antigens. Capillary electrophoresis of *P. americana* extract was carried out in our laboratories (Figure 2).

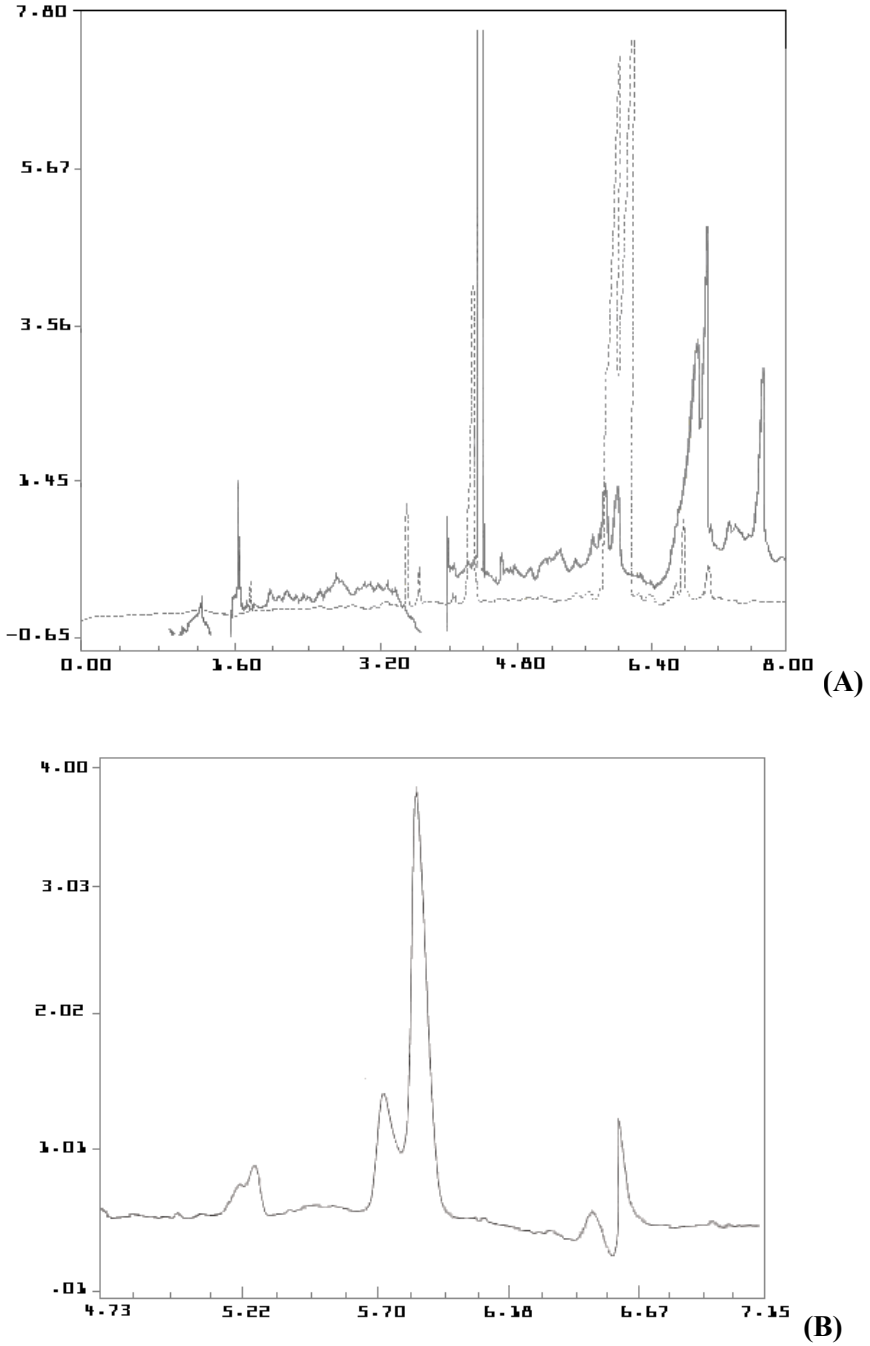

Figure 2. Capillary electrophoresis of the argentinian *Periplaneta americana* extract. (**A**) Electropherograms of *P. americana* extract (solid line), and *Triatoma infestans* extracts (adult insects) (dotted line). (**B**) Electropherogram of *P. americana* extract, from 4.73 to 7.15 min run.

The overlapping of both electropherograms showed that some *T. infestans* peaks matched those of *P. americana* (Figure 2A), which accounted for some epitopes in common between *P. americana* and *T. infestans* proteins, in agreement with previous reports on the basis of absorption techniques, RAST inhibition, and isoelectric focusing [(10)].

Furthermore, electropherograms (Figure 2) showed to be distinctive for each argentinian insect, *P. americana* and *T. infestans*, being therefore appropriate to characterize each extract under study. Consequently, the complete electropherogram of *P. americana* extract is shown in Figure 2A, while the insert from 4.73 to 7.15 min run of this extract is shown in Figure 2B. So that the argentinian *P. americana* extract under study has been characterized according to the protein electropherogram for comparison purposes with *P. americana* extracts from other sources. Likewise for the argentinian *T. infestans* extract (Figure 2B, dotted line).

The outcome of the vaccine therapy application to allergic patients and controls over three-years was assessed by measuring total immunoglobulin E (IgE) by PRIST, and specific serum IgE and IgG values before and after immunotherapy using RAST (see Materials and Methods) that is a blood radioimmunoassay currently used for detection of patient's serum specific IgE antibodies for allergens. In this instance, allergens are those present in the argentinian *P. americana* and *T. infestans* extracts.

In fact, IgE is the antibody associated with type I allergic response. Allergens (each *P. americana* and *T. infestans* extract) are covalently bound to a solid phase (cellulose discs) and further incubated with the serum of the allergic patient. The serum IgE antibodies are specific to the allergen, and are cross-linked with the immobilized allergen. Afterwards, the percentage of IgE binding to the immobilized allergenic proteins was detected by using a radioactively labeled secondary antibody (labeled anti-human IgE) [(39, 40)].

Radioallergosorbent test inhibition (RAST inhibition) was established for assessing specificity, just preventing the reaction of the IgE-containing serum with the solid phase. If the

serum is preincubated with a varying amount of insect extract, then the protein interferes with the binding of the serum to the adsorbed proteins. This procedure is called the inhibition assay [39, 40].

The total serum IgE baseline mean value of patients and controls under study was 230.50 kU/L. The mean specific IgE value in the immunotherapy group was, before treatment: 0.985 PRU/mL; and after three-years-treatment: 0.29 PRU/mL; $p < 0.02$. The specific IgE in the control group accounted for 1.02 PRU/mL; and IgE-Rast-anti *Pa* after three-years-treatment: 1.12 PRU/mL.

The specific serum IgG values before and after immunotherapy accounted for: IgG-RAST baseline value in the immunotherapy group, before treatment: 36.85 IU/mL; and after three-years-treatment: 216.42 IU/mL; $p < 0.001$. The IgG-RAST baseline value in the control group was 48.6 IU/mL; and after three-years-treatment: 66 IU/mL.

According to the results, the detection of IgE in serum of allergic patients after immunotherapy with the argentinian *P. americana* extract decreased, while the specific IgG was increased, in agreement with previous reports [6].

The *P. americana* extract yielded silver stained protein bands by SDS-PAGE in the range 20-220 kDa. Proteins accounting for 160, 90, and 42/46 kDa were recognized as allergenic by the patient serum prior to desensitization treatment by electroblotting. After three-years-immunotherapy, the total IgE serum values decreased and the specific IgE-double bands (42/46 kDa) disappeared, showing their allergenic relevance.

Also, after three-years-treatment the symptom scores and the serum levels of the interleukins IL-2, IL-4 and IL-4R were reported to be lower than at the beginning of the treatment [37].

Several reports on the clinical efficiency of immunotherapy are known. Recently, cockroach allergy and allergen immunotherapy have been reported [46]. The clinical response to specific immunotherapy was associated in some house dust mite allergic patients (asthma/allergic rhinitis) with decreased cysteinyl leukotriene releasibility by blood leukocytes [47].

Immunotherapy has been also reported to prevent an allergic disease progression and the development of new sensitization, especially in children [48]. House dust mite sublingual immunotherapy showed to be effective after one-year-treatment on allergen-specific nasal and skin reactivity, but not in reducing rhinoconjunctivitis symptoms, in children with perennial allergic rhinitis and conjunctivitis symptoms mono-sensitized to the mites *Dermatophagoides pteronyssinus* and *D. farinae* [49].

Clinical improvement in patients with asthma and rhinitis after immunotherapy with cockroach extract was associated with immunological changes [50]. After one year treatment, specific IgE levels slightly decreased, while IgG4 levels increased significantly in the immunotherapy group in distinct bands. Also increase in IgG4/IgG1, and decrease in symptoms score of the patients were correlated after immunotherapy [50]. X-ray of some crystalline allergens, together with allergen disease markers and new immunotherapy designs also supported decrease in asthma symptoms and severity [51].

A guideline on allergen-specific immunotherapy in IgE-mediated allergic diseases has been reported by German, Austrian and Swiss allergy associations, together with scientific societies and professional specialists associations, according to the criteria of the Association of the Scientific Medical Societies in Germany [52].

Allergen-specific immunotherapy has been recently reported as effective for treatment of mice allergic to *Periplaneta americana* with a liposome-entrapped vaccine composed of mouse Tregitopes (regulatory T-cell epitopes present in the heavy and light chains of IgG) 289 and 167, each with the cockroach allergen Per a 9, and Per a 9 alone [53]. All these treatments reduced allergen-induced airway tissue inflammation and remodeling, *via* different mechanisms.

Cockroach allergy has been recognized as important IgE-mediated type I hypersensitivity since 1964 [54]. Cockroach, like other allergens, contains trypsin-like enzyme activity that contributes to allergenicity and airway inflammation by activating proteinase-activated receptors (PARs) (activation of calcium signaling and/or ERK1/2 phosphorylation *via* PAR2). Three serine

proteinases (endopeptidases) were recently identified in *Blattella germanica* that may, *via* PAR2 activation, play different roles for allergen sensitization *in vivo* [55]. PAR-2, Toll-like receptor (TLR), and C-type lectin receptors seem to be important for cockroach allergens to get into epithelial cells to mediate allergen uptake, dendritic cell maturation, antigen-presenting cell (APC) function in T-cell polarization, and cytokine production [56].

The arthropod allergens and their use as allergy markers for diagnosis have been reported [21]. Glutathione *S*-transferases (GST) from arthropods can elicit allergic reactions. The allergen Per a 5, a GST from *P. americana*, was cloned [57]. Two GST homologue (Per a 5) genes are available in the Genbank, providing the possibility of producing recombinant Per a 5 (rPer a 5) in order to study its role in allergic reactions. Classes, isoforms, and allergenicity of GST of *P. americana* have been recently reported [58].

WHO/IUIS allergen nomenclature database [31] is the official site for the systematic allergen nomenclature that is approved by the World Health Organization (WHO) and International Union of Immunological Societies (IUIS) Allergen Nomenclature Sub-committee. This allergenic proteins database contains important allergens from *Blatella germanica* and *P. americana* cockroaches: Bla g 1–11 and Per a 1–10. These cockroach allergens can be subdivided into more than 10 protein groups on the basis of highly varying physiological functions. They have been identified in cockroach faeces, eggs or exoskeletons.

The search of *Periplaneta americana* found 37 items in the Allergome Database [59], which accounted for Per a 1 to Per a 13, developed as: Per a; Per a 1 (Per a 1.0101; Per a 1.0102; Per a 1.0103; Per a 1.0104; Per a 1.0105; Per a 1.0201); Per a 2 (Per a 2.0101); Per a 3 (Per a 3.0101; Per a 3.0201; Per a 3.0202; Per a 3.0203); Per a 4; Per a 5 (Per a 5.0101; Per a 5.0102); Per a 6 (Per a 6.0101); Per a 7 (Per a 7.0101; Per a 7.0102; Per a 7.0103); Per a 8; Per a 9 (Per a 9.0101); Per a 10 (Per a 10.0101), Per a 11 (Per a 11.0101), Per a 12 (Per a 12.0101); Per a 13 (Per a 13.0101); Per a FABP (Fatty Acid Binding Protein, Lipocalin). Homologous, possibly cross-reactive allergens have been described in cockroach species [59].

Also a Compare Allergen Database is available online [60], which lists clinically relevant and peer-reviewed protein allergens with bibliography and species identification.

4. Conclusions

Arthropods are a widespread phylum that comprises varied members, such as insects, arachnids, centipedes and crabs. Common allergies are usually related to house dust mites and cockroaches. Routine diagnosis of arthropod allergy is carried out by skin prick tests and/or specific IgE antibody assays in extracts.

In the present paper extracts of the argentinian cockroach *Periplaneta americana* were fractionated by sequencial column chromatography yielding allergenic glycoprotein fractions in the range of 20-200 kDa. Therefore, the glycoprotein nature of the antigens from *P. americana* extract was demonstrated.

Allergens are composed of a variety of enzymes that enable natural biological processes. These enzymes are a source of several airway diseases and production of specific antibodies.

Cockroach allergy has been often associated with asthma and rhinitis in patients of Argentine. Therefore, the antigenicity, allergenicity, and specificity of *P. americana* glycoproteins were tested by using rabbit antisera. In addition, both immunoglobulins, IgE and IgG, were detected in rabbit and atopic human sera treated with *P. americana* extract, after immunization with it.

The cross-reactivities of *Blatella germanica* and *P. americana* as well as *Triatoma infestans* and *P. americana* were assessed, supporting previous reports of Alonso's research group (see Results and Discussion).

Since rabbits were immunized with complete Freund's adjuvant and each insect extract (see Material and Methods), the presence of the adjuvant ensured the prevalence of circulating IgG antibodies. Consequently, when testing *P. americana* extract against the antiserum two precipitin lines of different intensity were obtained, indicating IgG antibodies besides IgE. However, the lack of precipitation bands in the case of the *Dermatophagoides pteronyssinus* house dust mite extract showed that the immune response of this house mite dust occurs mainly through IgE type I reactions, and not circulating IgG antibodies.

Various allergic diseases have been treated for years by immunotherapy. The immunogenic properties of *P. americana* extract have been also evaluated by vaccine therapy. After three-years-treatment, optimal outcomes were recorded in atopic patients.

Some conclusions of this study are,

(a) The results show that atopic patients are exposed to dangerous immunogenicity when going to rural areas due to the demonstrated cross-reactivity between the urban cockroach *P. americana* and the rural vinchuca *T. infestans*.

(b) Immunotherapy has shown to be effective for the treatment of allergic patients (asthma/rhinitis).

(c) Capillary electrophoresis of *P. americana* and *T. infestans* showed matching of some bands supporting the occurrence of common epitopes.

(d) In addition, capillary electrophoresis was demonstrated to be a useful tool for characterization of allergenic insect extracts from different sources.

(e) At last, allergens are useful in routine allergy diagnosis as disease markers.

(f) The prevalence of specific IgE-antibodies to cockroach allergens varies considerably, depending on geographical regions and regional exposure to cockroach allergens.

The question arises whether the cockroach species of *P. americana* from the northern hemisphere, and even from specific regions, are the same as those found in Buenos Aires and other areas of Argentine. There may be variations in cockroach species and allergens depending on geographic location. Further investigation is being carried out.

Acknowledgements

We thank the Hospital de Clínicas and Universidad de Buenos Aires (Argentina) for the research facilities support; Ministerio de Ciencia, Tecnología e Innovación Productiva (Mincyt, Argentina) for electronic library facilities. A.B.P. is a Senior Research Member of CONICET.

Conflicts of Interest

The authors declare that there are no conflicts of interest.

References

(1) Alonso, A.; Scavini, L.M.; Rodríguez, S.M.; Pionetti, C.H. *Allergol. Immunopathol. (Madr.)* 1980, 8, 111-116.

(2) Irañeta, S.; Albónico, J.; Alonso, A. *J. Invest. Allergol*. Clin. Immunol. 1999, 9, 235-240.

(3) Alonso, A. *Polutantes ambientales no convencionales.* [Unconventional environmental pollutants]. Article in Spanish. https://www.ciencias.org.ar/user/DOCUMENTOS/Cucarachas y vinchucas en patología respiratoria.pdf. Accessed on 18 January 2020.

(4) Alonso, A.; Seoane, M.A.; Irañeta, S.G.; Scavini, L.M.; Rodríguez, S.M.; Marino, G.A. *Allergol. Immunopathol. (Madr.)* 1989, 17, 307-311.

(5) Albónico, J.F. Propiedades inmunoquímicas de los antígenos de la *Periplaneta americana* y su vinculación con la rinitis y el asma bronquial. [Immunochemical properties of the antigens of the *Periplaneta americana* and its connection with rhinitis and bronchial asthma]. *Tesis de Doctorado en Medicina*. Ph.D. Thesis in Medicine in Spanish. División Alergia, Departamento de Medicina, Hospital de Clínicas "José de San Martín", Facultad de Medicina, Universidad de Buenos Aires. Director de Tesis: Prof. Alonso, A., Buenos Aires, Argentina, 1993.

(6) Alonso, A.; Albónico, J.F.; Scavini, L.M.; Rodríguez, S.M.; Pionetti, C.H.; Mouchián, K. *Allergol. Immunopathol. (Madr.)* 1987, 15, 109-115.

(7) Alonso, A.; Albónico, J.F.; Scavini, L.M.; Rodríguez, S.M.; Pionetti, C.H.; Mouchian, K. *Rev. Hosp. Clín. (B. Aires)* 1988, 4, 15-25.

(8) Alonso, A.; Albónico, J.F.; Mouchián, K.; Pionetti, C.H. *Prensa Méd. Argent.* 1993, 80, 589-593.

(9) Alonso, A.; Albónico, J.F., Mouchián, K., Scavini, L.M. *Ann. Allergy (Abst.)* 1995, 74, 78.

(10) Alonso, A.; Marino, G.A.; Scavini, L.M.; Rodríguez, S.M. *J. Investig. Allergol. Clin. Immunol.* 1992, 2, 154-161.

(11) Alonso, A; Albónico, J.F.; Rodríguez, S.M.; Mouchián, K.; Marino, G.A.; Scavini, L.M. *J. Investig. Allergol. Clin. Immunol.* 1996, 6, 301-306.

(12) Alonso, A.; Potenza, M.; Crespo, O.; Rodríguez, S. *An. Soc. Cient. Argent.* 2003, 232, 23-38.

(13) Alonso, A.; Irañeta, S.G.; Rodríguez, S.R.; Mouchián, K.; Albónico, J.F. *An. Soc. Cient. Argent.* 2011, 244, 21-35.

(14) Alonso, A.; Albónico, J.F.; Mouchián, K.; Rodríguez, S.R.; Irañeta, S.G.; Pionetti, *C.H. Rev. Asoc. Méd. Argent.* 2014, 127, 22-31.

(15) Alonso, A.; Caccuri, R.L.; Scavini, L.M.; Rodríguez, S.M.; Marino, G.A. J. *Investig. Allergol. Clin. Immunol.* 1994, 4, 197-202.

(16) Rodriguez, R.M.; Irañeta, S.G.; Olgiati, M.L.; Soprano, L.L.; Mouchián, K.; Alonso, A.; *Integr. Mol. Med.* 2018, 5, 1-4.

(17) Caraballo, L.; Zakzuk, J.; Lee, B.W.; Acevedo, N.; Soh, J.Y.; Sánchez-Borges, M.; Hossny, E.; García, E.; Rosario, N.; Ansotegui, I.; Puerta, L.; Sánchez, J.; Cardona, V. *World Allergy Organ. J.* 2016, 9, 20.

(18) El-Gamal, Y.M.; Hossny, E.M.; El-Sayed, Z.A.; Reda, S.M. *J. Allergy Clin. Immunol.* 2017, 140, 1240-1243.

(19) Perzanowski, M.S.; Chew, G.L.; Aalberse R.C.; de Blay, F. Chapter 1. Allergic asthma, 7-33. In: Bonnefoy, X.; Kampen, H.; Sweeney, K. *Public Health Significance of Urban Pests.* WHO. European Centre for Environment and Health, Bonn. WHO Regional Office for Europe, Copenhagen, Denmark, 2008.

(20) Bachmann, A.O. *Rev. Soc. Entomol. Argent.* 1967, 29, 11-16.

(21) Hilger, C.; Kuehn, A.; Raulf, M.; Jakob, T. *Allergo J. Int.* 2014, 23, 172-178. Correction: *Allergo J. Int.* 2014, 23, 281.

(22) Hintze-Podufal, C.; Vetter, R. *Entomol. Gener.* 1996, 20, 169-175.

(23) Todorović, D.; Ilijin, L.; Mrdaković, M.; Vlahović, M., Filipović, A., Grčić, A., Perić-Mataruga, V. *Int. J. Radiat. Biol.* 2019, 95, 1185-1193.

(24) Taxonomy browser (*Blaptica dubia*). *Taxonomy ID 132935*. *National Center for Biotechnology Information*. Accessed on January 2020.
https://www.ncbi.nlm.nih.gov/Taxonomy/Browser/wwwtax.cgi?id=132935.

(25) Patterson, M.L.; Slater, J.E. *Clin. Exp. Allergy* 2002, 32, 721-727.

(26) Wang, X.-Y.; He, Z.C.; Song, L.-Y.; Spencer, S.; Yang, L.X.; Peng, F.; Liu, G.-M.; Hu, M.-H.; Li, H.B.; Wu, X.-M.; Zeng, S.; Hilgenfeld, R.; Stöckigt, J.; Zhao, Y.; Qian, J.F. *Cancer Ther.* 2011, 10, NP12-NP23.

(27) Eggleston, P.A. *J. Allergy Clin. Immunol.* 2003, 112, 265-267.

(28) Bennett, G. *Lancet* 1993, 341, 732.

(29) Arwa, H.M.A.M.; Eltaib, S.A.L.; Yassir, M; Amina, E.M. *Amer. J. Res. Commun*. 2018, 6, 33-52.

(30) Arlian, L.G.; Morgan, M.S.; Neal, J.S. *Curr. Allergy Asthma Rep*. 2002, 2, 401-411.

(31) www.allergen.org. World Health Organization (WHO) and International Union of Immunological Societies (IUIS) Allergen Nomenclature Database. Accessed on 18 January 2020.

(32) Dhooria, M.S. *Fundamentals of Applied Acarology*. Springer, Singapore, 2016.

(33) Alonso, A.; Mouchián, K.; Soto, M.M.; Albónico, J.F.; Pionetti, C.H.; Rodríguez, S.R.; Irañeta, S.G. *Rev. Asoc. Méd. Argent*. 2014, 127, 19-26.

(34) Alonso, A.; Irañeta, S.; Rodríguez, S.; Scavini, L. *J. Invest. Allergol. Clin. Immunol*. 1998, 8, 365-369.

(35) Alonso, A.; Mouchián, K.; Potenza, M.; Bignone, M.L. *Allergol. Immunopathol. (Madr.)* 2003, 31, 215-220.

(36) Alonso, A.; Potenza, M.; Mouchián, K.; Albónico, J. *Allergol. Immunopathol. (Madr.)* 2003, 31, 278-281.

(37) Alonso, A.; Albónico, J.F.; Mouchián, K.; Scavini, L.M.; Irañeta, S.G.; Pionetti, C.H. *J. Investig. Allergol. Clin. Immunol.* 1999, 9, 299-304.

(38) Bailey, G.S. 135: Ouchterlony Double Immunodiffusion. In: Walker, J.M. (ed.). *The Protein Protocols Handbook.* VII: *Immunochemical Techniques*. Humana Press, New Jersey, 1996, pp. 749-752.

(39) Hamilton, R.G. Assessment of human allergic diseases. In: Rich, R.R.; Fleisher, T.A.; Shearer, W.T.; Schroeder Jr., H.W.; Frew, A.J.; Weyand; C.M. (eds.), *Clinical Immunology: Principles and Practice*. Fourth Edition, Chapter 97, Part eleven: *Diagnostic Immunology*. Elsevier Ltd., printed in China, pp. 1192-1201, 2013.

(40) Rich R.R.; Fleisher, T.A.; Shearer, W.T.; Schroeder, H.; Frew, A.J.; Weyand; C.M. (eds.), *Clinical Immunology: Principles and Practice*. Fifth Edition, Chapter 97, Part eleven: *Diagnostic Immunology*. Elsevier, Canada, 2019.

(41) Oakley, B.; Kirsch, D.; Morris, R. *Anal. Biochem*. 1980, 105, 361-363.

(42) Mahmood, T.; Yang, P.-C. *N.* Am. *J. Med. Sci*. 2012, 4, 429-434.

(43) Sun, B.Q.; Lai, X.X.; Gjesing, B.; Spangfort, M.D.; Zhong, N.S. *Chin. Med. J*. 2010, 123, 3540-3544.

(44) Scott-Taylor, T.H.; Axinia, S.-C.; Amin, S.; Pettengell, R. *Immun. Inflamm*. Dis. 2018, 6, 13-33.

(45) Calderon, M.A.; Casale, T.B.; Nelson, H.S.; Demoly, P. *J. Allergy Clin. Immunol*. 2013, 132, 1322-1336.

(46) Kleine-Tebbe, J.; Hamilton, R.G.; Goodman, R.E. *J. Allergy Clin. Immunol*. 2019, 143, 1342-1344.

(47) Saraçlar, Y.; Sekerel, B.E.; Kalayci, O.; Adalioğlu, G.; Tuncer, A. *J. Investig. Allergol. Clin. Immunol*. 1998, 8, 98-104.

(48) Boquete, M.; Carballada, F.; Expósito, F.; González, A.L. *Allergol. Immunopathol. (Madr.)* 2000, 28, 89-93.

(49) Aydogan, M.; Eifan, A.O.; Keles, S.; Akkoc, T.; Nursoy, M.A.; Bahceciler, N.N.; Barlan, I.B. *Respir. Med.* 2013, 107, 1322-1329.

(50) Srivastava, D.; Gaur, S.N.; Arora, N.; Singh, B.P. *Eur. J. Clin. Invest.* 2011, 41, 879-888.

(51) Pomés, A.; Mueller, G.A.; Randall, T.A.; Chapman, M.D.; Arruda, L.K. Curr. *Allergy Asthma Rep*. 2017, 17, 25.

(52) Pfaar, O.; Bachert, C.; Bufe, A.; Buhl, R.; Ebner, C.; Eng, P.; Friedrichs, F.; Fuchs, T.; Hamelmann, E.; Hartwig-Bade, D.; Hering T.; Huttegger, I.; Jung, K.; Klimek, L.; Kopp, M.V.; Merk, H.; Rabe, U.; Saloga, J.; Schmid-Grendelmeier, P.; Schuster, A.; Schwerk, N., Sitter, H., Umpfenbach, U.; Wedi, B.; Wöhrl, S.; Worm, M.; Kleine-Tebbe, J. Commenting Participants and Facilitators: Kaul, S.; Schwalfenberg, A. *Allergo J. Int.* 2014, 23, 282-319.

(53) Prangtaworn, P.; Chaisri, U.; Seesuay, W.; Mahasongkram, K.; Onlamoon, N.; Reamtong, O.; Tungtrongchitr, A.; Indrawattana, N.; Chaicumpa, W.; Sookrung, N. *Nature - Sci. Rep*. 2018, 8, 15480.

(54) Bernton, H.S; Brown, H. *J. Allergy* 1964, 35, 506-513.

(55) Polley, D.J.; Mihara, K.; Ramachandran, R.; Vliagoftis, H.; Renaux, B.; Saifeddine, M.; Daines, M.O.; Boitano, S.; Hollenberg, M.D. *Clin. Exp. Allergy* 2017, 47, 946-960.

(56) Do, D.C.; Zhao, Y.; Gao, P. *Allergy* 2016, 71, 463-474.

(57) Wei, J.-F.; Yang, H.; Li, D.; Gao, P.; He, S. *Mediators Inflamm*. 2014, 2014, ID 591468.

(58) Sookrung, N.; Reamtong, O.; Poolphol, R.; Indrawattana, N.; Seesuay, W.; Saelim, N.; Tantilipikorn, P.; Bunnag, C.; Chaicumpa, W.; Tungtrongchitr, A. *Nature - Sci. Rep*. 2018, 8, 484.

(59) www.allergome.org. The Platform for Allergen Knowledge. The Allergome Team. Accessed on 18th January 2020.

(60) https://comparedatabase.org. COMPARE, Comprehensive Protein Allergen Resource. Allergen Database. Accessed on 18th January 2020.

Anales de la Asociación Química Argentina

STRUCTURAL AND SPECTROSCOPIC PROPERTIES OF SOME DOUBLE OXALATES CONTAINING Mg(II) AND A DIVALENT FIRST ROW TRANSITION METAL CATION

María M. Torres [1,2], Daniel Palacios [1,2], Ana C. González-Baró [3], Vicente L. Barone [3] and Enrique J. Baran [3,*]

[1] *Departamento de Ciencias Exactas y Naturales, Universidad Nacional de la Patagonia Austral, 9400-Río Gallegos, Argentina.*

[2] *Departamento de Ciencias Básicas, UTN-Facultad Regional Santa Cruz, 9400-Río Gallegos, Argentina.*

[3] *Centro de Química Inorgánica (CEQUINOR, CONICET/UNLP), Facultad de Ciencias Exactas, Universidad Nacional de La Plata, Bvd.120 N° 1465, 1900-La Plata, Argentina.*

[*] *Autor Corresponsal E-mail: baran@quimica.unlp.edu.ar*

Resumen

Se preparó y caracterizó una serie de oxalatos dobles de estequiometría $MgM(C_2O_4)_2 \cdot 4H_2O$ (con M = Mn, Fe, Co, Ni, Zn). Su comportamiento estructural fue investigado por medio de difractometría de rayos X en polvos, mostrando una fuerte analogía estructural con la llamada forma-β, de los oxalatos complejos simples de composición $M(C_2O_4)_2 \cdot 2H_2O$. El comportamiento espectroscópico vibracional de estos oxalatos dobles fue investigado por espectroscopía de infrarrojo y Raman. Los resultados estructurales y espectroscópicos confirmaron claramente las fuertes analogías estructurales existentes entre esta nueva serie de oxalatos dobles y los de estequiometría $MM'(C_2O_4)_2 \cdot 4H_2O$, α-$MC_2O_4 \cdot 2H_2O$ y β-$MC_2O_4 \cdot 2H_2O$.

Abstract

A series of double metal oxalates of stoichiometry $MgM(C_2O_4)_2 \cdot 4H_2O$ (with M = Mn, Fe, Co, Ni, Zn) have been prepared and characterized. Their structural behavior was investigated by means of X-ray powder diffractometry, showing a strong structural analogy to the so-called β-modification of the related simple oxalate complexes of composition $M(C_2O_4)_2 \cdot 2H_2O$. The vibrational spectroscopic behavior of these double metal oxalates was investigated by infrared and Raman spectroscopy. The structural and spectroscopic

results clearly confirmed the strong structural analogies between this new series of double oxalates and those of $MM'(C_2O_4)_2{\cdot}4H_2O$, α-$MC_2O_4{\cdot}2H_2O$ y β-$MC_2O_4{\cdot}2H_2O$ stoichiometry.

Palabras clave: Oxalatos metálicos dobles conteniendo Mg(II); difractometría de rayos X en polvos; características estructurales; espectros de IR y Raman; comportamiento vibracional.

Keywords: Double metal oxalates containing Mg(II); X-ray powder diffractometry; structural characteristics; IR and Raman spectra; vibrational behavior.

1. Introduction

Oxalates are of considerable interest because many of them exist as natural minerals and, in addition, in coordination chemistry the oxalate anion can adopt different coordination modes to bind metals to form infinite chains, sheets and networks, leading to a very rich structural chemistry [1-3].

In recent years we have investigated the vibrational-spectroscopic behavior of different oxalate complexes of the type $M^{II}C_2O_4{\cdot}2H_2O$ [4-7]. The complexes with M^{II} = Mg, Fe, Co and Ni present two polymorphic forms called α-modification (monoclinic, space group C2/c, Z = 4) and β-modification (orthorhombic, space group Cccm, Z = 8). They are generated from a bidimensional structural arrangement in which the oxalate anions act as tetradentate ligands, interacting with two vicinal M^{II} cations. The structure is completed with two water molecules, above and below each cation, generating an approximately octahedral $M^{II}O_6$ coordination sphere around each metal center. The two polymorphic forms originate from small differences in the stacking pattern of the three-dimensional pile up of successive sheets, which causes a rearrangement of the hydrogen bonds between the sheets [1,8].

Most recently, we have also investigated the structural and spectroscopic behavior of different double metal oxalates of composition $MM'(C_2O_4)_2{\cdot}4H_2O$ (M and M' different divalent metal cations of the first row transition metal series). It was found that these complexes show a strong structural analogy to the orthorhombic, so-called β-modification, of the related simple oxalato complexes of composition $MC_2O_4{\cdot}2H_2O$ [9]. This founding was highly surprising because in these simple oxalates the modification is the thermodynamically most stable form [1,8].

In order to attain a wider insight into the general behavior of these mixed-metal oxalates we have now investigated a series of complexes containing simultaneously Mg(II) and one first row divalent transition metal cation. These systems are specially interesting in the discussed

context, because α-$MgC_2O_4 \cdot 2H_2O$ is easily obtained whereas the corresponding β-modification is relatively difficult to generate [6,10].

The following complexes were prepared and analyzed: $MgMn(C_2O_4)_2 \cdot 4H_2O$, $MgFe(C_2O_4)_2 \cdot 4H_2O$, $MgCo(C_2O_4)_2 \cdot 4H_2O$, $MgNi(C_2O_4)_2 \cdot 4H_2O$ and $MgZn(C_2O_4)_2 \cdot 4H_2O$. Attempts to obtain pure samples of the similar Cu(II) complex, $MgCu(C_2O_4)_2 \cdot 4H_2O$, were unsuccessful despite the numerous variations in the synthetic procedure that were performed (cf. also [9]).

2. Materials and Methods

2.1. Synthesis of the compounds

The investigated double oxalates, of composition $MgM(C_2O_4)_2 \cdot 4H_2O$ were prepared as follows: To 20 mL of an aqueous 0.2 M solution of $MCl_2 \cdot nH_2O$ at ~ 90 °C, 20 mL of a hot (ca. 90 °C) 0.8 M solution of oxalic acid was added with stirring. To this solution, 20 mL of a hot aqueous solution of 0.2 M $M'Cl_2 \cdot nH_2O$ was dropwise added. After a few minutes the complexes precipitated out. They were separated by filtration, washed with hot water and finally dried in vacuum over H_2SO_4. The purity of the obtained complexes was checked by elemental analysis (C and H) using a Carlo Erba model EA 1108 elemental analyzer. The water content was determined, independently, by heating a known sample amount to a constant weight at 100 °C, 120 °C, and 150 °C and determining the loss of weight.

2.2. X-ray powder diagrams

The obtained complexes were characterized by X-ray powder diffractometry, with a Rigaku-Denki diffractometer and monochromatic (Ni-filtered) Cu-Kα radiation (λ = 1.5418 Å), using NaCl as an external calibration standard.

2.3. Vibrational spectra

The infrared spectra, in the spectral range between 4000 and 400 cm-1, were recorded with a FTIR-Bruker-EQUINOX-55 spectrophotometer, using the KBr pellet technique. Raman spectra were obtained in the same spectral range with a Thermo Scientific DXR Raman microscope, using the 532 nm line of a Thermo Scientific solid-state laser diode pump for excitation.

3. Results and Discussion

3.1. Structural characteristics

As mentioned in the Introduction, the dihydrated metal oxalates of stoichiometry $M^{II}(C_2O_4)\cdot 2H_2O$, with M^{II} = Mg, Fe, Co and Ni present two polymorphic forms, called α- and β-modifications. Thermodynamically, the α-modification is the most stable form and the $\beta \rightarrow \alpha$ transformation is irreversible [1,11].

The structural characteristics of the now prepared double-metal oxalates were derived from the analysis of the corresponding X-ray powder diffractograms. These diagrams are practically identical for the full series of complexes, and show again a close relationship to that of the β-modification of the $M^{II}(C_2O_4)\cdot 2H_2O$ complexes.

These relationships become clearly evident by inspection of the diagrams presented in Figure1. In this figure, we have compared the X-ray powder diagrams of α-$CoC_2O_4\cdot 2H_2O$ [12] with those of the respective β-modification [12], the now prepared $MgCo(C_2O_4)_2\cdot 4H_2O$ oxalate and the previously investigated $MnCo(C_2O_4)_2\cdot 4H_2O$ [9]. As can be seen, both double metal oxalates, that containing Mg(II) and the $MnCo(C_2O_4)_2\cdot 4H_2O$ present very similar X-ray powder diagrams, which also resemble that of β-$CoC_2O_4\cdot 2H_2O$.

These comparisons strongly suggest that all the new oxalates of stoichiometry $MgM(C_2O_4)\cdot 4H_2O$ also belong to the β-modification of the simple $M(C_2O_4)\cdot 2H_2O$ metal oxalates.

3.2. Vibrational spectra

In our previous papers we have demonstrated that the vibrational (IR and Raman) spectra of the α- and β-modifications of the $M(C_2O_4)\cdot 2H_2O$ complexes are totally identical, confirming the close structural relationship between them [4-7]. Therefore, this methodology is not useful to distinguish between these two polymorphic forms.

The FTIR spectra of the previously prepared $MM'(C_2O_4)2\cdot 4H_2O$ complexes [9] as well as those now prepared, containing Mg(II) as one of the metal cations are also similar to those recorded for the two polymorphs of the simple dihydrated oxalates. On the other hand, the spectra of all these new double metal oxalates are practically identical.

As examples of the measured spectra, Figure 2 shows the FTIR and Raman spectra of $MgCo(C_2O_4)2\cdot 4H_2O$ and Figure 3 those of $MgMn(C_2O_4)2\cdot 4H_2O$. The assignment of both pairs of spectra is presented in Table 1.

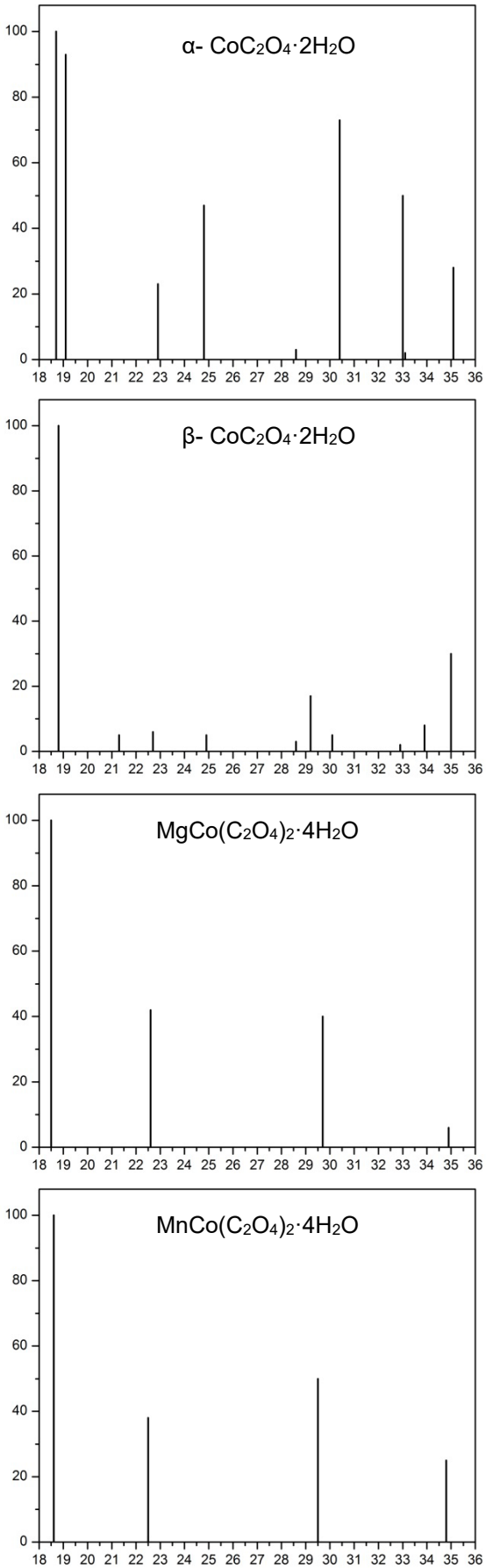

Figure 1. Comparison of the powder diagrams of α-$CoC_2O_4 \cdot 2H_2O$, β-$CoC_2O_4 \cdot 2H_2O$, $MgCo(C_2O_4)_2 \cdot 4H_2O$ and $MnCo(C_2O_4)_2 \cdot 4H_2O$ in the 2θ range between 18 and 36°.

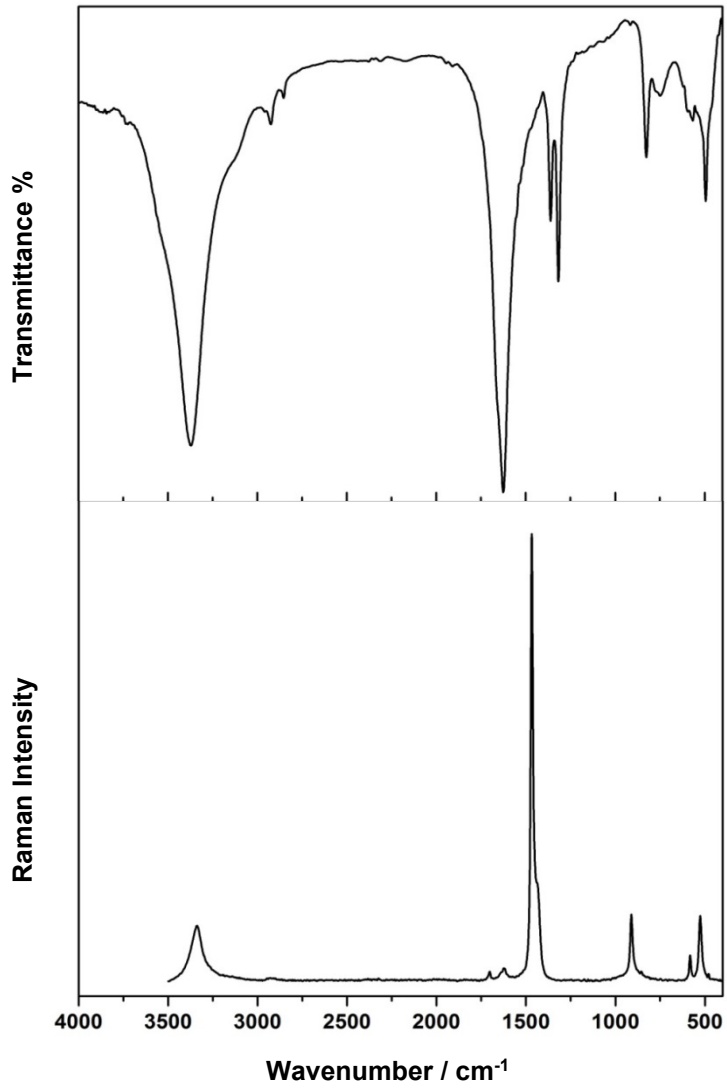

Figure 2. FTIR (above) and Raman spectra (below) of $MgCo(C_2O_4)_2{\cdot}4H_2O$.

Table 1. Assignments of the FTIR and FT-Raman spectra of $MgCo(C_2O_4)_2{\cdot}4H_2O$ and of $MgMn(C_2O_4)_2{\cdot}4H_2O$ (Band positions in cm^{-1}).

$MgCo(C_2O_4)_2{\cdot}4H_2O$		$MgMn(C_2O_4)_2{\cdot}4H_2O$		Assignments
Infrared	**Raman**	**Infrared**	**Raman**	
3552 sh				
3370 vs, 3129 sh	3350 s	3390 vs, 3157 sh	3340 sh, 3335 s	ν(OH) (H_2O)
2924w, 2852vw	2928 vw	2928w, 2852vw	2923 vw	
1657sh, 1625vs	1703vw,1625w	1657sh, 1632 vs	1706vw,1643vw 1617 w	ν_{as}(CO)
	1467 vs		1462 vs	ν_s(C-O)+ν(C-C)
	1400 sh		1419 w sh	ν_s(C-O)+δ(OCO)
1361 s, 1317 vs		1363s, 1318 vs		ν_s(C-O)+δ(OCO)
	911 m 854 vw		907 s, 855 vw	ν(C-C)
825 s		819 vs		ν(C-C)+δ(OCO)
751 m,br		727m		$\rho(H_2O$
	581 w, 526 m	568 m	577m, 516 s	δ_{ring}
618m, 566m, 494 s	479 vw	498 s	480 vw	δ_{ring}

vs, very strong; s, strong; m, medium; w, weak; vw, very weak; sh, shoulder; br,broad.

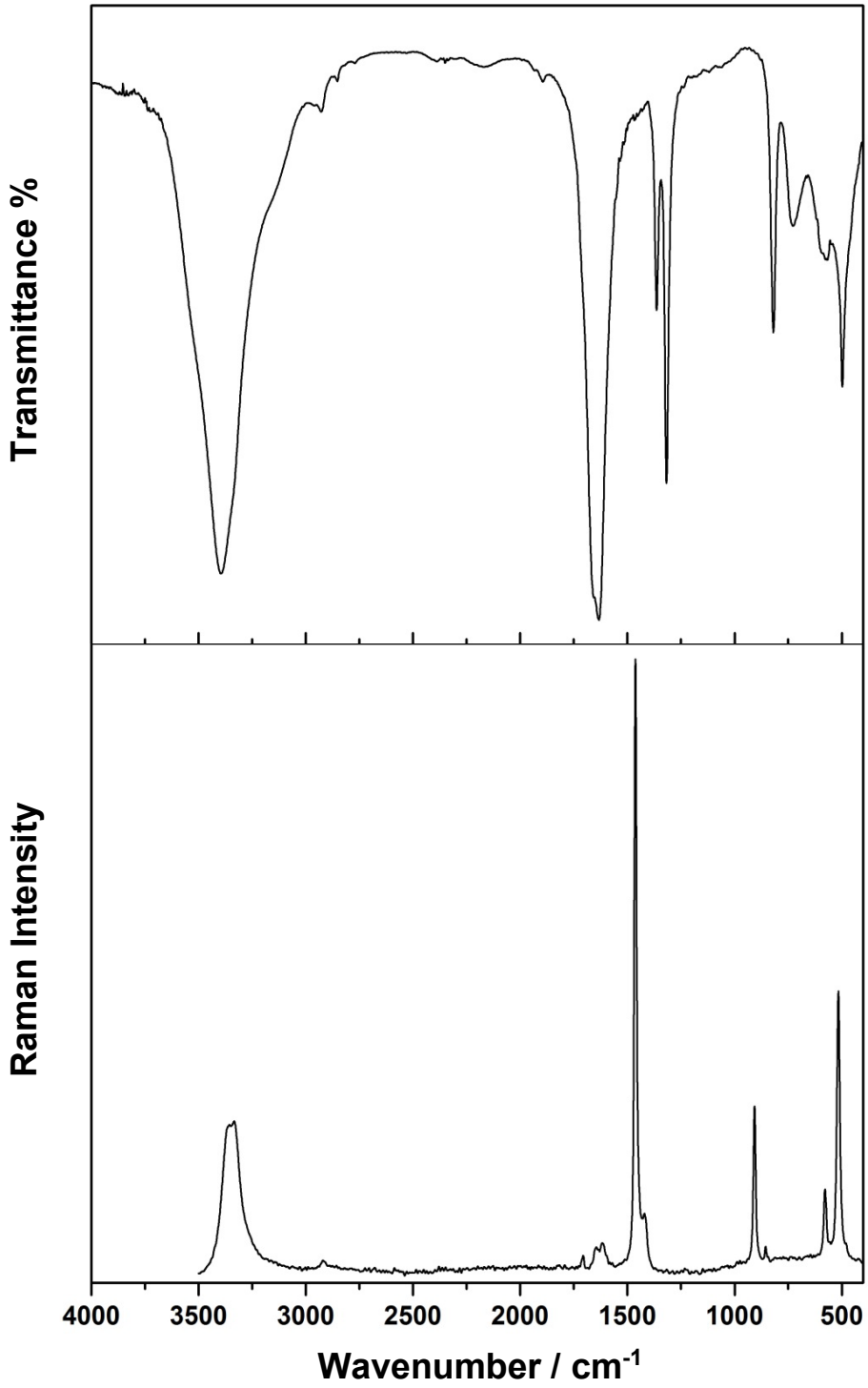

Figure 3. FTIR (above) and Raman spectra (below) of $MgMn(C_2O_4)_2{\cdot}4H_2O$.

As described above the vibrational unit conformed by the two oxalate groups bonded to the cations in a planar arrangement, possesses the approximate D_{2h} point group, whose irreducible representation is given by $\Gamma = 6A_g + 2B_{1g} + 2B_{2g} + 5B_{3g} + 3Au + 6B_{1u} + 6\ B_{2u} + 3B_{3u}$ (*cf.* also [5,6]). Due to the presence of a symmetry center one may expect the operativity of the so-called exclusion principle. Therefore, phonons with u-parity are only IR active and those with g-parity

are only Raman active, a fact that becomes immediately apparent by inspection of the results presented in Table 1.

Some brief additional comments on the performed assignments are given as follows:

- The strongest IR band corresponds to the antisymmetric carboxylate stretching vibration, ν_{as}(CO), whereas the strongest Raman line is assigned to the respective symmetric stretching, partially coupled with one of the ν(C-C) modes.

- The fact that the ν_{as}(CO) vibration generates also two very weak signals in the Raman spectra, suggests the presence of either weak coupling or distortional effects in the unit cell, which partially activate originally forbidden vibrations.

- The proposed assignment $\nu_{as}(CO) > \nu_{s}(CO)$ is in agreement with the results of former studies of similar systems in solution [14,15] as well as with our own studies of other metal oxalato-complexes [4-7].

- The ν(C-C) stretching vibrations and OCO deformation modes are found in the ranges that are usual for these vibrations [4-7,15].

- The band related to the stretching motions of the water molecules is very strong and well defined in the IR spectra and somewhat weaker in the Raman spectra. Its position suggests that the water hydrogen atoms are involved in relatively strong H-bonds [15,16]. The strength of these bonds are similar to that found in the previously investigated double oxalates $MM'(C_2O_4)_2{\cdot}4H_2O$[9] as well as in natural and synthetic glushinskite, $MgC_2O_4{\cdot}2H_2O$ [6].

- As suggested in other previously investigated cases, it is assumed that the bending mode of water, δ(H_2O), is overlapped by the strongest IR band and attains not enough intensity in the Raman spectra.

- The assignments in the lower-frequency range, and especially that of one of the torsion modes of the bound water molecules, ρ(H_2O), are also supported by our previous deuteration experiments with related complexes [6,7].

4. Conclusions

A series of double metal oxalates of composition $MgM(C_2O_4)_2{\cdot}4H_2O$ (MgM = MgFe, MgNi, MgZn, MgNi, MgMn) were prepared and characterized. X-ray powder diffractometry shows that they present a strong structural analogy to the so-called β-modification of the related simple oxalates of the type $MC_2O_4{\cdot}2H_2O$ and to the previously investigated series

$MM'(C_2O_4)_2{\cdot}4H_2O$ [9]. This fact is highly surprising because in these simple oxalates the β-modification is less thermodynamically stable and irreversible turns to the most stable α-form. Besides, the vibrational spectroscopic behavior of all these groups of complexes is totally similar, confirming additionally the close structural analogies between the $MM'(C_2O_4)_2{\cdot}4H_2O$, $MgM(C_2O_4)_2{\cdot}4H_2O$, α-$MC_2O_4{\cdot}2H_2O$ and β-$MC_2O_4{\cdot}2H_2O$ complexes.

Acknowledgements

This work was supported by the UNPA and the UNLP. ACGB is a member of the Research Career from CONICET.

References

(1) E.J. Baran, *J. Coord. Chem.*, 2014, 67, 3734-3768.

(2) O.E. Piro, E.J. Baran, *Crystallogr. Rev.*, 2018, 24, 149-175.

(3) V.N. Serezhkin, Yu. Artem'eva, L.B. Serezhkina, Yu.N. Mikhailov, *Russ. J. Inorg. Chem.*, 2005, 50, 1019-1030.

(4) M.C. D'Antonio, A. Wladimirsky, D. Palacios, L. Coggiola, A.C. González-Baró, E.J. Baran, R.C. Mercader, *J. Braz. Chem. Soc.*, 2009, 20, 445-450.

(5) N. Mancilla, V. Caliva, M.C. D'Antonio, A.C. González-Baró, E.J. Baran, *J. Raman Spectr.*, 2009, 40, 915-920.

(6) M.C. D'Antonio, N. Mancilla, A. Wladimirsky, D. Palacios, A.C. González-Baró, E.J. Baran, *Vibrat. Spectr.*, 2010, 53, 218-221.

(7) A. Wladimirsky, D. Palacios, M.C. D'Antonio, A.C. González-Baró, E.J. Baran, *J. Argent. Chem. Soc.*, 2011, 98, 71-77.

(8) E.J. Baran, P.V. Monje, *Oxalate Biominerals*, in: A. Sigel, H. Sigel, R.K.O. Sigel (Eds.), *Metal Ions in Life Sciences*, Vol. 4, J. Wiley, Chichester, 2008, pp. 219-254.

(9) M.C. D'Antonio, M.M. Torres, D. Palacios, A.C. González-Baró, V.L. Barone, E.J. Baran, *Anales Asoc. Quím. Argent.*, 2018, 154, 41-48.

(10) L. Walter Lévy, J. Perrotey, *Bull. Soc. Chim. Fr.,* 1970, 1697-1704.

(11) R. Deyrieux, A. Péneloux, *Bull. Soc. Chim. Fr.,* 1969, 2675-2681.

(12) R. Deyrieux, Ch. Berro, A. Péneloux, *Bull. Soc. Chi. Fr.,* 1973, 25-34.

(13) G.M. Begun, W.H. Fletcher, *Spectrochim. Acta*, 1963, 19, 1343-1349.

(14) A.R. Hind, S.K. Bhargava, W. van Bronswijk, S.C. Grocott, S.L. Eyer, *Appl. Spectr.*, 1998, 52, 683-691.

(15) H. Siebert, *Anwendungen der Schwingungsspektroskopie in der Anorganischen Chemie*, Springer, Berlin, 1966.

(16) E. Libowitszky, Monatsh. *Chem.*, 1999, 130, 1047-1059.

Anales de la Asociación Química Argentina

EVALUACIÓN DE DOS MÉTODOS PARA LA EXTRACCIÓN DE PECTINA DEL BAGAZO DE SÁBILA (*ALOE BARBADENSIS MILLER*)

EVALUATION OF TWO METHODS FOR PECTIN EXTRACTION OF ALOE BAGASSE (*ALOE BARBADENSIS MILLER*)

Maria E. Moreno [1,*], Dra. C. Caridad Curbelo [2], Dra. C. Lourdes Crespo [3]

[1]*Universidad Nacional Experimental Francisco de Miranda. Falcón, Venezuela.*

[2]*Universidad Politécnica "José Antonio Echevarría". La Habana, Cuba.*

[3]*Universidad de Camagüey "Ignacio Agramonte Loynaz". Camagüey, Cuba.*

[*]*Autor Corresponsal E-mail: mariumoreno@gmail.com*

Resumen

Esta investigación se enfocó desde la perspectiva de aplicar métodos de extracción, tanto hidrólisis ácida como hidrodestilación, para comparar rendimientos y calidad de la pectina obtenida a partir del bagazo de sábila producto del procesamiento de las hojas. En primer lugar, se caracterizó fisicoquímicamente el bagazo. Seguidamente, se estableció un diseño de experimentos factorial multinivel (2^3) para comparar ambas técnicas tomándose para ello la relación sólido- solvente y el tiempo de contacto como factores experimentales. Resultando el mayor rendimiento con la técnica de la hidrodestilación (11,7 %) en condiciones de relación sólido-solvente alta y a mayor tiempo de contacto. La pectina obtenida es de gelificación rápida, soluble en agua y de alto metoxilo. En el espectro IR se observaron los picos característicos de los grupos funcionales de la pectina.

Abstract

This investigation was focused from the perspective of applying extraction methods, both acid hydrolysis and hydrodistillation, to compare yields and quality of the pectin obtained from the aloe bagasse resulting from the processing of the leafs. Firstly, bagasse was physicochemically characterized. Subsequently, a multilevel factorial design of experiments (2^3) was established to compare both techniques, taking the solid-solvent relationship and contact time as experimental factors. The highest yield resulting with the hydro-distillation technique (11.7%) under conditions of high solid-solvent ratio and longer contact time. The

pectin obtained is of rapid gelation, soluble in water and of high methoxyl. The characteristic peaks of the functional groups of pectin were observed in the IR spectrum.

Palabras clave: sábila, pectina, hidrólisis ácida, hidrodestilación.

Keywords: aloe, pectin, acid hydrolysis, hydrodestilation.

1. Introducción

La sábila es muy usada debido a sus propiedades curativas [(1)]; la especie que se cultiva es la especie conocida como *Aloe barbadensis Miller*, esta variedad por presentar un alto grado de aloína (23 al 30%) y otros componentes en sus hojas, es el de mayor demanda para la industria nacional e internacional [(2)]. Además de sus grandes propiedades beneficiosas es la que mejor se adapta al clima de Venezuela y la mayormente explotada [(3)].

Se conoce que, el *Aloe vera*, posee propiedades curativas y sus cristales son utilizados en la obtención de productos farmacéuticos, alimentos, bebidas, golosinas y de belleza. También su resina es utilizada en la elaboración de pinturas con propiedades anticorrosivas por su contenido de antraquinonas con muy buenos resultados [(4)] y del aprovechamiento de los residuos, producto del procesamiento, solo se reporta su uso para la biorremediación de suelos [(5)]. Es importante señalar que, los desechos sólidos de la sábila están compuestos por polisacáridos como la celulosa, pectina y hemicelulosas [(6)].

Este cultivo representa una fuente importante de residuos vegetales después de su procesamiento industrial, que dificultan su manejo y debido a su lenta degradación se convierten en un problema de impacto ambiental (pérdida de espacio físico, impacto paisajístico, contaminación por deposición, acumulación y descomposición de desechos orgánicos, generación de plagas, etc.) Se considera que del 30 a 60% del peso total de la planta de sábila corresponde al desecho o bagazo residual [(7)].

Por ello el presente trabajo se enfoca en la utilización de este residuo como materia prima para la obtención de pectina empleando dos técnicas de extracción. Las pectinas son polisacáridos importantes en los alimentos por sus propiedades funcionales, se usan mucho como agentes gelificantes, espesantes y estabilizantes. Este polisacárido se encuentra en los espacios intercelulares de los tejidos vegetales y les confiere propiedades específicas de firmeza y textura[(8)].

La pectina es en la actualidad un ingrediente muy importante en la industria alimenticia para la elaboración de gelatina, helados, salsas y queso; también es empleada en la industria

farmacéutica, para modificar la viscosidad de sus productos, en la industria de los plásticos como agentes clarificantes y aglutinante [9].

En Venezuela la pectina utilizada en la industria de alimentos y farmacéutica posee un alto costo ya que es importada [10], lo que incentiva a la búsqueda de fuentes alternas para su obtención, y a través de mejoras en las técnicas de extracción para obtener un proceso eficiente y de alto valor agregado, tanto económico como operacional.

Existe una amplia información respecto a pectinas, principalmente se encuentran estudios realizados sobre su extracción a partir de diferentes materias primas vegetales como cacao [11,12], café [13], limón [14], naranja [15], plátano [16], cambúr [17], maracuyá [18], manzana [19], pera [20], zapote [21], nopal [22], guayaba [23], mango [24], níspero [25], melocotón [26] entre otros. De la pectina extraída a partir del bagazo de sábila no existe información como la existente de otras frutas [27].

La abundante información respecto a la extracción de pectinas y de sus usos demuestra la importancia que tiene este compuesto, principalmente en la industria alimenticia. La gran variedad de materias primas para su obtención y las diferentes metodologías implementadas dan posibilidades de ampliar el estudio sobre el tema.

Esta investigación se planteó utilizar dos métodos para la extracción de pectina del residuo del procesamiento de Sábila. En esta se comparan el método tradicional (Hidrólisis ácida) empleado a nivel industrial y la Hidrodestilación, buscando comparar rendimientos, calidad y pureza de la pectina obtenida, tomando en cuenta que es un producto ampliamente utilizado en la industria de alimentos.

Hay que señalar que el proceso de extracción de pectina es un proceso de transferencia de masa sólido – líquido, de tal manera que cuando se ponen en contacto estas fases con diferente composición es posible que ocurra la transferencia de algunos de los componentes presentes de una fase hacia la otra y viceversa. Los componentes de la fase sólida pueden separarse por disolución selectiva de la parte soluble con un disolvente adecuado. Esta operación se conoce también como lixiviación. El sólido debe estar finamente dividido para que el disolvente líquido pueda hacer un contacto más íntimo con la fase sólida. Por lo general, el componente deseable es soluble, mientras que el resto del sólido es insoluble [28].

En este caso, la materia sólida a emplear es el bagazo de Sábila (Aloe vera), de donde se extraerá el componente pectina. Si se permite el contacto del material sólido y el solvente por un tiempo determinado, las dos fases alcanzarán un equilibrio y se logrará la transferencia de componentes de una fase a otra para su posterior separación y purificación del componente de interés.

Existen diversos procesos de extracción, su selección se basa en las diferencias existentes en las propiedades físicas, más que en las químicas de las fases en contacto. Tales procesos dependen de la diferencia de composición que alcancen las fases en el equilibrio o bien, en la diferencia de velocidad de transferencia de masa que tienen los constituyentes de una mezcla [28].

Para la extracción industrial de pectina el proceso más utilizado es la hidrólisis ácida. En esta técnica la materia prima es suspendida en agua caliente con la cantidad necesaria de un ácido fuerte y con agitación constante. Después de un tiempo de contacto la solución resultante es separada de los sólidos no solubles mediante filtración y luego se mezcla con alcohol para que la pectina precipite. La fase sólida obtenida es extraída y purificada lavándola con alcohol etílico. Por último, la pectina purificada es secada y molida [18,29].

Otro proceso de extracción de pectina es la hidrodestilación la cual, consiste en separar mediante la adición de calor los diferentes componentes de una mezcla, aprovechando las diferencias de volatilidades de los compuestos. En este método, la materia vegetal es colocada en contacto directo con el solvente (agua), luego aplicándole calor se comienza a destilar cuando alcanza el punto de ebullición. El vapor del solvente generado por el incremento de la temperatura extrae consigo compuestos contenidos en el interior del material vegetal [30, 31].

De acuerdo a esto para llevar a cabo esta investigación se seleccionaron como métodos de extracción la hidrólisis ácida y la hidrodestilación. El primero por ser el método más utilizado y empleado a nivel industrial y el segundo para establecer la influencia que puede tener la presencia o no del ácido en el rendimiento de pectina. Además, las pectinas son utilizadas en alimentos y se hace necesario el empleo de técnicas que no dejen residuos en el producto final y con la hidrodestilación se cumple esa condición.

Desde el punto de vista ambiental se reutiliza un desecho que ocasiona daños al ambiente, mientras que en el ámbito económico, genera beneficios a las empresas que tienen a la sábila como materia prima de sus procesos, ya que estarían reutilizando lo desechado, logrando de esta manera, la posibilidad de ampliar su línea de producción al generar productos aptos para el consumo humano.

2. Materiales y Métodos

Se utilizó como materia prima el bagazo de sábila fresco, el cual fue acondicionado para análisis fisicoquímicos posteriores.

Para la caracterización fisicoquímica del bagazo de sábila se emplearon métodos estandarizados: Determinación de humedad [32]. Determinación de Carbono Orgánico [33].

Determinación de pH 34. Determinación de nitrógeno y proteínas [35]. Contenido de cenizas [36]. Densidad [37]. Contenido total de pectina [38] y Acidez [39].

Los métodos empleados para la extracción de la pectina fueron el de hidrólisis ácida utilizando ácido clorhídrico y la hidrodestilación utilizando agua como solvente.

Para la obtención de la pectina en la hidrólisis ácida se tomó como referencia la investigación de Moreno et al. 27, en la cual se presentan las condiciones experimentales de pH= 1,5; temperatura= 90 °C y tiempo= 60 minutos, para el máximo rendimiento de pectina.

Para comparar los rendimientos de ambos métodos de extracción, se fijaron como factores la relación soluto – solvente, el tiempo de extracción y el método utilizado, estableciéndose dos niveles para cada uno y como variable respuesta se mantiene el rendimiento de pectina. Se fijó un diseño de experimentos multifactorial, cuyas características se muestran en la Tabla 1; Se utilizó el software Statgraphics Centurion XV.

Tabla 1. Diseño de experimentos 2^k para comparación de métodos de extracción

Variables independientes	Niveles
Procedimiento de extracción	-1 (hidrólisis ácida) 1 (hidrodestilación)
Relación soluto / solvente	-1 (baja) 0,05 1 (alta) 0,15
Tiempo de extracción	-1 (40 minutos) 1 (60 minutos)

Para llevar a cabo la hidrodestilación, se hizo el montaje del equipo (Figura 1) se pesó el bagazo seco (5 gramos/ 15 gramos) y se agregó en un balón de destilación junto con el agua destilada (100 mL). Se dejó hervir la mezcla por un tiempo (40 / 60 minutos), de acuerdo a la combinación de factores que se estaba evaluando a la temperatura de ebullición del solvente. Luego, se dejó enfriar y se filtró. Al líquido obtenido se le agregó etanol en proporción 1:1,5 para que precipitara la pectina, se dejó reposar 12 horas, para luego hacer el filtrado de la pectina. Esta se secó en la estufa a 40 °C, se pesó y se almacenó en bolsas cerradas.

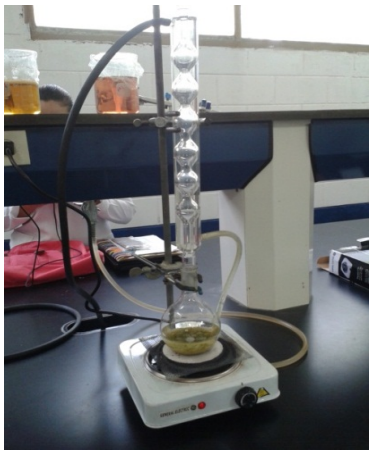

Figure 1. Equipo para la Hidrodestilación.

Se realizó la hidrólisis ácida pesando el bagazo (5 / 15 gramos) y se agregaron 100 mL de agua acidulada con ácido clorhídrico a un pH de 1,5 durante 40 / 60 minutos y en agitación constante a una temperatura fija de 90 °C. Una vez transcurrido ese tiempo se dejó enfriar y se filtró.

Al líquido obtenido se le agregó etanol en proporción 1:1,5; para que la pectina precipitara, se dejó reposar 12 horas y se filtró la pectina formada. Esta se lavó con etanol en proporción 1:1 y se secó en una estufa a 40°C, se pesó y se guardó en bolsas herméticas.

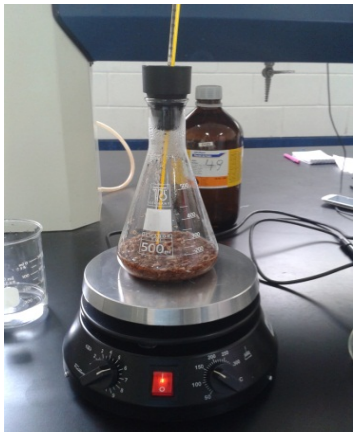

Figure 2. Hidrólisis ácida.

Una vez obtenida la pectina se le determinó el grado de esterificación; porcentaje de metoxilo y porcentaje de ácido anhidrourónico y se caracterizó por Espectroscopia IR, para ello se utilizó un equipo de IR NICOLET Magna IR 560.

3. Resultados y Discusión

En la Tabla 2 se presentan los resultados de la caracterización fisicoquímica del bagazo, se determinó que posee alto porcentaje de humedad, cenizas y contenido de carbono.

En la Tabla 3 se observan los rendimientos obtenidos al ejecutar la combinación de factores, para el método de hidrodestilación se obtuvo 11,7 % en promedio, valor éste no muy alejado del obtenido con la hidrólisis ácida (10,61 %).

En la Tabla 4 se presenta el análisis de varianza para establecer comparación entre los dos métodos de extracción utilizados en base al rendimiento de pectina.

El valor-P es mayor que 0,05; por lo tanto, no existe una diferencia estadísticamente significativa entre la media de rendimiento entre un nivel de método de extracción y otro, con un nivel del 95,0 % de confianza.

Tabla 2. Caracterización fisicoquímica del bagazo de Sábila

Parámetros	Valor promedio
Humedad (%)	5,926 ± 0,8676
Ceniza (%)	4,918 ± 1,5645
Acidez (%)	0,122 ± 0,0004
Carbono orgánico (%)	7,539 ± 0,1182
Nitrógeno Amoniacal (%)	4,431± 0,0943
Proteína (%)	4,112± 0,0875
pH	6,438 ± 0,0104
Densidad (g/mL)	0,700 ± 0,0002
Contenido total de pectina (%)	14,988 ± 1,1321

Table 3. Rendimientos de pectina obtenidos en la comparación de los métodos de extracción.

Corrida	Bloque	Método de extracción (HA/HD)	Relación sólido- solvente (g bagazo/mL solvente)	Tiempo de extracción (Minutos)	Rendimiento (%)
1	1	1	-1	-1	0
2	1	-1	-1	-1	0
3	1	1	1	1	11,53
4	1	1	1	-1	9,7
5	1	1	-1	1	0
6	1	-1	1	-1	7,37
7	1	-1	1	1	10,79
8	1	-1	-1	1	0
9	2	-1	1	1	10,43
10	2	-1	1	-1	8,39
11	2	1	-1	-1	0
12	2	1	1	-1	9,15
13	2	-1	-1	1	0
14	2	1	1	1	11,89
15	2	1	-1	1	0
16	2	-1	-1	-1	0

Table 4. Resultados del análisis estadístico para rendimiento por Método de extracción.

Fuente	Suma de Cuadrados	Gl	Cuadrado Medio	Razón-F	Valor-P
Entre grupos	1,74901	1	1,74901	0,06	0,8100
Intra grupos	407,759	14	29,1257		
Total (Corr.)	409,508	15			

.

El diagrama de Pareto (Figura 3) permite plantear que todas las variables estudiadas tienen influencia significativa con un 95 % de confianza y con efecto positivo, indicando que en la medida que se incremente la relación sólido - solvente y el tiempo de extracción se incrementará el rendimiento de pectina.

También se observa que la interacción de las variables relación sólido- solvente y tiempo de extracción tiene una influencia significativa y efecto positivo; así como la interacción del método de extracción y relación sólido solvente, según se observa en la figura.

De los resultados obtenidos se observa que todas las variables tienen efectos positivos sobre el rendimiento de pectina siendo el más significativo la relación sólido -solvente dando por sentado que a mayor relación sólido-solvente mayor será el rendimiento de pectina.

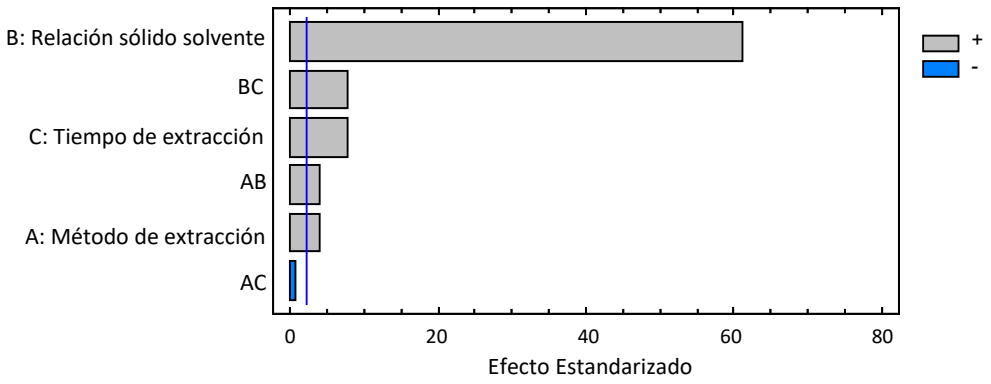

Figura 3. Diagrama de Pareto para la comparación de métodos de extracción.

El análisis realizado anteriormente se comprueba en la tabla ANOVA (Tabla 5) donde se reporta en la última columna el valor-P para cada variable y sus posibles interacciones y solo las que tienen este valor inferior a 0,05 resultan significativas sobre el rendimiento de pectina para un 95 % de confianza. También se reporta la razón – F, el cual permite evaluar la validez de los parámetros en el modelo matemático ajustado. Para las variables e interacciones que resultaron significativas este estadígrafo (Fexp) es mayor que Fcrítica, que resultó de 4,54.

El estadístico R-Cuadrada indica que el modelo, así ajustado, explica 99,796 % de la variabilidad en rendimiento. El estadístico R-cuadrada ajustada, que es más adecuado para comparar modelos con diferente número de variables independientes, es de 99,66 % y el estadístico de Durbin-Watson (DW) prueba los residuos para determinar si hay alguna correlación significativa basada en el orden en que se presentan los datos. Este valor se ubicó en 2,76.

En la Figura 4 se observa el comportamiento del rendimiento de pectina frente a los principales factores estudiados. Siendo el factor relación sólido-solvente el que tuvo mayor influencia sobre la variable respuesta.

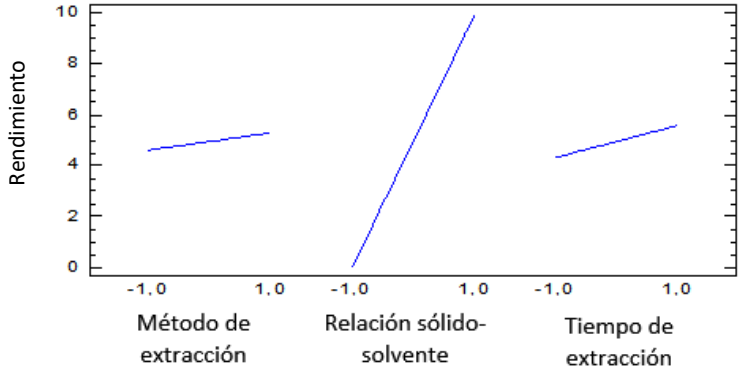

Figura 4. Comportamiento del rendimiento de pectina frente a los principales factores experimentales.

También se puede precisar que el máximo rendimiento se obtuvo con el método de extracción hidrodestilación a una relación alta de sólido-solvente y a mayor tiempo de contacto. El máximo rendimiento alcanzado con este método fue de 11,7 % en base seca. Es importante destacar que, a relación baja de sólido-solvente; para ambos métodos; no se obtuvo pectina; esto ocurrió tanto a 40 minutos como a 60 minutos. Esto puede deberse a que al ser poca la cantidad de bagazo, no es posible obtener una pectina en cantidad suficiente como para coagular y luego precipitar.

Con la hidrólisis ácida el máximo rendimiento de pectina alcanzado fue de 10,61% en base seca con un tiempo de contacto de 60 minutos. Igualmente, para baja relación sólido-solvente no fue posible obtener pectina.

De la Figura 5 se puede determinar que todas las interacciones de los factores estudiados presentan efectos positivos, siendo más significativa la interacción BC (Relación sólido-solvente y tiempo), esto se evidenció al momento de realizar la aplicación de los métodos de extracción, ya que los máximos rendimientos se obtuvieron a alta relación sólido –solvente y a mayor tiempo de contacto.

En la Tabla 6 se muestran los resultados obtenidos para la caracterización química; las pectinas extraídas por ambos métodos presentan bajo grado de esterificación y gelificación rápida.

En cuanto al contenido de metoxilo ambas califican como pectinas de alto metoxilo, ya que para ambas este valor se ubicó por encima de las especificaciones internacionales. Al comparar el contenido de ácido anhidrourónico se puede observar que la pectina extraída por la hidrólisis ácida posee un valor superior respecto a la pectina extraída por hidrodestilación. Tomando en cuenta que el contenido de ácido anhidrourónico indica el grado de pureza de la pectina extraída, se puede afirmar que la pectina extraída por hidrólisis ácida es de mayor pureza que la obtenida por hidrodestilación.

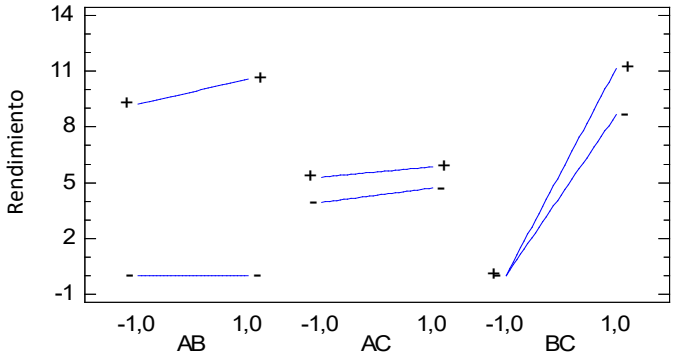

Figura 5. Efecto de las interacciones sobre el rendimiento de pectina.

Tabla 6. Caracterización química de la pectina obtenida

Método	Grado de Esterificación (%)	Contenido de Metoxilo (%)	Contenido de Ácido anhidrourónico (%)
Hidrólisis ácida	75,47	12,40	46,64
Hidrodestilación	62,79	16,74	18,03
Especificaciones Internacionales*	81,50	Min. 6,70	Min. 65

* USP, FCC

Al comparar las características de las pectinas se observan diferencias entre ellas a pesar de ser extraídas de la misma materia prima. En primer lugar, el grado de esterificación obtenido con los diferentes métodos aplicados, ambos son superiores al 60% pero se encuentran por debajo del exigido en las especificaciones internacionales. Por lo que las pectinas extraídas por ambos métodos presentan bajo grado de esterificación y gelificación rápida.

En cuanto al contenido de metoxilo ambas califican como pectinas de alto metoxilo, ya que para ambas este valor se ubicó por encima de las especificaciones internacionales.

Y al comparar el contenido de ácido anhidrourónico se puede observar que la pectina extraída por la hidrólisis ácida posee un valor superior respecto a la pectina extraída por hidrodestilación. Tomando en cuenta que el contenido de ácido anhidrourónico indica el grado de

pureza de la pectina extraída, se puede afirmar que la pectina extraída por hidrólisis ácida es de mayor pureza que la obtenida por hidrodestilación.

Se puede observar en las Figuras 6 y 7 los espectros IR obtenido para la pectina extraída para el método de hidrodestilación e hidrólisis ácida respectivamente, las bandas de particular importancia para la determinación del grado de esterificación son aquellas que aparecen alrededor de 1581cm^{-1} y 1712cm^{-1} para la pectina extraída por hidrólisis ácida y alrededor de 1576 cm^{-1} y 1731 cm^{-1} para la pectina extraída por hidrodestilación y son indicadoras de grupos carboxilos libres y esterificados provenientes de la pectina.

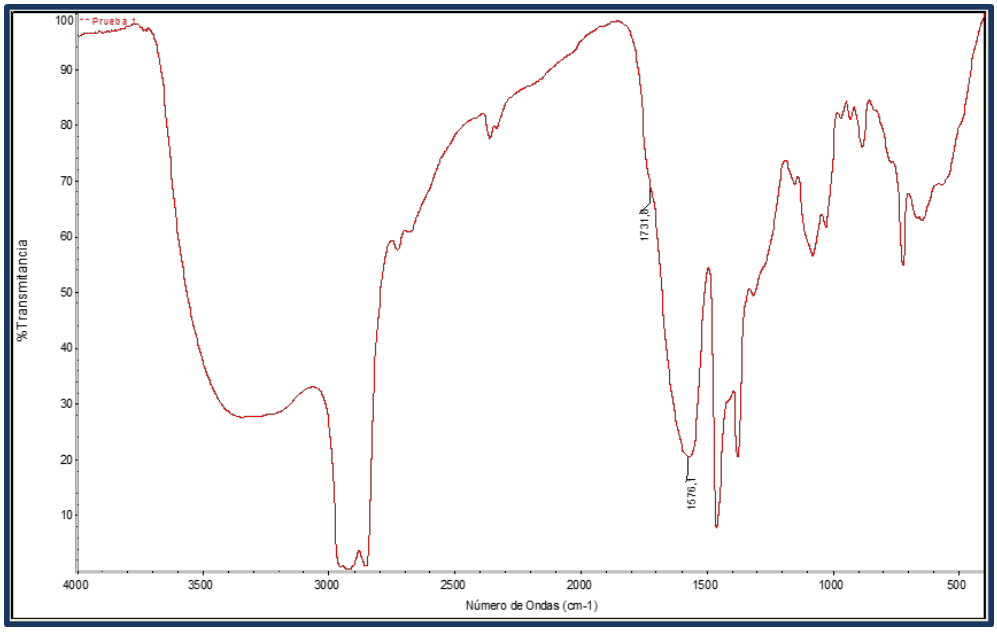

Figura 6. Espectro IR de la pectina obtenida por Hidrodestilación.

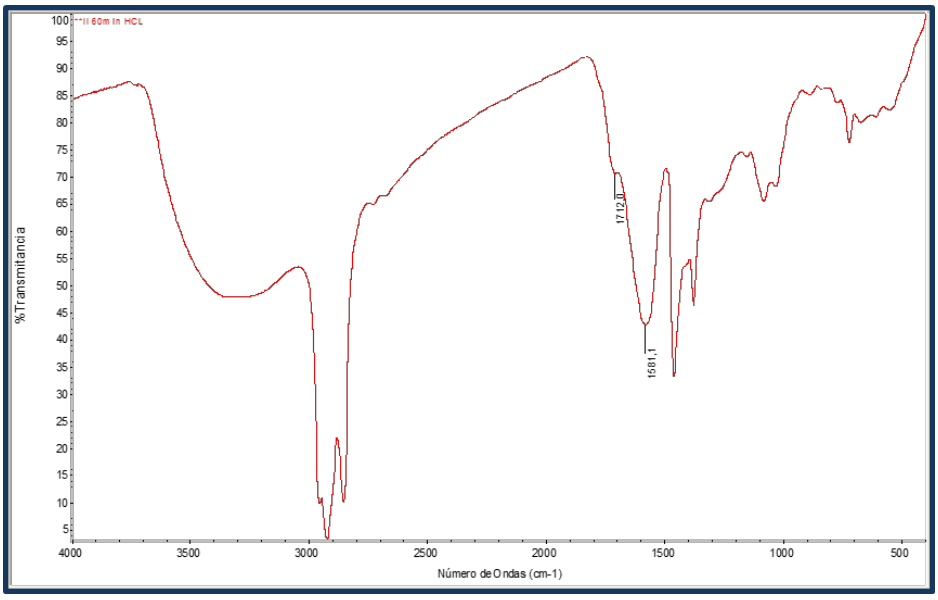

Figura 7. Espectro IR de la pectina obtenida por Hidrólisis ácida.

En ambos espectros se observa un pico ancho de 3100 y 3400 cm^{-1} debido a las vibraciones de tensión del O-H, lo cual indica que existen muchos grupos O ─ H en la estructura de la pectina. La banda de 2930 cm^{-1} corresponde a la tensión del C ─ H de los grupos CH_2.

En todos los espectros se observan picos alrededor de 1300 y 1400 cm^{-1}, estos corresponden a la banda de vibración de tensión del C─O─H.

Los picos a 1100 y 1200 cm^{-1} son la banda de vibración de tensión asimétrica del C─O─C, e indican la abundancia de los grupos metoxilos (─O─CH_3).

4. Conclusiones

El rendimiento de pectina alcanzado con el método de hidrodestilación fue de 11,7 % y para la hidrólisis ácida fue de 10,61 %, no presentando diferencias significativas entre ellos.

La pectina extraída es de gelificación rápida, soluble en agua y de alto metoxilo, presentando mayor pureza la obtenida por hidrólisis ácida.

La pectina extraída es apta para su uso en la industria alimentaria ya que la misma cumple con las características exigidas para pectinas comerciales..

Referencias

(1) Álvarez G. *Análisis Comparativo de Costos y Rentabilidad del Cultivo de Sábila (Aloe barbadensis Miller). Revista Agraria -Nueva Época*. 2005, 2(2), 35-42.
http://www.uaaan.mx/DirInv/portal_agraria/agraria/Agr_NE_II_02_files/Contenido-AgrariaNE_II01.pdf. Accesado en: enero 2018.

(2) Romero M, Tofiño A, Aarón M. Sábila. *Generalidades sobre el manejo del cultivo de la sábila en la guajira colombiana. Boletín de investigación. Corporación Colombiana de Investigación Agropecuaria, CORPOICA*. 2010. 20 pp. https://es.scribd.com/document/422680136/44290-56650 . Accesado en: enero 2018.

(3) Piña H. *Circuito agroalimentario Zábila. Coro, estado Falcón, Venezuela. Fundacite-UNEFM*. 2010.156 pp. ISBN 978-980-245-025-1

(4) Prato M, Ávila R, Donquis C, Medina E, Reyes R. *Antraquinonas en Aloe vera barbadensis de zonas semiáridas de Falcón, Venezuela, como inhibidores de la corrosión". Revista Multiciencias*. 2008; 8(2):148-145. http://www.redalyc.org/pdf/904/90480203.pdf . Accesado en: diciembre 2017.

(5) Acosta Y, Paolini *J. Dinámica de la masa microbiana (C y N) en un suelo de la Península de Paraguaná tratado con residuos orgánicos. Revista Multiciencias*. 2006, 6(2), 217-232.
https://produccioncientificaluz.org/index.php/multiciencias/article/view/16635. Accesado en: enero 2018.

(6) Pérez, L. *Condiciones para la producción de etanol carburante a partir de los desechos sólidos de sábila sacarificados. Instituto Tecnológico de Mérida. Yucatán- México.* 2008.
https://fdocuments.es/document/fermentacion-de-sabila.html Accesado en: enero 2018.

(7) *NATURAVEN C.A.* (http://www.naturaven.com/). Accesado en: enero 2018.

(8) Waldron K. *Cell wall polysaccharides: composition and structure. Comprehensive glycoscience*. 2007
https://onlinelibrary.wiley.com/doi/abs/10.1002/jsfa.2304. Accesado en: enero 2018.

(9) Herbstreith & Fox. *The specialists for pectins.* http://herbstreith-fox.de/produkte/englisch/einstant.htm. Accesado en: enero 2018.

(10) Camejo C, Ferrer A, Ferrer B, Peña J, Cedeño M. *Extracción y caracterización de pectina en limones injertados de la región Zulia.Rev. Fac. Agron. (LUZ)*.1996, 13, 641-645.
http://www.revencyt.ula.ve/storage/repo/ArchivoDocumento/fagro/v22n3/art4.pdf . Accesado en: enero 2018.

(11) Betancourt, L, Llano, J. *Extracción de pectinas a partir de subproductos del beneficio del Cacao*. 2009.
https://www.semanticscholar.org/paper/Extracci%C3%B3n-de-pectinas-a-partir-de-los-subproductos-Latorre-Moreno/c4181bf46e48b937d0b627f53cea 4ca3992c75b1

https://core.ac.uk/download/pdf/47237189.pdf Accesado en: enero 2018.

(12) Barazarte H, Sangronis E, Unai E. *La cáscara de cacao (Theobroma cacao L.): una posible fuente comercial de pectinas. Archivos Latinoamericanos de Nutrición. Órgano oficial de la Sociedad latinoamericana de nutrición*. 2008. 58(1):64-70.
http://ve.scielo.org/scielo.php?script=sci_arttext&pid=S0004-06222008000100009 Accesado en: febrero 2018.

(13) Zapata J. *Extracción de pectinas de subproductos del café, la nueva opción. Revista electrónica del centro de la ciencia y la investigación farmacéutica*. 2009. (6):4-7
https://core.ac.uk/download/pdf/47237189.pdf Accesado en: marzo 2018.

(14) Baltazar R, Carbajal D, Baca N, Salvador D. *Optimización de las condiciones de extracción de pectina a partir de cáscaras de limón francés (Citrus médica) utilizando la metodología de la superficie de respuesta. Agroindustrial Science. Escuela de Ingeniería Agroindustrial. Universidad de Trujillo. Perú*. 2013, 2: 77-89
http://revistas.unitru.edu.pe/index.php/agroindscience/article/view/500 Accesado en: enero 2018.

(15) Devia, J. *Proceso para producir pectinas cítricas. Revista Universidad EAFIT, Medellín, Colombia*. 2003, 129: 21-30
http://publicaciones.eafit.edu.co/index.php/revista-universidad-eafit/article/view/918 Accesado en: febrero 2018.

(16) Vásquez R. *Extracción de Pectina a partir de la cáscara de plátano (Musa AAB, subgrupo plátano) clon Hartón. Rev. Fac. Agron. (LUZ)*. 2008. 318-333.
http://ve.scielo.org/scielo.php?script=sci_arttext&pid=S0378-78182008000200008 Accesado en: marzo 2018.

(17) Arellanes A, Jaraba M, Mármol Z, Páez G, Aiello C, Rincón M. Obtención y caracterización de la pectina extraída de la cáscara de cambúr manzano (Musa AAB). Rev. Fac. Agron. (LUZ). 2011, 28:523-539
https://produccioncientificaluz.org/index.php/agronomia/article/download/26899/27525 Accesado en: enero 2018.

(18) Álvarez A, Burgos F. Comparación de las técnicas de extracción de pectina a partir de la cáscara de parchita amarilla (Passiflora edulis F.flavicarpa). Trabajo de grado. Universidad Central de Venezuela (UCV). Caracas, Venezuela. 2012.
http://saber.ucv.ve/bitstream/123456789/3521/1/TEG_Alvarez_Burgos.pdf. Accesado en: febrero 2018.

(19) Untiveros G. Obtención y caracterización de pectinas de alto y bajo metoxilo de la manzana variedad Pachacamac. Revista de la Sociedad Química Perú. 2003. 69 (3):155-162.
http://www.scielo.org.pe/pdf/as/v3n2/a05v3n2 Accesado en: marzo 2018.

(20) Casamayou E. Obtención y caracterización de pectina en polvo a partir del bagazo de pera. Trabajo de grado. Universidad Nacional Jorge Basadre Grohmann. Facultad de Ingeniería en Industrias Alimentarias. Tacna-Perú. 2008.
http://repositorio.unajma.edu.pe/bitstream/handle/123456789/283/Bladimir_Tesis_Bachiller_2017.pdf?sequence=1&isAllowed=y
http://ve.scielo.org/scielo.php?script=sci_arttext&pid=S0378-78182005000300004 Accesado en: enero 2018.

(21) Alegría P, Jordán J, Hoyos S, Olga L, Prado C, Julián A. Evaluación del comportamiento de la pulpa del fruto zapote (Matisia cordata) frente a procesos de transformación industrial. Revista Facultad de Ciencias Agropecuarias. Universidad del Cauca, Colombia. 2005, 3(1):41-46.
https://dialnet.unirioja.es/descarga/articulo/6117974.pdf Accesado en: enero 2020.

(22) Aza M, Méndez M. Extracción de pectina de Nopal (Opuntia ficus indica) por medio ácido aplicando dos niveles de temperatura, tiempo y estado de madurez. Trabajo de grado. Universidad Técnica del Norte. Facultad de Ingeniería Agroindustrial. Ibarra- Ecuador. 2011.
http://repositorio.utn.edu.ec/bitstream/123456789/743/1/03%20AGI%20293%20TESIS.pdf Accesado en: enero 2018.

(23) Chacín J, Marín M, D'Addosio R. Evaluación del contenido de pectina en diferentes genotipos de guayaba de la zona Sur del lago de Maracaibo. Revista Multiciencias, Ene-Abr 2010,10(1): 7-12.
Disponible en:http://redalyc.uaemex.mx/src/inicio/ArtPdfRed.jsp?iCve=90415596002 Accesado en: febrero 2018.

(24) Gamboa M. Aprovechamiento de los residuos obtenidos del proceso de despulpado del mango (Mangifera indica l.), de las variedades Smith, Tommy Atkins, Haden y bocado como materias primas para

la obtención de pectinas Tesis de maestría. Universidad de Oriente, Venezuela. 2009. https://www.yumpu.com/es/document/view/14333252/tesis-udo-ribibudoeduve-universidad-de-oriente. Accesado en: marzo 2018.

(25) Chasquibol N, Arroyo E, Morales J. Extracción y caracterización de pectinas obtenidas a partir de frutos de la biodiversidad peruana. Redalyc. Ingeniería Industrial. 2008, (26):175-199. http://www.search.ask.com/?gct=hp&o=APN11773A&sysid=539&qrsc=2871&l=dis&sver=3&t_type=1&dateOfInstall=2015-09-26&d=539-180-0&v=7.6-981-0&apn_ptnrs=%5EBRQ Accesado en: enero 2018.

(26) Pagán, J. Degradación enzimática y características físicas y químicas de la pectina del bagazo de melocotón". Tesis de doctorado. Universitat de Lleida. 1995.
Disponible en: http://www.cervantesvirtual.com/descargaPdf/degradacion-enzimatica-y-caracteristicas-fisicas-y-quimicas-de-la-pectina-del-bagazo-de-melocoton--0/. Accesado en: febrero 2018.

(27) Moreno M, Márquez D, Heredia N. Evaluación del bagazo de Sábila para la extracción de pectina a escala de laboratorio". Cienciamatria. Revista Interdisciplinaria de Humanidades, Educación, Ciencia y Tecnología. 2017. 3(5):117-132. ISSN: 2542-3029.
https://cienciamatriarevista.org.ve/index.php/cm/article/view/16 Accesado en: enero 2018.

(28) Foust A, Wenzel L, Clump C, Maus L, Bryce L. *Principios de operaciones unitarias. Segunda edición. México. CECSA*. 2006.752pp. ISBN 0-471-26897-6.

(29) Maldonado Y, Salazar S, Millones C, Torres E, Vásquez E. *Extracción de pectina mediante el método de hidrólisis ácida en frutos de maushan (Vasconcellea weberbaueri (Harms) V.M. Badillo) provenientes del distrito de San Miguel de Soloco región Amazonas. Revista Aporte Santiaguino*, 2010, 3(2):177-184.
http://revistas.unasam.edu.pe/index.php/Aporte_Santiaguino/article/view/437 Accesado en: enero 2018.

(30) Rojas J, Perea A, Stashenko E. *Obtención de aceites esenciales y pectinas a partir de subproductos de jugos cítricos. VITAE. Revista de la facultad de Química Farmacéutica*.2009, 16 (1):110-115.
http://www.scielo.org.co/scielo.php?pid=S0121-40042009000100013&script=sci_abstract&tlng=es Accesado en: febrero 2018.

(31) Cerpa M. Hidrodestilación de aceites esenciales. Modelado y caracterización. Tesis de doctorado. Universidad de Valladolid. España. 2007.
http://www.anipam.es/downloads/43/hidrodestilacion-de-aceites-esenciales.pdf Accesado en: marzo 2018.

(32) *Official Methods of Analysis of the Association of Official Analytical Chemists. AOAC 14004*. (2000). Determinación de humedad.
Disponible en: https://www.aoac.org/official-methods-of-analysis-21st-edition-2019/

(33) *Método de Walkley & Black. Carbono orgánico*.
https://inta.gob.ar/sites/default/files/script-tmp-cox__microescala.pdf

(34) *COVENIN Norma 1315:1979. Alimentos. Determinación del pH. Norma venezolana*.
http://www.sencamer.gob.ve/sencamer/normas/1315-79.pdf

(35) *International Standard Organization. (2006). Method 20483. Determination of the nitrogen content and calculation of the crude protein content- Kjeldhal method. ISO 20483*.
https://www.iso.org/standard/35435.html

(36) *COVENIN Norma 1155:1981. Alimentos. Determinación de Ceniza. Norma venezolana*.
http://www.sencamer.gob.ve/sencamer/normas/1155-81.pdf

(37) *COVENIN Norma 367. Alimentos. Determinación de densidad. Norma venezolana.*
http://www.sencamer.gob.ve/sencamer/normas/367-98.pdf

(38) NMX-F-347-S- 1980. Frutas y derivados. Determinación de pectina. Norma Mexicana.
https://www.colpos.mx/bancodenormas/nmexicanas/NMX-F-347-S-1980.PDF

(39) *Official Methods of Analysis of the Association of Official Analytical Chemists. AOAC 939.05. (2000). Determinación de Acidez libre.*
https://www.aoac.org/official-methods-of-analysis-21st-edition-2019/

Anales de la Asociación Química Argentina

SÍNTESIS Y CARACTERIZACIÓN DE CALIX[4]ARENO FUNCIONALIZADO CON GRUPOS SULFÓNICOS INCLUIDO EN UNA MATRIZ DE SÍLICE-TITANIA

María B. Colombo Migliorero[1], Sandra M. Bonilla Castañeda[2], Sergio A. Fernandes[2], Valeria Palermo[1,*], Patricia G. Vázquez[1], Gustavo P. Romanelli[1,3]

[1]Centro de Investigación y Desarrollo en Ciencias Aplicadas "Dr. Jorge J. Ronco" (CINDECA), CCT La Plata CONICET-CIC-Departamento de Química, Facultad de Ciencias Exactas, Universidad Nacional de La Plata, 47 Nº 257, B1900AJK, La Plata, Buenos Aires, Argentina.

[2]Grupo de Química Supramolecular e Biomimética (GQSB), Departamento de Química, Universidade Federal de Viçosa, Campus Universitário, Avenida P.H. Rolfs, s/n, Viçosa, MG 36570-000, Brazil.

[3]CISAV, Facultad de Ciencias Agrarias y Forestales, Universidad Nacional de La Plata, Calles 60 y 119 s/n, B1904AAN, La Plata, Argentina..

[*]Autor Corresponsal E-mail: vpalermo@quimica.unlp.edu.ar

Resumen

Se reporta la síntesis de nuevos materiales sólidos constituidos por una matriz de sílice, titania y mixta de sílice-titania conteniendo ácido *p*-sulfónico calix[4]areno en su estructura llevados a cabo mediante la técnica sol-gel. La morfología, composición y características ácidas de los sólidos obtenidos fueron determinadas mediante técnicas de caracterización: difracción de rayos X, espectroscopía infrarroja con transformada de Fourier, titulación potenciométrica, adsorción/desorción de nitrógeno y microscopias electrónicas de barrido y transmisión. Los materiales preparados, gracias a contener en su estructura ácido *p*-sulfónico calix[4]areno, presentan prometedoras aplicaciones en el campo de la catálisis heterogénea, para la síntesis de compuestos orgánicos.

Abstract

The synthesis of new solids constituted by a silica, tinania, and silica-titania matrix, containing *p*-sulfonic acid calix[4]arene is reported. The samples were prepared by the sol-gel process. The morphology, composition and acid characteristics of the obtained solids were elucidated by many techniques, such as X ray diffraction, Fourier transform infrared spectroscopy, potentiometric titration, adsorption/desorption of nitrogen and scanning and transmission electron microscopies. The samples have promising application in

the heterogeneous catalysis field, especially in organic synthesis, since they contain *p*-sulfonic acid calix[4]arene in the structure.

Palabras clave: Ácido p-sulfónico calix[4]areno, Sol-gel, Sílice, Titania, Catálisis heterogénea.

Keywords: p-sulfonic acid calix[4]arene, Sol-gel, Silica, Titania, Heterogeneous catalysis.

1. Introducción

A finales del siglo XX una nueva disciplina llamada Química Verde, emergió con el objetivo de remediar los efectos negativos producidos por la humanidad, principalmente causados por el desarrollo industrial. Entre los factores más importantes que afectan al medioambiente se encuentran la enorme cantidad de recursos naturales consumidos y los desechos generados vertidos al aire, ríos y suelos. La Química Verde abarca no sólo la Química, sino que incluye a la ciencia de los materiales, ingeniería y biotecnología. Desde sus postulados, incentiva el diseño y aplicación de procesos químicos que tiendan a utilizar de manera eficiente la materia prima; evitar el uso de reactivos y solventes tóxicos; eliminar (o reducir) el uso y generación de sustancias peligrosas. El desarrollo de tecnologías limpias es fundamental para optimizar la sustentabilidad de los diferentes procesos químicos e industriales [1-3].

Los iniciadores de esta disciplina, Anastas, Sheldon y Trost, introdujeron nuevos parámetros para evaluar el grado de sustentabilidad de un proceso determinado, como por ejemplo la economía atómica que describe la conversión eficiente de los átomos implicados en el proceso, el factor E, que se define como la relación entre la masa de residuo producido y la masa de producto obtenido. El término desecho o residuo se aplica a la sustancia o energía que se genera en un proceso y no tiene ninguna aplicación. Además, el tratamiento de estos residuos consume tiempo, dinero y esfuerzo. Por lo tanto, el desarrollo de nuevas tecnologías tiene como precepto primordial prevenir la formación de residuos basándose en el concepto de residuo cero, es decir, todo lo que ingresa debe ser parte del producto final (economía atómica) [4-6].

Una de las estrategias para tornar más sustentable un proceso es el empleo de catalizadores en las reacciones químicas. A su vez, la catálisis heterogénea se prefiere a la catálisis homogénea, ya que facilita la separación del catalizador del medio de reacción, mediante filtración o centrifugación, permitiendo su reuso [7].

Por lo expuesto anteriormente se buscan nuevos compuestos que actúen como catalizadores altamente selectivos. Entre estos se encuentran los calixarenos, que son moléculas macrocíclicas, de la familia de los metaciclofanos, que consisten en varias unidades de fenol

(generalmente de cuatro a ocho), conectadas a través de puentes de metileno en posición orto respecto al grupo hidroxilo [8,9]. Los calixarenos tienen un potencial latente para ser considerados como la tercera generación de supramoléculas, después de ciclodextrinas y éteres corona, en la formación de complejos anfitrión-huésped (host-guest). La conformación inicial del cono se estabiliza por las interacciones intramoleculares de enlace de hidrógeno entre los grupos hidroxilos (Figura 1) [10]. En estado sólido las moléculas orgánicas se alojan en la cavidad de los calixarenos, pero se ha demostrado que los calixarenos solubles en agua pueden formar complejos con moléculas orgánicas pequeñas, donde el proceso de inclusión está regido por efectos electrostáticos y conformacionales [11,12]. De este modo, los calixarenos sirven como una excelente "plataforma" para diseñar el sitio del receptor para la unión específica de átomos y moléculas participantes. Estas propiedades son de gran interés en biomedicina ya que los calixarenos aumentan la solubilidad y la biodisponibilidad de los fármacos [13-15].

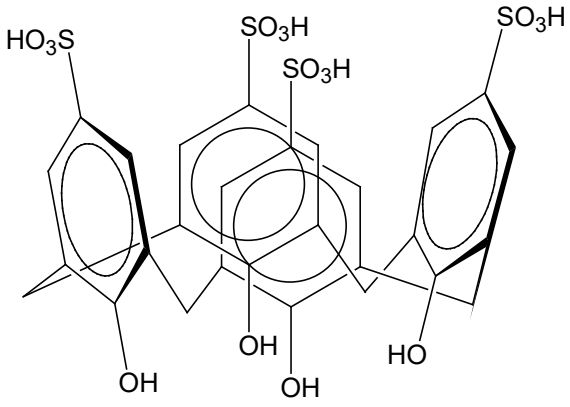

Figura 1. Estructura molecular del ácido *p*-sulfónico calix[4]areno (CX_4SO_3H)

Una aplicación interesante de los calixarenos es como sensores moleculares para la detección de varios cationes metálicos, aniones y aminoácidos gracias a la incorporación de grupos fluorogénicos [16,17] y en la remediación de aguas subterráneas contaminadas y efluentes industriales [17,18]. Asimismo, hay numerosas investigaciones sobre la actividad catalítica de los calixarenos en la síntesis de compuestos orgánicos de interés farmacológico [19-21]. Recientemente se ha realizado la inclusión de calixarenos en una matriz de sílice y fue utilizado con éxito como catalizador heterogéneo en la síntesis de heterociclos [22-25] y en reacciones de esterificación [26].

La utilización de sílice como soporte es muy común debido a las ventajas que presenta, tales como alta área superficial, gran estabilidad mecánica, térmica y química [27]. Por su parte, los óxidos mixtos de sílice y titania tienen numerosas aplicaciones en el campo de la catálisis, tanto como soportes o como catalizadores, debido a sus excelentes propiedades obtenidas por la combinación de ambos óxidos [28,29].

El método tradicionalmente empleado para preparar los óxidos de sílice y titanio incluye la técnica sol-gel, que data de mediados del Siglo XIX. Este método involucra la formación de una suspensión coloidal, llamada sol, a partir de la hidrólisis y condensación de los alcóxidos correspondientes y catalizado por un ácido o una base. Posteriormente el sol gelifica en una fase líquida continua y, finalmente, por evaporación del solvente, se obtiene el xerogel deseado [30]. Las características estructurales de los materiales preparados pueden modificarse regulando las diferentes variables y condiciones de la técnica sol-gel. De este modo, una gran variedad de materiales sílice-titania con propiedades bien definidas han sido reportados [28,29,31]. Al explorar estas posibilidades, en este trabajo investigamos la síntesis de un nuevo material que consiste en el agregado de diferentes cantidades de ácido *p*-sulfónico calix[4]areno incluido en un material mixto de sílice-titania, obtenido mediante la técnica sol-gel.

2. Materiales y Métodos

2.1. Síntesis de los materiales

El ácido *p*-sulfónico calix[4]areno (CX_4SO_3H, Figura 1), fue sintetizado siguiendo los procedimientos descriptos en la bibliografía [32,33].

La preparación de CX_4SO_3H (fase activa) incluido en la matriz de sílice se realizó a temperatura ambiente, disolviendo tetraetilortosilicato (TEOS, 16 mmol) en etanol absoluto (4,65 mL). Luego se agregaron, con agitación constante, 0,309 mmol de CX_4SO_3H, para obtener un material con 5% de fase activa y, finalmente, agua destilada (1,07 mL) (Figura 2.a). La mezcla se agitó magnéticamente durante 2 h y el gel formado se dejó reposar a temperatura ambiente y presión atmosférica hasta peso constante, obteniendo un sólido denominado CX_4SO_3H-Si (calixareno incluido en sílice (5% p/p)).

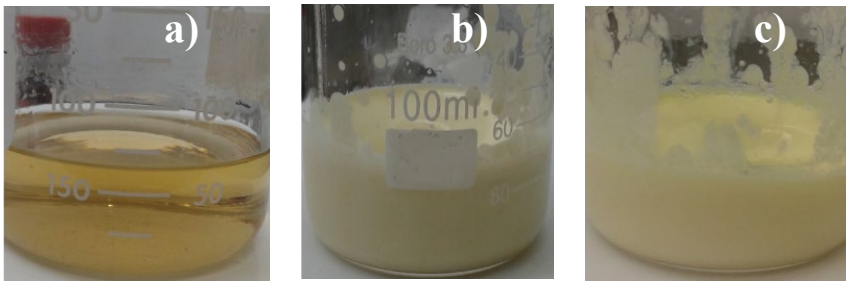

Figura 2. Geles de los materiales sintetizados con CX_4SO_3H: a) incluido en sílice, CX_4SO_3H-Si; b) incluido en titania, CX_4SO_3H-Ti; c) incluido en sílice-titania, CX_4SO_3H-Si-Ti.

La obtención de CX_4SO_3H incluido en la matriz de titania se realizó utilizando como precursor isopropóxido de titanio IV (TIP, 16 mmol), bajo las mismas condiciones que la síntesis de la sílice, para obtener un material con 5% p/p de fase activa (Figura 2.b). La mezcla se mantuvo

con agitación magnética durante 2 h y el gel formado se dejó reposar a temperatura ambiente y presión atmosférica hasta peso constante. El sólido obtenido se denominó CX_4SO_3H-Ti (calixareno incluido en titania (5 % p/p)).

La síntesis del CX_4SO_3H incluido en la matriz de sílice-titania se realizó a temperatura ambiente, disolviendo 8 mmol de TEOS y 8 mmol de TIP en etanol absoluto (4,65 mL), relación 1:1. Luego se añadieron 0,309 mmol de CX_4SO_3H, con agitación constante, y se añadió agua destilada (1,07 mL) (Figura 2.c). Luego, se mantuvo durante 2 h con agitación magnética y, finalmente, se dejó reposar a temperatura ambiente hasta peso constante. El sólido obtenido fue denominado CX_4SO_3H-Si-Ti (ácido p-sulfónico calix[4]areno incluido en el material mixto sílice-titania de proporción 1:1 (5% p/p)).

2.2. Caracterización de los materiales sintetizados

Las imágenes digitales fueron tomadas con una cámara LG G Pro Lite 8MP.

Para la Difracción de Rayos X (XRD), se utilizó un equipo Philips modelo PW-1390 (control de canal) y PW-1394 (control de motor), con registrador gráfico de barrido incorporado. Se usó radiación Cu Kα (α = 1,5417 Å), filtro de Ni, 20 mA y 40 kV en la fuente de alta tensión. Ángulo de barrido (2θ) comprendido entre 5° y 60°, velocidad de barrido de 2 °/min y amplitud de la escala vertical 2000 cuentas/seg.

Las propiedades texturales, como el área superficial de los sólidos (S_{BET}), se determinaron mediante adsorción-desorción de nitrógeno utilizando un equipo Micromeritics Accusorb 2100.

La caracterización por Espectroscopia Infrarroja por Transformada de Fourier (FT-IR) se realizó en un equipo Bruker IFS 66, usando pastillas de aproximadamente 1% p/p de la muestra en KBr, en el rango entre 400 y 4000 cm^{-1}, con una resolución de 2 cm^{-1}.

La estimación de las propiedades ácidas de los materiales se realizó por medio de titulación potenciométrica con *n*-butilamina. Se llevó a cabo en un equipo Metrohm 794 Basic Titrino con un electrodo de doble unión. Se agregaron 0,025 mL/min de solución de *n*-butilamina en acetonitrilo (0,05 N) a una cantidad conocida (0,05 g) del sólido de interés, previamente suspendido en acetonitrilo (90 mL), y agitado por un período de 3 h.

Se utilizó Microscopía Electrónica de Barrido (SEM) para la obtención de las micrografías de los sólidos, empleando un equipo Philips Modelo 505, a un potencial de trabajo de 15 kV, soportando las muestras sobre grafito y metalizándolas con oro. El mismo equipo fue utilizado

para realizar el análisis químico semicuantitativo (EDS) y el mapeo de la distribución de los elementos.

Por su parte, el Microscopio Electrónico de Transmisión (TEM) utilizado fue un JEOL, modelo 100 CX, operado a 100 kV. Las muestras se prepararon suspendiendo el material en agua destilada y llevándolo 15 min a baño ultrasónico para favorecer la dispersión. Posteriormente, se colocaron gotas de esta suspensión sobre una grilla provista con un film de Formvar® y se dejó secar durante 30 min. Todo el procedimiento se realizó a temperatura ambiente.

2.3. Ensayo catalítico

La actividad catalítica de los materiales preparados se evaluó en la síntesis de la julolidina I (2-bromo-3b,5,6,6a,7,9,9a,10,11,12a-decahidrofuro[3,2-c]furo[2'3':4,5] pirido[3,2,1-ij]quinolina). La reacción entre *p*-bromo anilina (0,5 mmol), formaldehído (1,5 mmol) y 2,3-dihidrofurano (1,5 mmol), asistida por el catalizador (0,5% mol) y en ausencia de solvente, fue llevada a cabo en un horno de microondas a 150 ºC (Esquema 1).

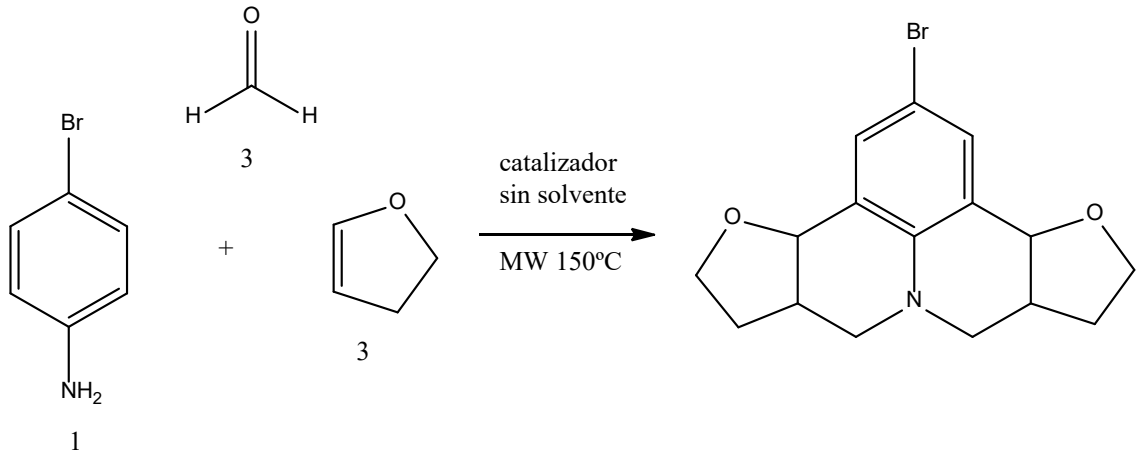

Esquema 1. Síntesis julolidina I

3. Resultados y Discusión

Comenzando con la caracterización, en la Figura 3 se presentan los registros fotográficos de los sólidos obtenidos usando la técnica sol-gel: sílice, titania y la mezcla de sílice-titania con el ácido *p*-sulfónico calix[4]areno (CX_4SO_3H) incluido en las diferentes matrices. Puede observarse la diferencia de textura y morfología de los geles secos: en el caso del material de sílice predominan características vítreas que no se observan en los materiales conteniendo titania. Esta diferencia puede atribuirse a que las reactividades de los alcóxidos de titanio son considerablemente más altas que las de los alcóxidos de silicio [30].

Figura 3. Geles secos sintetizados con CX_4SO_3H a temperatura ambiente: a) CX_4SO_3H-Si; b) CX_4SO_3H-Ti; c) CX_4SO_3H-Si-Ti.

Por lo tanto, deben tomarse precauciones durante la síntesis binaria del sistema sílice-titania para evitar la homocondensación [34]. El grado de homogeneidad depende de los parámetros de procesamiento, como la naturaleza y reactividad química de los sustratos, la concentración de agua y la secuencia de adición, el pH del medio, el tiempo y la temperatura de reacción [35]. Debido a esto, la incorporación de titania en la sílice vítrea influye en las propiedades finales del gel.

Aunque la sílice tiene alta estabilidad térmica, su estabilidad química disminuye a altas temperaturas, donde la presencia de agua es baja, resultando en la formación de hidroxilos superficiales. Se ha demostrado que la incorporación de titania mejora la estabilidad química [35].

En la fotografia correspondiente a CX_4SO_3H-Ti (Figura 3.b), las partículas presentan la apariencia de un polvo amarillento sin textura vitrea, en tanto que el sólido mixto CX_4SO_3H-Si-Ti (Figura 3.c), tiene una apariencia parecida a la titania.

En la Figura 4 se muestran los difractogramas de Rayos X obtenidos para los materiales sintetizados. Puede apreciarse que las bandas anchas de los soportes solapan las bandas angostas propias del calixareno, lo cual es evidencia de una buena dispersión de la fase activa dentro del soporte.

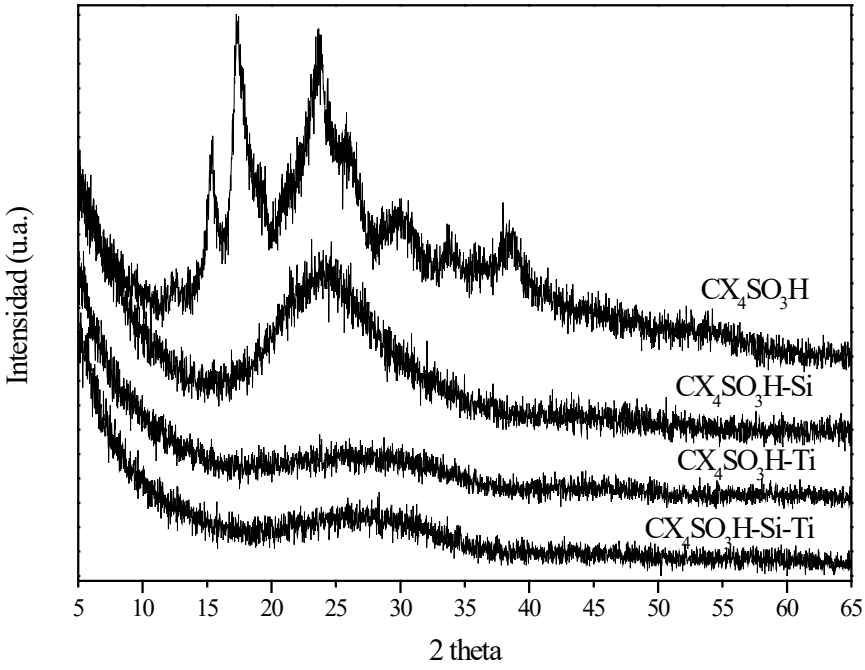

Figura 4. XRD de los materiales sintetizados.

Mediante las curvas de adsorción-desorción de nitrógeno es posible obtener información sobre el tipo de porosidad del sólido según la forma de las isotermas, las cuales se clasifican en cinco tipos principales [36]. En la Figura 5 se presentan las isotermas de los materiales sintetizados. La isoterma correspondiente al ácido *p*-sulfónico calix[4]areno puro podría asimilarse a una isoterma de tipo II sin la histéresis característica de estos sólidos (Figura 5.a), que están bien representados en la isoterma de los materiales a base de titania (Figura 5.c) y del óxido mixto de sílice-titania (Figura 5.d). Este tipo de isoterma es característica de sólidos poco porosos, con microporosidad y un área de entre 2 a 7 m^2 por g. En el caso del material conteniendo sílice (Figura 5.b) puede distinguirse una isoterma de tipo IV, que posee meso y macroporosidad. Al ser obtenida mediante la técnica de sol-gel, la gelificación de estas especies ramificadas produce la formación de regiones mesoporosas con un tamaño de poros entre 2 y 50 nm.

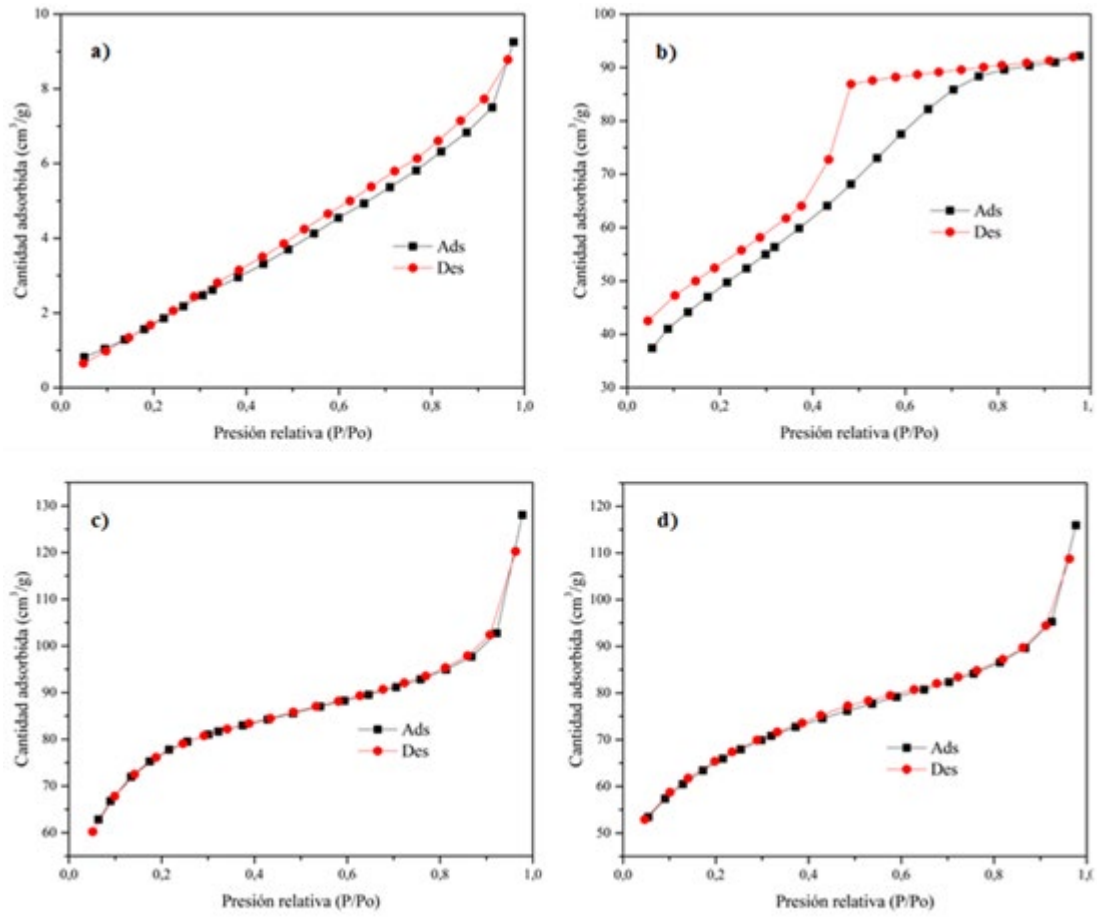

Figura 5. Isotermas de adsorción-desorción de N_2: a) CX_4SO_3H; b) CX_4SO_3H-Si; c) CX_4SO_3H-Ti; d) CX_4SO_3H-Si-Ti.

En la Figura 6 se grafican los espectros FT-IR obtenidos para los materiales sintetizados. Puede observarse que CX_4SO_3H-Si presenta las bandas características de la estructura de la sílice amorfa: νO-Si-O 1100 cm^{-1}, δO-Si-O 800 y 1196 cm^{-1}, νSi-OH 950 cm^{-1}, δSi-OH 1640 cm^{-1} y δO-H 3500 cm^{-1}.[37] A su vez, CX_4SO_3H-Ti muestra las bandas correspondientes a la titania pura: a 620-800 cm^{-1} que se asigna a los enlaces Ti-O y Ti-O-Ti, a 1625 cm^{-1} que corresponde al modo de flexión de las moléculas de H_2O de hidratación, y a 3300-3400 cm^{-1} que se asigna al grupo -OH [38-40]. En tanto, CX_4SO_3H-Si-Ti muestra los picos tanto de la sílice como de la titania. La incorporación de la titania en la sílice se evidencia por la existencia de la banda de vibración Ti-O-Si en 945 cm^{-1} [40-42]. En todos los casos los espectros del calixareno incluido en los materiales muestran las bandas características del soporte puro.

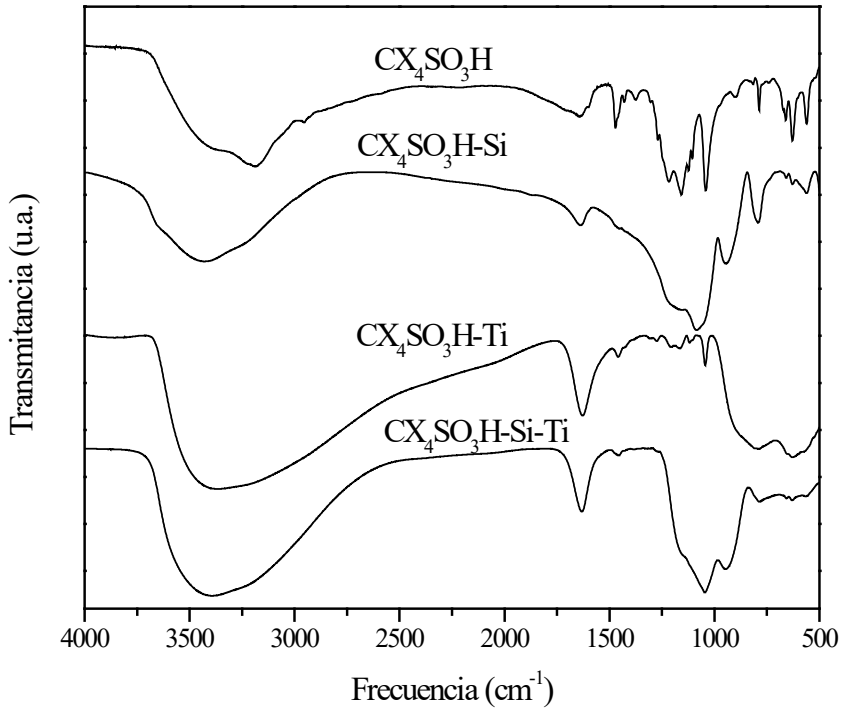

Figura 6. FT-IR de los materiales sintetizados.

Un gel ideal de TiO_2-SiO_2 consistiría solo en enlaces Si-O-Si y Si-O-Ti, que pueden detectarse por medio de FT-IR. La banda en el rango de 945-960 cm^{-1} es típica para vidrios TiO_2-SiO_2 o silicato de titanio cristalino. Si el gel no fuera homogéneo, se produciría la cristalización de TiO_2 [43,44].

La titulación potenciométrica con *n*-butilamina permite determinar las propiedades ácidas de una dispersión de partículas sólidas, a través de la medida de la diferencia de potencial del electrodo (E). Asimismo, para interpretar los resultados, se sabe que el potencial de electrodo inicial (Ei) indica la máxima fuerza ácida de los sitios, y los valores (meq/g sólido) donde se alcanza el *plateau*, indica el número total de sitios ácidos. La fuerza ácida de los sitios superficiales puede clasificarse de acuerdo a los siguientes rangos: sitio muy fuerte, Ei > 100 mV, sitio fuerte, 0 < Ei < 100 mV; sitio débil, -100 < Ei< 0 mV, y sitio muy débil, Ei < -100 mV [45].

En la Figura 7 se muestran las curvas de titulación potenciométrica obtenidas para los materiales sintetizados. Observamos en el gráfico de la izquierda (Figura 7.a), la alta acidez que posee el ácido *p*-sulfónico calix[4]areno, la cual concuerda con datos de acidez medidos utilizando otras técnicas de titulación reportados por Shinkai y col. [10].

En la Figura 7.b se muestran las curvas obtenidas para los materiales con el ácido *p*-sulfónico calix[4]areno incluido, donde se observa que la acidez de estos materiales es menor que la observada para el ácido *p*-sulfónico calix[4]areno puro, posiblemente esta disminución de

la acidez se debe a interacciones entre los grupos ácidos del calixareno con el soporte. Se sabe que los grupos OH de los calixarenos forman fuertes enlaces de hidrógeno intramoleculares. Esto afecta las propiedades de disociación ácida de estos grupos [46]. Sin embargo, los tres materiales, aunque poseen una acidez menor a la del ácido *p*-sulfónico calix[4]areno puro, siguen manteniendo elevada acidez, siendo la fuerza ácida de CX_4SO_3H-Si-Ti intermedia entre CX_4SO_3H-Si y CX_4SO_3H-Ti. La acidez de estos materiales los hace promisorios para su uso como catalizadores ácidos heterogéneos, especialmente en reacciones de síntesis orgánicas, por ejemplo, en aquellas reacciones en las que ya se ha evaluado el uso de los calixarenos como catalizadores en medio homogéneo [21-24,47].

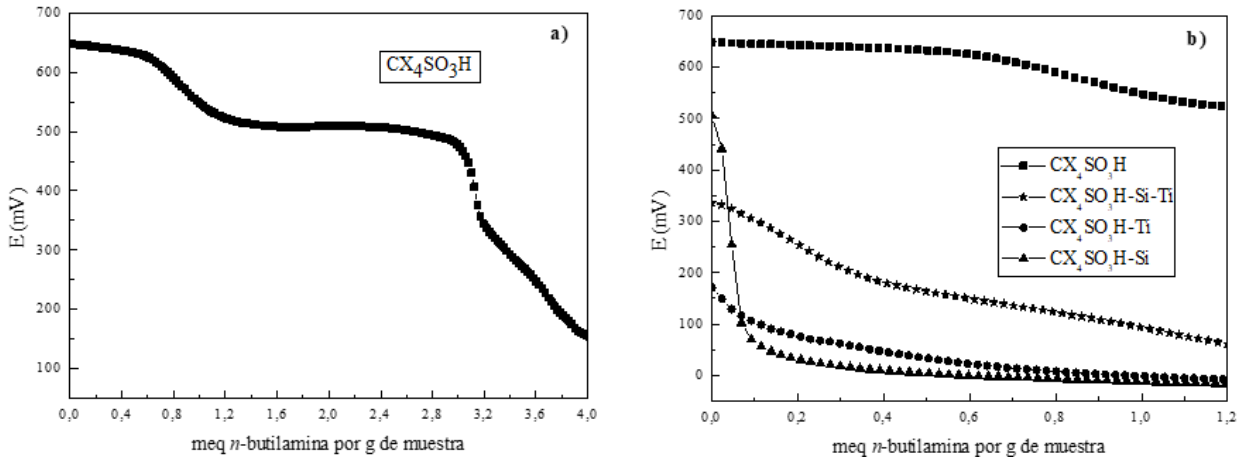

Figura 7. Titulación potenciométrica de: a) CX_4SO_3H; b) materiales con CX_4SO_3H incluido.

La caracterización de los materiales preparados se completó con micrografías SEM y TEM. En la Figura 8 se muestran las micrografías SEM y TEM obtenidas para el ácido *p*-sulfónico calix[4]areno puro y para los materiales con el calixareno incluido en los diferentes soportes.

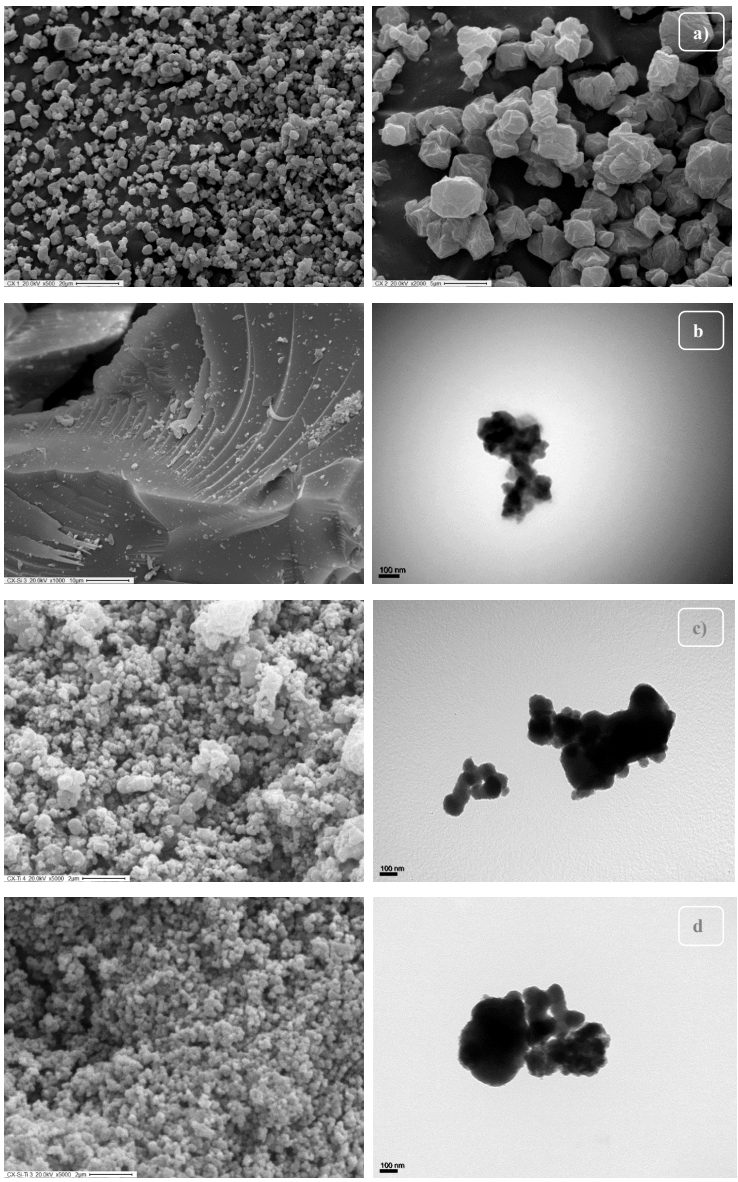

Figura 8. Micrografías a) SEM de CX_4SO_3H x500 (izquierda) y x2000 (derecha); b) SEM x1000 (izquierda) y TEM (derecha) de CX_4SO_3H–Si; c) SEM x5000 (izquierda) y TEM (derecha) de CX_4SO_3H–Ti; d) SEM x5000 (izquierda) y TEM (derecha) de CX_4SO_3H–Si-Ti.

Puede observarse para CX_4SO_3H partículas de tamaño y forma uniformes (Figura 8.a) y al estar incluido en sílice, CX_4SO_3H-Si (Figura 8.b) la estructura en láminas característica de este soporte [48], mientras que en las micrografías de CX_4SO_3H-Ti (Figura 8.c) se observa una aglomeración de las partículas redondeadas de titania con una morfología definida y homogénea [49]. Por último, para el material que contiene una mezcla de titania y sílice (Figura 8.d) puede observarse que predomina la morfología característica de la titania [50].

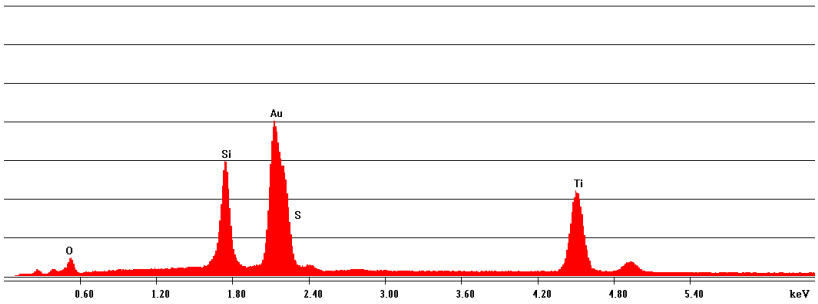

Figura 9. Análisis elemental cuantitativo de CX_4SO_3H-Si-Ti.

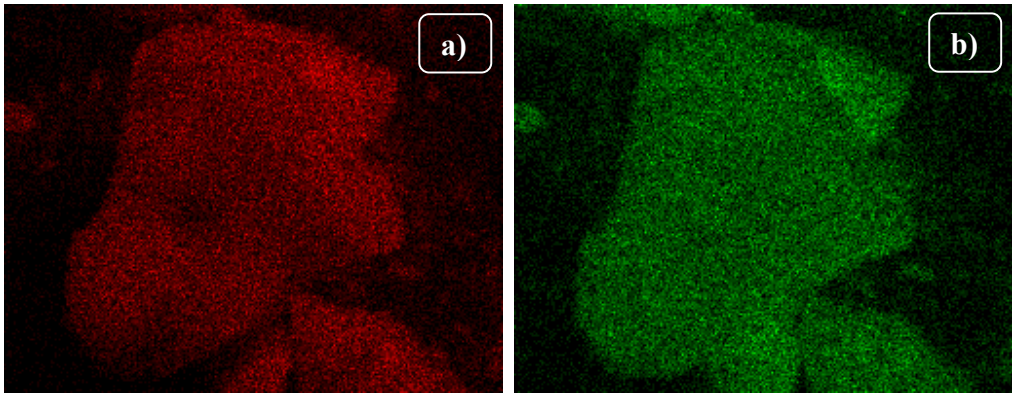

Figura 10. Mapeo de a) Si y b) Ti en CX_4SO_3H-Si-Ti.

Al material nuevo, CX_4SO_3H-Si-Ti, se le realizó un análisis elemental semicuantitativo (EDS), que permite determinar la presencia de titanio y silicio en la matriz (Figura 9). Asimismo, el mapeo de estos elementos muestra una distribución uniforme y homogénea de titanio y silicio en el material (Figuras 10.a y 10.b). Esto comprueba la correcta formación del óxido mixto sílice-titania, en concordancia con los resultados obtenidos por espectroscopia FT-IR.

Por último, los materiales preparados conteniendo al ácido *p*-sulfónico calix[4]areno incluido en los diferentes soportes, fueron evaluados como catalizadores en la síntesis de la julolidina I (Esquema 1) en ausencia de solvente y bajo irradiación de microondas. Los tres materiales mostraron muy buenos rendimientos en la reacción: CX_4SO_3H-Si 92%, CX_4SO_3H-Si-Ti 89%, CX_4SO_3H-Ti 73%. El catalizador pudo ser recuperado con facilidad del medio de reacción, para ser reutilizado.

4. Conclusiones

En base a los resultados obtenidos por las diversas técnicas de caracterización, se puede concluir que se sintetizó exitosamente un soporte mixto a base de sílice y titania, con características que difieren de los dos óxidos que lo constituyen. Por otro lado, la inclusión de ácido *p*-sulfónico calix[4]areno tanto en la sílice, titania como en el soporte mixto fue satisfactoria.

Estos materiales, al conservar las propiedades ácidas propias del ácido *p*-sulfónico calix[4]areno son promisorios para su uso como catalizadores ácidos, particularmente en síntesis orgánica. Lo novedoso de estos materiales es que el ácido *p*-sulfónico calix[4]areno, al estar incluido, permite condiciones de reacción heterogéneas que facilitan la recuperación del catalizador y su posterior reuso.

Agradecimientos

Los autores agradecen a Lilian Osiglio, Graciela Valle, Juan Tara, Mariela Theiller y German Kürten por las caracterizaciones realizadas, y a UNLP, CONICET y ANPCyT por el financiamiento recibido.

Referencias

(1) Ballini, R. *Eco-Friendly Synthesis of Fine Chemicals*. The Royal Society of Chemistry, Cambridge, 2009.

(2) Manley, J.B.; Anastas, P.T.; Cue, B.W. *J. Clean. Prod*. 2008, 16, 743-750.

(3) Farrauto, R.J.; Heck, R.M. *Catal. Today* 2000, 55, 179-187.

(4) Sheldon, R.A. *Green Chem*. 2007, 9, 1273-1283.

(5) Trost, B.M. *Science* 1991, 254, 1471-1477.

(6) Anastas, P.T.; Kirchhoff, M.M. *Acc. Chem. Res*. 2002, 35, 686-694.

(7) Sheldon, R.A.; Arends, I.; Hanefeld, U. *Green Chemistry and Catalysis*, WILEY-VCH, Weinheim, 2007.

(8) Gutsche, C.D. *Calixarenes. An Introduction*. 2nd Ed. The Royal Society of Chemistry, Cambridge, 2008.

(9) Sasaki, S.; Aisawa, S.; Hirahara, H.; Sasaki, A.; Narita, E. *Chem. Lett*. 2004, 33, 790-791.

(10) Shinkai, S. Tetrahedron 1993, 49, 8933-8968.

(11) Shinkai, S.; Araki, K.; Matsuda, T.; Nishiyama, N.; Ikeda, H.; Takasu, I.; Iwamoto, M. *J. Am. Chem. Soc.* 1990, 112, 9053-9058.

(12) Arena, G.; Contino, A.; Gulino, F.G.; Magri, A.; Sciotto, D.; Ungaro, R. *Tetrahedron Lett*. 2000, 41, 9327-9330.

(13) Yu, G.; Chen, X. *Theranostics* 2019, 9, 3041-3074.

(14) Cagil, E.M.; Hameed, O.; Ozcan, F. *Mat. Sci. Eng. C.* 2019, 100, 466-474.

(15) Yang, W.; Otto, D.P..; Liebenberg, W.; de Villiers, M.M. *Curr. Drug Discov. Technol*. 2008, 5, 129-139.

(16) Kumar, R.; Sharma, A.; Singh, H.; Suating, P.; Seok Kim, H.; Sunwoo, K.; Shim, I.; Gibb, B.C.; Seung Kim, *J. Chem. Rev.* 2019, 119, 9657-9721.

(17) Yilmaz, M., Erdemir, S. Turk. *J. Chem*. 2013, 37, 558-585.

(18) Khan, S.; Qureshi, I.; Shifa, M.S.; Waziri, A.H. Int. *J. Environ. An. Ch*. 2019, 99, 1123-1134.

(19) Tashakkorian, H.; Lakouraj, M.M.; Rouhi, M. *Int. J. Med. Chem*. 2015, ID 738202, 1-8.

(20) Durmaz, M.; Halay, E.; Bozkurt, S. *Beilstein J. Org. Chem*. 2018, 14, 1389-1412.

(21) Liberto, N.A.; Baptista Simões, J.; de Paiva Silva, S.; da Silva, C.J.; Modolo, L.V.; de Fátima, Â.; Silva, L.M.; Derita, M.; Zacchino, S.; Portilla Zuñiga, O.M.; Romanelli, G.P.; Fernandes, S.A. *Bioorg. Med. Chem.* 2017, 25, 1153-1162.

(22) Rezende, T.R.M.; Varejão, J.O.S.; Sousa, A.L.L.D.A.; Castañeda, S.M.B.; Fernandes, S.A. *Org. Biomol. Chem.* 2019, 17, 2913-2922.

(23) Ferreira de Paiva, W.; Bastos Braga, I.; de Assis, J.V.; Bonilla Castañeda, S.M.; Sathicq, Á.G.; Palermo, V.; Romanelli, G.P.; Natalino, R.; da Silva, M.J.; Terra Martins, F.; Senra Gonçalves de Carvalho, G.; Wilson Amarante, G.; Fernandes, S.A.; *Tetrahedron*, 2019, 75, 3740-3750.

(24) Palermo, V.; Sathicq, A.; Liberto, N.; Fernandes, S.; Langer, P.; Jios, J.; Romanelli, G. *Tetrahedron Lett.* 2016, 57, 2049-2054.

(25) Sathicq, Á.G.; Liberto, N. A.; Fernández, S.A.; Romanelli, G.P. *C. R. Chimia* 2015, 18, 374-378.

26. de Assis, J.V.; Abranches, P.A.S.; Braga, I.B.; Zuñiga, O.M.P.; Sathicq, A.G.; Romanelli, A.G.; Sato, A.G.; Fernades, S.A. *RSC Advances*, 2016, 6, 24285-24289.

(27) Ferré, M.; Cattoen, X.; Wong Chi Man, M.; Pleixats, R. *Chemistry Select*, 2016, 1, 6741-6748.

(28) Aguado, J.; van Grieken, R.; López-Muñoz, M.J.; Marugán, *J. Appl. Catal. A Gen*. 2006, 312, 202-212.

(29) Davis, R.; Liu, Z. *Chem. Mater*. 1997, 9, 2311-2324.

(30) Wright, J.D.; Sommerdijk, N.A.J.M. *Sol-Gel Materials Chemistry and Applications*. Taylor & Francis Group, Boca Raton, 2001

(31) Dutoit, D.C.M.; Schneider, M.; Baiker, A. *J. Catal*. 1995, 153, 165-176.

(32) Gutsche, C.D.; Iqbal, M. *Org. Synth*. 1989, 68, 234-236.

(33) Shinkai, S.; Araki, K.; Tsubaki, T.; Arimura, T.; Manabe, O. *J. Chem. Soc. Perkin Trans*. 1 1987, 2297-2299.

(34) de Lange, R.S.A.; Hehhink, J.H.A.; Kelzer, K.; Burggraaf, A.J. *J. Non-Cryst. Solids* 1995, 191, 1-16..

(35) Lenza, R.F.S.; Vasconcelos, W.L. *Mater. Res.* 2002, 5, 497-502.

(36) Brunauer, S.; Emmet, P.H.; Teller, E. *J. Am. Chem. Soc*. 1938, 60, 309-319.

(37) Martínez, J.; Ruíz, F. *Rev. Mexi. Fis.* 2002, 48, 142-149.

(38) Caldeira, L.; Vasconcelos, D.C.L.; Nunes, E.H.M.; Costa, V.C.; Musse, A.P.; Hatimondi, S.A.; Nascimento, J.N.; Grava, W.; Vasconcelos, W.L. *Ceram. Int.* 2012, 38, 3251-3260.

(39) Burgos, M.; Langlet, M. *Thin Solid Films* 1999, 349, 19-23.

(40) Musić, S.; Gotić, M.; Ivanda, M.; Popović, S.; Turković, A.; Trojko, R.; Sekulić, A.; Furić. K. *Mater. Sci. Eng. B* 1997, 47, 33-40.

(41) Shao, G.; Hilonga, A.; Kim, Y.; Kim, J.; Elineema, G.; Quang, D.; Jeon, S.; Kim, H. *Chem. Eng. J.* 2012, 122, 198-199.

(42) Gao, X.; Wachs, I.E. *Catal. Today* 1999, 51, 233-254.

(43) Schraml-Marth, M.; Walther, K.L.; Wokaun, A.; Handy, B.E.; Baiker, A. *J. Non-Cryst. Solids* 1992, 143, 93-111.

(44) Minehan, W.T.; Messing, G.L.; Pantano, C.G. J. Non-Cryst. Solids 1989, 108, 163-168.

(45) Cid, R.; Pecchi, G. *Appl. Catal*.1985, 14, 15-21.

(46) Gutsche, C.D. *Acc. Chem. Res*. 1983, 16, 161-170.

(47) Rostami, M.E.; Gorji, B.; Zadmard, R. *Tetrahedron Lett*. 2018, 59, 2393-2398.

(48) Colombo Migliorero, M.; Palermo, V.; Vázquez, P.; Romanelli. G. *J. Renew. Mater*. 2017, 5, 167-173.

(49) Palacio, M.; Villabrille, P.I.; Romanelli, G.P.; Vázquez, P.G.; Cáceres, C.V. *Appl. Catal. A: Gen*. 2012, 417-418, 273-280.

(50) Aziz, R.A.; Sopyan, I. *Indian J. Chem*. 2009, 48A, 951-957.